UNIVERSITY OF OKLAHOMA

GRADUATE COLLEGE

THE CHANGING HYDROCLIMATE OF THE UNITED STATES GREAT PLAINS: METEOROLOGICAL AND CLIMATOLOGICAL IMPACTS ON WATER RESOURCES

A DISSERTATION

SUBMITTED TO THE GRADUATE FACULTY

in partial fulfillment of the requirements for the

Degree of

Doctor of Philosophy

By

PAUL XAVIER FLANAGAN
Norman, Oklahoma
2018

Downloaded from SHAREOK. Persistent Handle URL: https://hdl.handle.net/11244/316316

THE CHANGING HYDROCLIMATE OF THE UNITED STATES GREAT PLAINS: METEOROLOGICAL AND CLIMATOLOGICAL IMPACTS ON WATER RESOURCES.

A DISSERTATION APPROVED FOR THE
SCHOOL OF METEOROLOGY

BY

Dr. Jeffrey B. Basara, Chair

Dr. Jason C. Furtado

Dr. Elinor R. Martin

Dr. Michael Richman

Dr. Xiangming Xiao

© Copyright by PAUL XAVIER FLANAGAN 2018
All Rights Reserved.

Acknowledgments

I would like to extend my utmost gratitude to the numerous individuals without whom this project would not have been possible. First, I would like to thank my advisor, Dr. Jeffrey Basara for guiding me through this entire process. Without his ample expertise, aid and extensive knowledge this project would not be where it is today. No matter what difficulties arose through this process, he was there to lend a helping hand. I do not think I would be where I am in my career without having him as my advisor. I would also like to thank my Ph.D. committee, Dr. Jason Furtado, Dr. Elinor Martin, Dr. Michael Richman and Dr. Xiangming Xiao. Throughout this entire project their guidance and expertise has helped shape this project into the form you see below.

Next, I would like to thank the Climate, Hydrology, Ecosystem, and Weather (CHEWe) research group, especially Hayden Mahan, Ryann Wakefield and Jordan Christian. Through thick and thin you have all had my back. The conversations we've had in our office about life, science and whatever else came our way helped me push through the darker days to get to this point. Without all of you I don't know if I could have gotten all the way to the finish line. I would also like to thank Dr. Benjamin Cook, who helped inspire this project from the start. His guidance was crucial in shaping this project from the initial NASA NESSF graduate fellowship proposal to the finish project you see here. I would also link to thank the International Journal of Climatology, Journal of Hydrometeorology and the Journal of Climate for their aid in publishing the work contained within this dissertation, along with the numerous coauthors whose aid was instrumental in getting those studies published.

Finally I would like to thank my family and friends for their support throughout this project. Without all of you I would never have been able to push through to the end in one piece. Lastly, a

large amount of thanks to my girlfriend Chelsea. Without her love and support it would not have been possible for me to get this project done. You pushed me through thick and thin and wouldn't let me give up on myself. Thank you so much, I love you.

Table of Contents

	Page
Acknowledgements	iv
Table of Contents	vi
Abstract	viii
Chapter 1: Introduction	1
Chapter 2: Analysis of the Great Plains Annual Climate	
2.1: Introduction	4
2.2: Data and Methods	6
2.2.1: Global Historical Climatology Network-Daily Data	6
2.2.2: Asynchronous Difference Index	13
2.3: Great Plains' Temperature and Precipitation Climatology	14
2.4: Results	15
2.4.1: Spatial ADI Analysis	15
2.4.2: Temporal ADI Analysis	21
2.4.3: Daily ADI	26
2.4.4: Weekly ADI	30
2.5: Discussion	34
Chapter 3: Primary Atmospheric Drivers of Pluvial Years in the United States Great Plains	
3.1: Introduction	41
3.2: Data and methods	43
3.2.1: Datasets	43
3.2.2: Definition of pluvial periods	45
3.2.3: Statistical methods	48
3.3: Results	51
3.3.1: Southern Great Plains pluvial analysis	51
3.3.2: Northern Great Plains pluvial analysis	53
3.3.3: Robustness of the pattern composite analysis	57
3.3.4: Heavy precipitation event analysis	59
3.3.5: Break composites	62
3.4: Discussion	64
Chapter 4: Role of Pacific Sea Surface Temperatures in United States Great Plains Pluvial Years	
4.1: Introduction	67
4.2: Data and Methods	72
4.2.1: Datasets	72
4.2.2: Calculating the Eddy Geopotential Height Index	72
4.2.3: Composite and Regression Analysis	73
4.2.4: Synoptic Wave Event Classification Scheme	74
4.3: Diagnosis of Synoptic Waves during Great Plains *Pattern* Pluvial Years	76
4.3.1: Synoptic Wave Event Statistics	76

4.3.2: Event Classification Composites 78
4.4: Diagnosis of Great Plains *Pattern* Pluvial Years 83
4.4.1: SST and Stream function Composites 83
4.4.2: Eddy Geopotential Height Index Linear Regression Analysis 89
4.5: Discussion 94

Chapter 5: Southern Great Plains Pluvial Year Case Study
5.1: Introduction 99
5.2: Atmospheric and Surface Datasets 100
5.3: Synoptic Diagnosis of the 2015 Southern Great Plains Pluvial 101
5.4: Climate Scale Diagnosis of the 2015 Southern Great Plains Pluvial 105
5.5: Discussion 108

Chapter 6: Summary and Conclusions
6.1: Introduction 111
6.2: Analysis of the Great Plains Annual Climate 111
6.3: Primary Atmospheric Drivers of Great Plains Pluvial Years 113
6.4: Links Between Great Plains' Pluvial Years and Pacific Sea Surface Temperatures 117
6.5: Southern Great Plains Pluvial Year Case Study Results 119
6.6: Final Remarks 120

References 123

Appendix 1 147

Abstract

In the United States Great Plains (GP), understanding precipitation variability is key in developing an understanding of the present and future availability of water in the region. Numerous studies have investigated the hydroclimate, or the part of the climate relating to the hydrology of a region, of the GP from the soils, surface, vegetation and their impacts on water resources. Even so, there is still more to be understood from a climatological perspective. Further, analysis of the GP climate in terms of temperature and precipitation maxima in relation to the hydroclimate is not yet complete. While drought and its associated drivers have been studied in the GP region, periods of excessive precipitation (pluvials) at seasonal to interannual scales have received less attention. Thus, analysis of the GP climate in terms of features that directly impact water is required to more fully understand the GP climate and future impacts to water availability.

The first part of this study investigated a long-term observational dataset to quantify the asynchronicity and address the impacts of climate variability and change. Global Historical Climate Network Daily (GHCN-Daily) data were utilized for this study; 352 GHCN-Daily stations were identified based on specific criteria and the dates of the precipitation and temperature maxima for each year were identified at daily and weekly intervals. An Asynchronous Difference Index (ADI) was computed by determining the difference between these dates averaged over each decade. Analysis of Daily and Weekly ADI revealed two physically distinct regimes of ADI (positive and negative), with comparable shifts in the timing of both the maximum of precipitation and temperature over all six states within the GP examined when comparing the two different regimes. Time series analysis of decadal average ADI yielded moderate shifts (~5-10 days from linear regression analysis) in ADI in several states with increased variability occurring over much of the study region.

Utilizing the ERA-20C dataset, a climatological analysis of GP pluvials was completed. Through an analysis of GP precipitation, the region was split into two subregions; the Northern Great Plains (NGP) and the Southern Great Plains (SGP). Analysis of ERA-20C geopotential heights during NGP and SGP pluvial years reveals atmospheric anomaly patterns associated with the occurrence of pluvial years. In the SGP, this pattern is depicted by negative height anomalies over the southwestern United States, coincident with a southward shifted jet stream over the north Pacific allowing a more frequent passage of synoptic waves toward the southern United States. The NGP pluvial pattern shows negative height anomalies over the northwestern United States and an anomalously extended jet stream over the northern North Pacific. Further, analysis of sea surface temperatures (SST) and streamfunction aids in explaining the occurrence of these pluvial years. During SGP above average precipitation (i.e., pluvial) years, central tropical Pacific SST anomalies occur concurrently with key atmospheric anomalies across the Pacific basin and North America and they contribute significantly to the occurrence of excessive rainfall, with no specific pattern of oceanic or atmospheric anomalies emergin during NGP pluvial years. When comparing the SGP pluvial of 2015 to that of 2007, differences in the height, SST and streamfunction anomaly fields described the overall differences between pluvial years driven by annual atmospheric anomalies and years which show no strong atmospheric annual anomaly feature associated with annual excessive precipitation. Overall, the results from this study reveal new insights to precipitation variability across the GP owing to local and global processes.

Chapter 1

Introduction

Given the overall importance of agricultural practices within the Great Plains (GP) of the United States (Fisher et al. 2007), water is a precious commodity. This is especially true given the climate variability within the region. From short to long-term drought, flash floods, and pluvial periods spanning seasons to years, the availability of water can dramatically change from one year to the next (e.g., Ting and Wang 1997; Ruiz-Barradas and Nigam 2005). To mitigate the impacts of this variability, local stakeholders must have knowledge of the availability of water in the coming growing season (Irmak et al. 2000; Alderfasi and Nielsen 2001; Kang et al. 2009) to successfully manage their agricultural business. Seeding strategies, crop diversity, crop acreage, herd count and other agricultural practices such as grazing depend highly on the availability of water in the coming months (e.g., Holechek 1996; Thurow and Taylor 1999; Graef and Haigis 2001; Kirigwi et al. 2004).

The ecosystem of the GP is highly dependent on the availability of water (Burke et al. 1991). This is due to the large area of grasslands which span the region. Short-term changes in water can have a dramatic impact on the health and diversity of the grassland ecosystem (Symstad and Jonas 2011). While this does not directly impact the population of the GP, these grasslands are commonly used for agricultural practices such as cattle grazing, and thus, have impacts to the local economy. Thus, understanding regional climate impacts on water availability and variability is important. The timing of abundant precipitation and the timing of heightened water stress in relation to each other can determine the successful growth and wellbeing of a region's ecology (e.g., Hughes 2000; Menzel et al. 2003, 2006; Badeck et al. 2004; Cleland et al. 2007; Bertin 2008).

To predict the changes to water availability over the region the drivers of variability of the regional climate (e.g., temperature, precipitation, etc.) must be thoroughly understood. While short to long-term dry periods (i.e., drought) have been examined extensively for the GP region, especially in relation to climate change (e.g., Ruiz-Barradas and Nigam 2010; McCrary and Randall 2010; Bukovsky and Karoly 2011; Wehner et al. 2011; Hoerling et al. 2012; Feng 2017), wet (pluvial) periods of significant, above-normal precipitation have not been similarly investigated (Cook et al. 2011). This is due to the perceived lack of direct, negative impacts caused by pluvial periods which creates a lack of necessity in examining their causes. Yet, understanding the variability of water in the GP is fundamental to being able to predict the dynamic changes in available water. Studies such as Hu and Huang (2009) and Trenberth and Guillemot (1996) have examined these wet periods over the GP, finding that modifications to water transport, atmospheric jets, synoptic wave occurrences and their location are key to pluvial events. However, these studies have focused on singular events or specific seasons. To develop a comprehensive knowledge base of GP water variability, pluvial events must be further investigated. For example, analyzing past pluvial events deepens the current knowledge of why pluvial events occur while diagnostic examination determines the conditions that lead to prior pluvial events and connections between the global system and the local climate of the GP. Finally, thorough knowledge of precursor and concurrent conditions for pluvial events aids in the development of pathways to predicting pluvial events over the GP on temporal scales related to seasonal prediction.

Overall, a knowledge gap exists when considering the GP climate and hydroclimate. Diagnosing the total impact of precipitation on water, thus predicting changes to this precious commodity are difficult over the GP. Developing an understanding of water variability requires an in depth examination into the nature of precipitation over the region. Regardless of the perceived

lack of negative impacts from long-term wet periods, understanding the drivers behind these events from a regional to global scale is necessary if the variability of water is to be understood across the GP region. Thus, the goal of this work is to delve into the climate of the GP with a focus on climatological and meteorological impacts, primarily precipitation, on the variability of water.

The purpose of this research is to develop a more complete understanding of the GP hydroclimate by filling in several knowledge gaps relating to precipitation variability. Thus, this project will investigate aspects of the GP climate that are not well understood. The hypothesis of this project is: Shifts in GP and global climate variability will result in changes to the GP hydroclimate. To evaluate this hypothesis, several research goals will be completed:

- Analyze the annual climate of the GP,
- Determine the primary atmospheric drivers of GP pluvial years utilizing climatological datasets,
- Diagnose the distinguishing features of pluvial years driven by these atmospheric patterns to determine predictable environmental processes associated with pluvial periods.

With these goals completed, conclusions into the effects of climate shifts on the GP hydroclimate can be made. Further, given the overwhelming focus of research on drought, this analysis of pluvial periods will close the knowledge gap and bring forth key insights into the effect of climate change on precipitation variability. As a whole, this work will expand the knowledge of the GP hydroclimate related to precipitation variability and associated drivers. The dissertation is organized as follows: Chapter 2 details an analysis into the GP annual climate, Chapter 3 details the primary atmospheric drivers of pluvial years, Chapter 4 details the diagnosis of these atmospheric patterns, Chapter 5 presents a SGP pluvial case study and Chapter 6 contains the conclusions.

Chapter 2

Analysis of the Great Plains Annual Climate

(Flanagan et al. 2017)

2.1 Introduction

The growing season (GS), which spans from March to October in the northern hemisphere during which plants and crops emerge after the cold season and grow until leaf fall (Linderholm 2006), is typically associated with increased temperature, and precipitation as well as increased variability in ground and surface moisture fluxes (e.g., Evapotranspiration (ET) and soil moisture (Illston et al. 2004; Durre et al. 2000; Teuling and Troch 2005). Recent climate change research has focused on the effects of global climate change on regional precipitation (e.g., Ruiz-Barradas and Nigam 2010; Long et al. 2012; Christian et al. 2015; Shi and Durran 2016; Bukovsky and Karoly 2011; Groisman et al. 2012), temperature (e.g., Long et al. 2012; Berg et al. 2015; Kunkel et al. 2010; Kumar et al. 2013), and plant health and phenology (e.g., Schlenker and Roberts 2009; Jamieson et al. 2012; Bertin 2008; Weltzin and McPherson 2003; Zeppel et al. 2014; Tubiello et al. 2002). However, while impacts of climate change on vegetation health have been studied, most have focused on specific plant and crop impacts (Schlenker and Roberts 2009; Jongen et al. 2011; Olesen and Bindi 2002; Tubiello et al. 2007) rather than regional GS climate.

Because small changes to temperature and precipitation trends incur significant impacts on vegetation during the GS, such impacts are extremely important to examine (Lobell and Asner 2003). The temperature magnitude, timing of temperature increases/decreases and overall maximum are important to crop phenology (e.g., Bertin 2008; Menzel et al. 2006; Hughes 2000; Menzel 2003; Cleland et al. 2007; Badeck et al. 2004) and can impact plant growth and maturity

(Menzel 2003). Thus, as temperature warms more quickly vegetation will mature earlier in the GS and shift the timing at which water stress will be higher due to quicker plant mass growth (Martyniak 2008) as the temperature magnitude and temperature maxima determine the timing of peak ET and thus the timing of peak water usage (Vivoni et al. 2008; Bartz and Brecht 2002; Blum 2010). If water availability is not sufficient for the vegetation, plant health can be adversely affected (Turner and Begg 1981; Blum 2010). At the same time, Schlenker and Roberts (2009) noted that the negative effects of extreme temperatures on corn crops during June and July could be mitigated by increases in precipitation. Thus the seasonality and variability of precipitation also yield significant impacts to vegetation health in concert with temperature.

Beyond the basic requirement of sufficient water for vegetation sustenance, the timing of precipitation can also impact plant health and crop production. Fay (2009) demonstrated that variations in precipitation impacted food resource availability while also finding that microbial processes are sensitive to soil moisture that can impact the availability of nitrogen in the soil. This leads to a sensitivity of nitrogen availability to trends in soil moisture and as the timing between rainfall events increases the availability of nitrogen decreases. Di et al. (1994) modeled the relationship between Normalized Difference Vegetation Index (NDVI) and precipitation and suggested that the response to NDVI from precipitation events changes throughout the GS and found that plants more effectively utilized water from precipitation events during the earlier and later portions of their growing cycle, but less so when the plant was more mature. Further, Di et al. (1994) noted that due to plant root depth and size, deeper soil moisture was more important later in the growing season than earlier. Thus, precipitation events are more important earlier in the season to maintain overall soil moisture storage essential to vegetation (Méndez-Barroso et al. 2009; Vivoni et al. 2008).

Unlike most grasslands and croplands around the world, the maxima in temperature and precipitation during the Great Plains (GP) of North America growing season do not occur at the same time whereby the maxima in precipitation precedes the climatological maxima in temperature. Because the agricultural industry in the Great Plains (GP) is of critical socioeconomic importance (Fischer et al. 2007), the impacts of climate change on the seasonality of precipitation and temperature, especially during the GS, are critically important. At the same time, numerous studies have noted changes in the timing of precipitation and temperature across interior portions of North America (e.g., Stewart et al. 2004; Regonda et al. 2005; Caesar et al. 2006; Schwartz et al. 2006). However, the asynchronicity (AS) between the timing of precipitation and temperature maxima have not been examined and yet are critical to GS processes in the region. Thus, the purpose of this study was to examine the climatological AS between the timing of precipitation and temperature maxima in the GP using historical observations to determine whether long-term changes in AS have occurred.

2.2 Data and Methods

2.2.1 Global Historical Climatology Network-Daily Data

To investigate the long-term trends in the AS of temperature and precipitation maxima, a climate data set of surface observations was required. The Global Historical Climatology Network's Daily (GHCN-Daily) dataset (Menne et al. 2012) was utilized for this study. A network of sensors that spans the globe and has been in operation for over 100 years, the dataset provides daily maximum temperature and precipitation observations from over 80,000 weather stations. Only stations contained within the GP of the United States (Fig. 2.1) were retained for this study which spanned from 1895 to 2015. Further, similar to Christian et al. (2015), the GP was defined

to include the states of Texas, Oklahoma, Kansas, Nebraska, South Dakota, and North Dakota. A length of period (>90 years) requirement was used to filter out stations with short periods of record. However, no filter was used to remove stations without continuous datasets during this period as few stations within the dataset have a continuous, long-term record of observations. Thus, earlier decades may not contain observations from all stations shown in Figure 2.1. After filtering was completed, a total of 352 stations were identified within the GP region. As seen in Figure 2.1, the distribution of stations covers the entire region, with few noticeable gaps. To focus only on the spring precipitation maximum and the summer temperature maximum consistent with the GS, the period was constrained from March through August of each year.

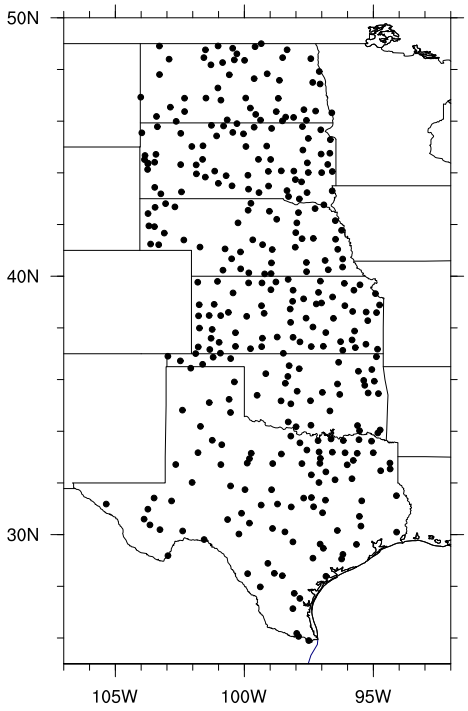

Figure 2.1: Map of the Great Plains showing the location of each GHCN-Daily station used in this study.

While the GHCN-Daily dataset is useful for climate studies due to its long period of record, biases exist in the daily data that can mask or artificially induce trends within the dataset (Karl et al. 1988). Additionally, the GHCN dataset is hindered by: time of observation bias (Karl et al. 1986), instrumentation bias (Quayle et al. 1991), station location change bias (Karl and Williams 1987) and a bias caused by urbanization near or at the station site (Karl et al. 1988). While bias correction algorithms exist for monthly averaged data a comparable method of removing these biases from the daily datasets does not exist. However, histogram analysis on the date of maximum temperature (Fig. 2.2) and precipitation (Fig. 2.3) from the GHCN-Daily dataset shows that dates from each state match the climatological date of the respective maxima (Fig. 2.4).

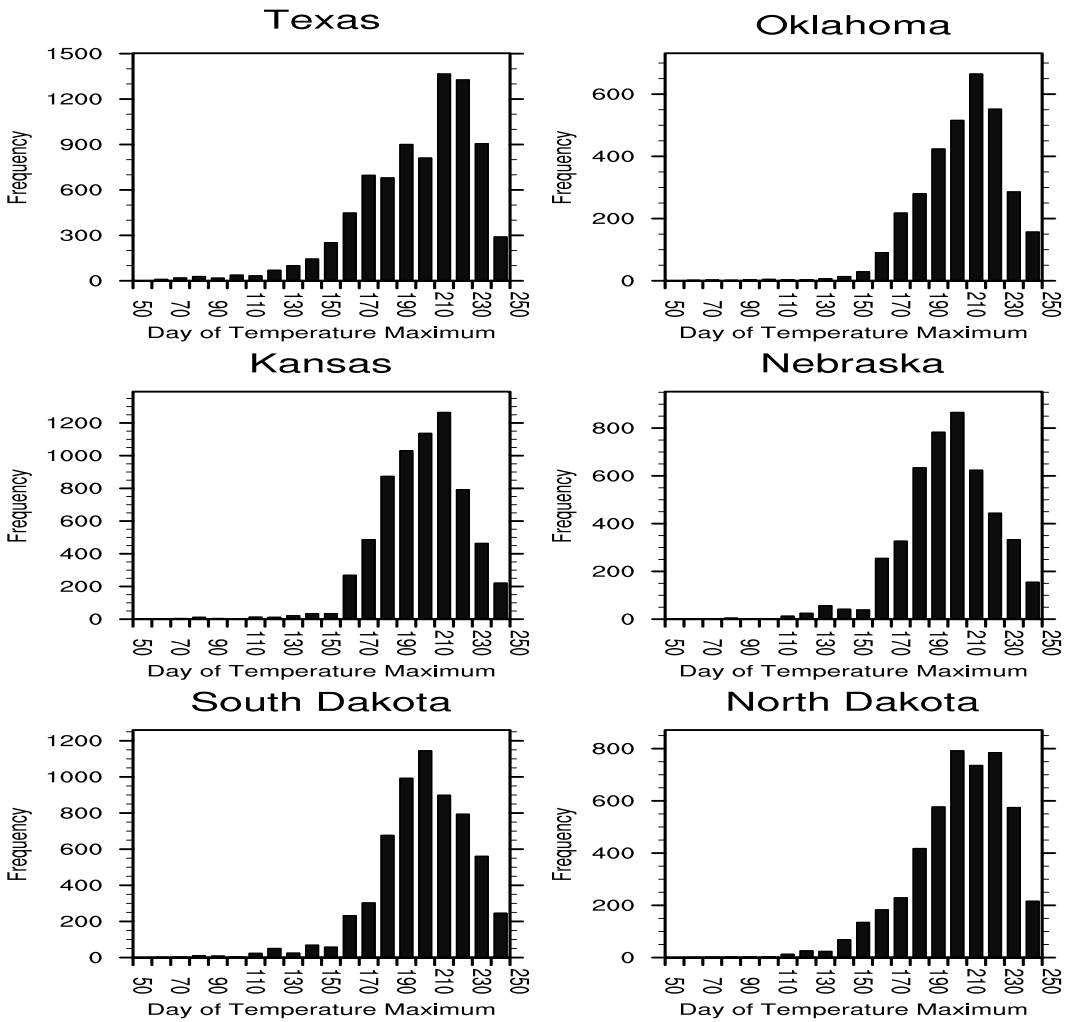

Figure 2.2: Histogram of dates for maximum temperature throughout the entire GHCN-Daily dataset for each state.

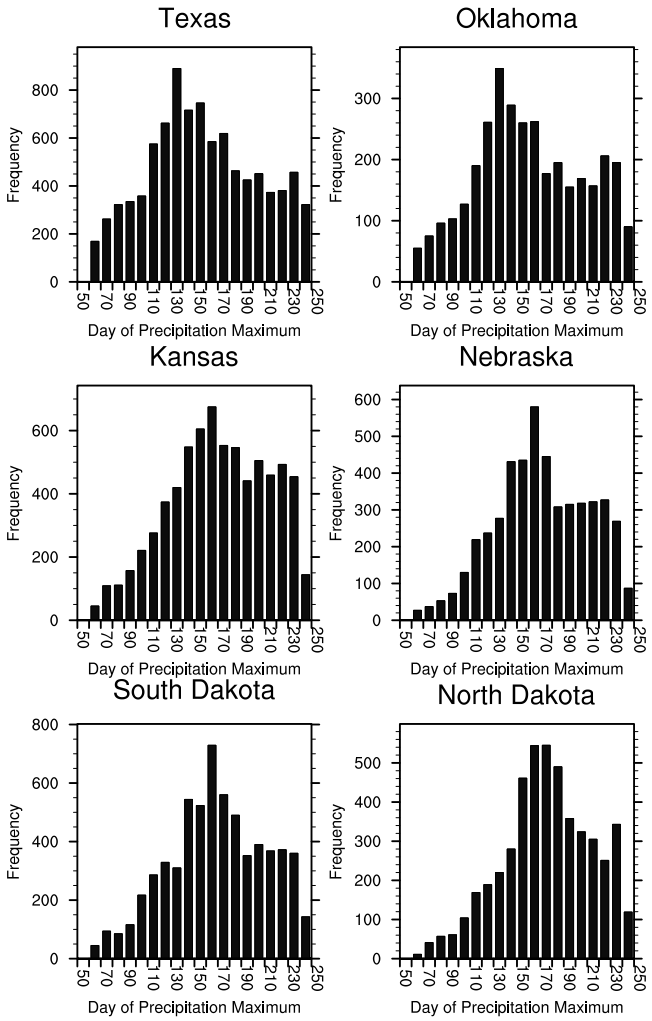

Figure 2.3: Same as figure 2.2, except for precipitation.

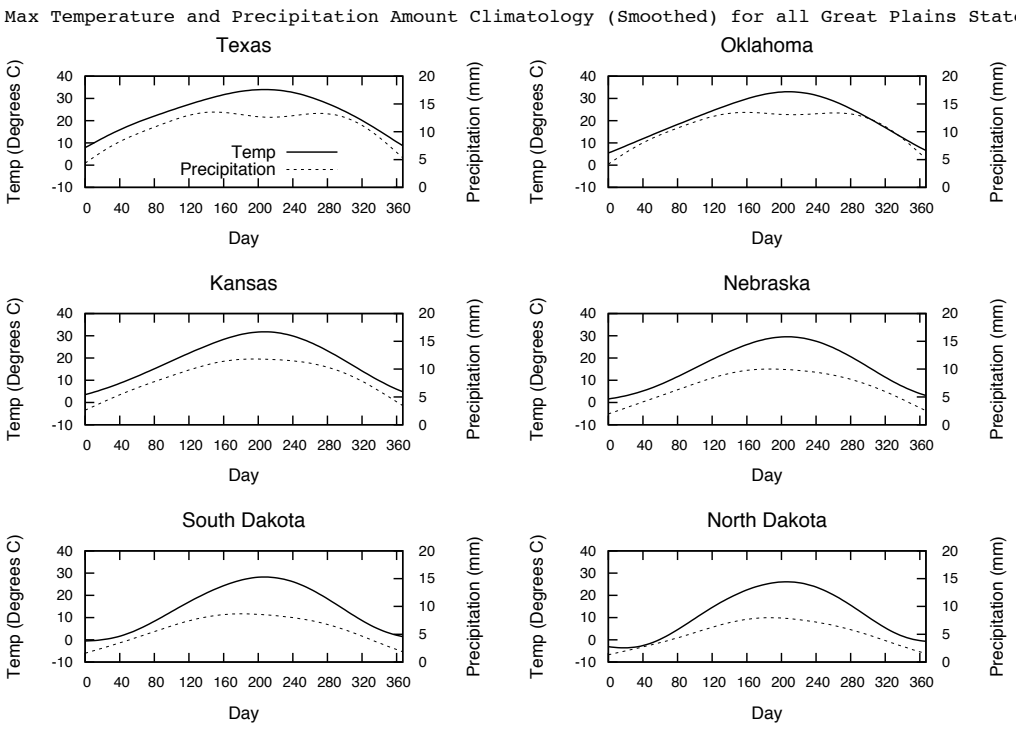

Figure 2.4. Temperature and precipitation climatology from the GHCN-Daily dataset. Dashed line is precipitation (mm) and the solid line is temperature (degrees C). Lines were smoothed due to the variability in the daily precipitation climatology.

2.2.2 Asynchronous Difference Index

To quantify the climatological difference between the maxima of temperature and precipitation, an index was created. The Asynchronous Difference Index (ADI) computes the difference between the dates of the two maxima which allows for a simplistic quantitative analysis of the dataset. For this study, the ADI was defined as the difference between the date of maximum temperature and the date of maximum precipitation, as shown in equation 1:

$$ADI = Dmax_{Temp} - Dmax_{Prec} \qquad \text{(Eq. 2.1)}$$

Where,

ADI = Asynchronous Difference Index

$Dmax_{Temp}$ = Date (day or week) of highest maximum temperature

$Dmax_{Prec}$ = Date (day or week) of maximum precipitation amount.

This formulation was developed to obtain a positive average ADI during climatological conditions. As seen in Figures 2.2 and 2.3, the dates of maximum precipitation and temperature cannot be approximated as normal distributions. However the ADI normalizes these two datasets and allows for a more simplistic statistical methodology to be utilized for analysis.

To deduce the effect of different methodologies in finding the "date" of maxima, two separate techniques of analyzing the data for the maximum date were utilized. First, the day of maximum temperature and precipitation was analyzed from the 352 stations for each year. The ADI was then developed from this dataset of daily maximum temperature and precipitation for each year (Daily ADI). Secondly, daily observations were averaged, or for precipitation the sum total was determined, for each week and then the maximum week within the period yielded the date of maximum. Weeks were designated as 1 through 26 for the study period, with the first week

starting on the third day of March for each year. This was done to exclude data from September in the last week of each period and constrain the dataset to the same period as the other two date methodologies. The ADI was then computed as the difference between the two-week numbers and then multiplied by 7 to obtain an approximation for the number of days (Weekly ADI). This was done so that a direct comparison between the daily and weekly results could be completed. Statistical analysis was then completed for each version of the ADI including the mean, standard deviation, Student's t-test significance tests, and linear regression. Student's t-tests were completed on the decadal ADI dataset using the 1890-1949 period as an estimate for the population statistic and the 1950-2015 period as the test statistic. The latter was assigned due to recent results noted by Christian et al. (2015) and Weaver et al. (2016) which found increasing variability of precipitation across the GP after 1950.

2.3 Great Plains' Temperature and Precipitation Climatology

Using the GHCN-Daily dataset, a climatology of precipitation and maximum temperature was created for each state within the study domain (Fig. 2.4). This daily climatology was then smoothed (using a kernel density estimate for a random collection of points) to remove the influences of fluctuations in the precipitation climatology. All six states have similar temperature climatology with a maximum in mid summary (late July, ~day 200), but differ in precipitation climatology. The four northern states have a peak of precipitation during early summer (June, ~day 160), but the southern states have a bimodal pattern of precipitation with one peak during spring (May, ~day 140) and another peak during fall (October, ~day 280). In this manuscript, the analyses focus on the study period from March to August, which includes both the climatological temperature maximum and the first (spring) climatological precipitation maximum. Ending the

study period at August removes the unwanted secondary precipitation maximum evident in the Texas and Oklahoma precipitation climatology that occurs in September/October and beyond the critical growing season.

2.4 Results

2.4.1 Spatial ADI Analysis

Climatologically, ADI yieldes features that commonly seen within the GP climate (Fig. 2.5). A strong gradient of ADI is analyzed over the Southern Great Plains (SGP), especially in Texas and Oklahoma. This matches well with the known gradient of precipitation that occurs within this region of the GP. Further to the north, a reversal of this gradient occurs and ADI was climatologically lower in the eastern portion of the Northern Great Plains (NGP) when compared to the western portions of this portion of the GP. The SGP mean ADI pattern is likely due to the overall east to west gradient of precipitation whereby climatologically more rainfall falls in the eastern portion of the SGP. This causes temperatures to reach their yearly maximum at a later date due to increased latent heat flux. Across the western portion of the SGP, less precipitation occurs, and temperature values increase more rapidly and earlier in the year. In the NGP domain, this pattern is more difficult to describe as the east to west gradient of rainfall still occurs in this portion of the GP as well and ADI is controlled more so by the date of maximum rainfall than temperature (Fig. 2.6). A gradient in the date of maximum rainfall occurs across the NGP (decreasing to the west) without a corresponding gradient in the date of maximum temperature and would yield higher ADI in the western portion of the NGP as seen in the mean ADI analysis (Fig. 2.5). The cause of the later date of maximum precipitation in the NGP compared to the SGP is due to mesoscale convective system (MCS) activity that occurs in the early summer within the GP, which

has been noted numerous times in previous studies (e.g., Rasmusson 1971; Wallace 1975; Easterling and Robinson 1985).

Spatial analysis of ADI standard deviation shows significant variability in the ADI (40-50 days), with (slightly) larger values (~50+) in the SGP compared to the NGP (~48; Fig. 2.7). This is expected, as the SGP is noted to have higher precipitation variability when compared to the NGP (Fig. 2.8; Weaver et al. 2016). The spatial pattern of variability in the date of maximum precipitation (Fig. 2.8a) depicts a pattern much like that of the overall ADI variability. These results demonstrate that the variability in the ADI is most likely due to the variability in the date of maximum precipitation more so than the date of the temperature maxima. This result mirrors what is seen in mean ADI, as the date of maximum precipitation appears to have more control on the climatological mean of ADI than the date of maximum daily temperature.

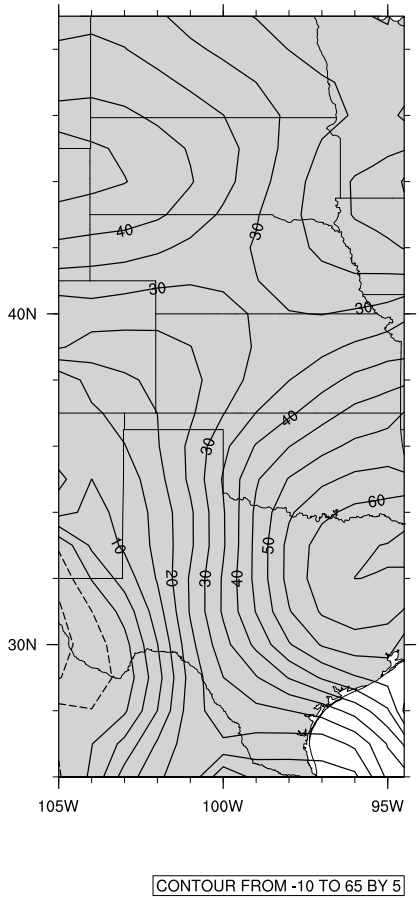

Figure 2.5: Mean ADI for the entire study period (1890-2015) from the GHCN dataset. Solid lines are for positive ADI and dashed lines represent negative ADI. Data was gridded using the Barnes Objective Analysis methodology in order to display smoother contours compared to contouring raw ADI at station level.

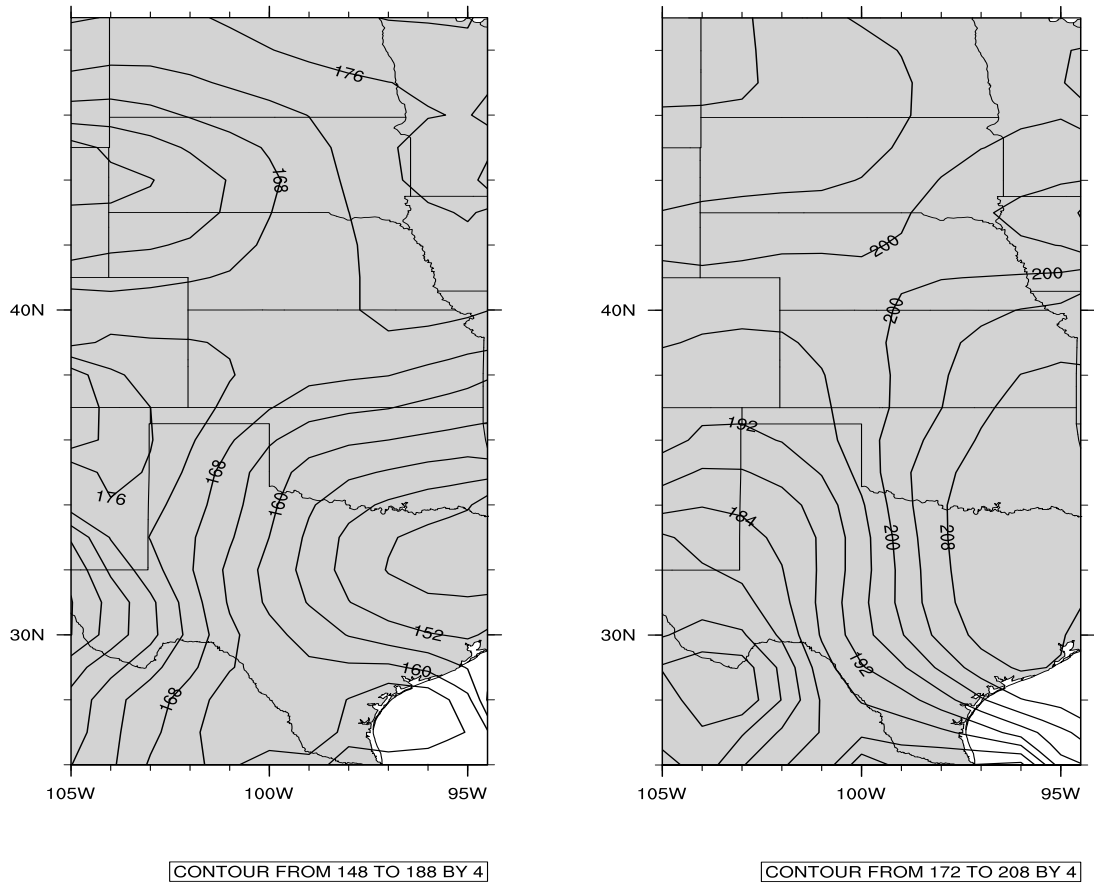

Figure 2.6: Same as figure 2.5, except for the date of maximum precipitation (a) and temperature (b)

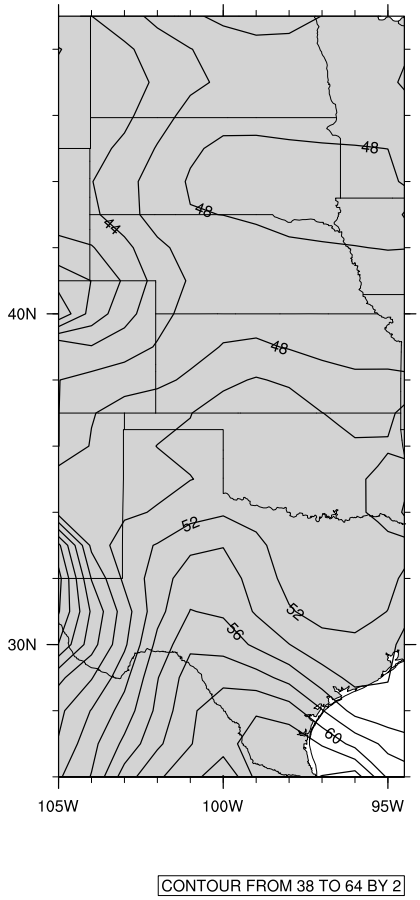

Figure 2.7: ADI standard deviation for the entire study period (1890-2015) from the GHCN dataset. Data was gridded using the Barnes Objective Analysis methodology in order to display smoother contours compared to contouring raw ADI at station level.

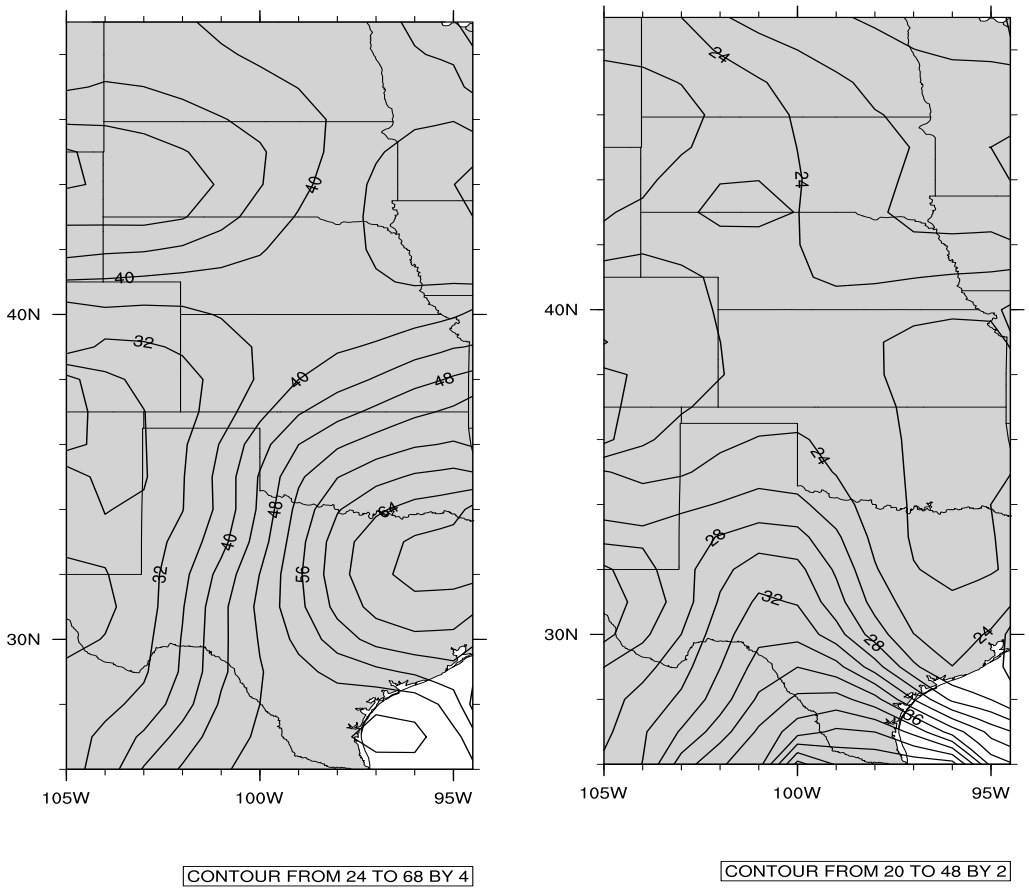

Figure 2.8: Same as figure 2.7, except for date of maximum precipitation (a) and temperature (b).

2.4.2 Temporal ADI Analysis

Histograms of all Daily (Fig. 2.9) and Weekly (Fig. 2.10) ADI values show a normal distribution around a positive value of ADI. This is expected, as climatologically within the period from March to August the temperature maximum occurs later than the precipitation maximum. Further, within the GP climate, it is difficult to get a precipitation and temperature maximum to occur on the same day, and few zero values of ADI were expected. However, a secondary peak in the negative range of ADI is not expected. To examine whether the valley in the zero values causes this to peak to exist as a function of the ADI itself (i.e., not a physical, real phenomenon) analysis of the average day/week of maximum temperature and precipitation is completed for each state (Table 2.1). Results demonstrate that the average date of maximum precipitation changes from approximately late May (positive ADI) to late July (negative ADI), an expected result given the MCS activity that occurs later in the warm season. However, the change of the average date of temperature maximum from late July (positive ADI) to late June (negative ADI) is not. Summertime temperature maxima over the GP is climatologically causes a strong mid-tropospheric ridge to develop over the region during the summer (Illston et al. 2004). Thus, a shift in the maximum temperature as systematic as shown via the negative ADI analysis does not have a simple explanation.

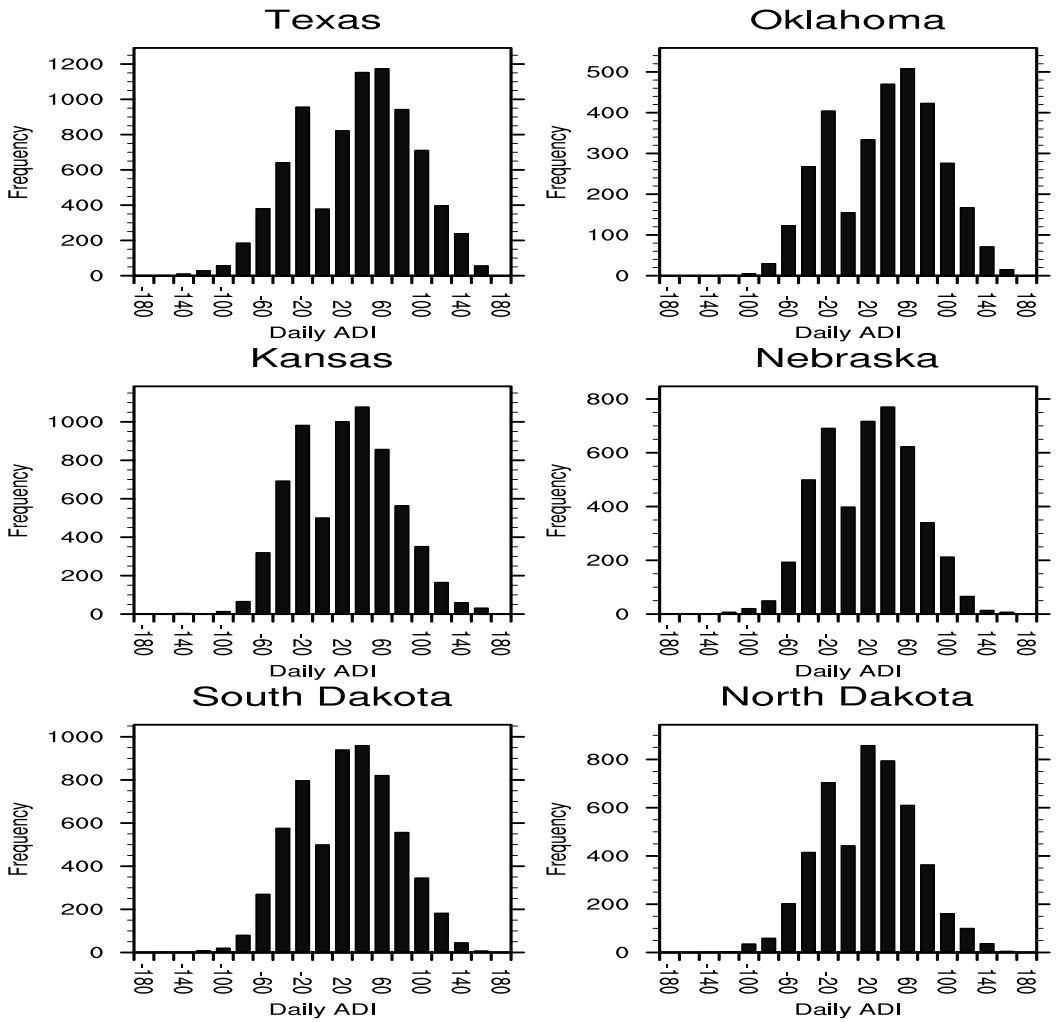

Figure 2.9: Histogram of Daily ADI values throughout the study period for each state.

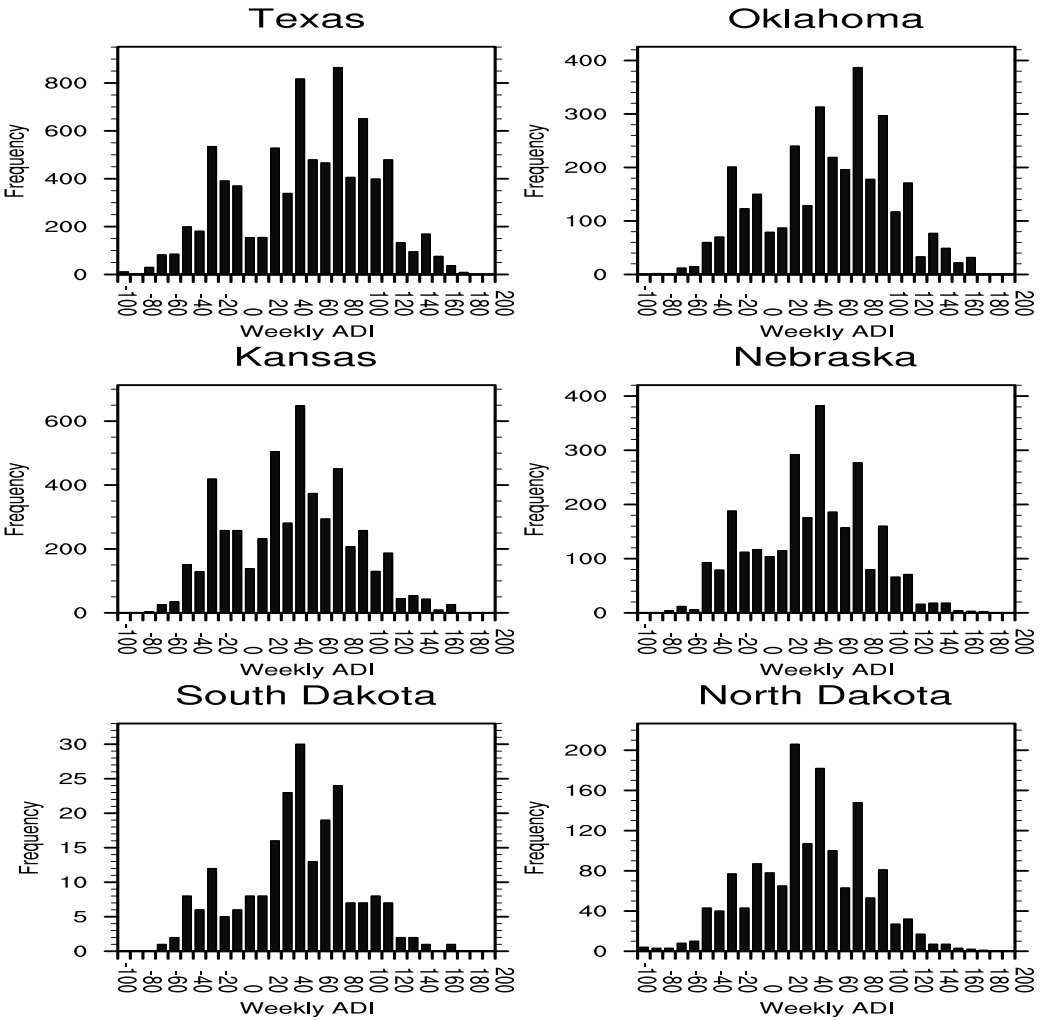

Figure 2.10: Same as figure 2.9, except for Weekly ADI.

Table 2.1: Average date of temperature and precipitation maxima, separated by state and for negative/positive ADI. The number of observations and the percent total are also shown.

Daily GHCN-Daily data		Temp.	Prec.	Number of obs.	Percent of total
Texas	Negative ADI	**177.66**	**209.03**	2261	27.80
	Positive ADI	**209.1**	**136.82**	5872	72.20
Oklahoma	Negative ADI	**192.16**	**216.8**	831	25.57
	Positive ADI	**211.91**	**140.66**	2419	74.43
Kansas	Negative ADI	**189.6**	**214.83**	2080	31.12
	Positive ADI	**208.5**	**149.6**	4604	68.88
Nebraska	Negative ADI	**184.84**	**210.54**	1460	31.71
	Positive ADI	**206.62**	**152.09**	3144	68.29
South Dakota	Negative ADI	**186.09**	**212.34**	1753	28.70
	Positive ADI	**209.52**	**150.67**	4354	71.30
North Dakota	Negative ADI	**186.03**	**211.53**	1420	29.65
	Positive ADI	**212.96**	**159.23**	3369	70.35
Weekly GHCN-Daily data		**Temp.**	**Prec.**	**Number of obs.**	**Percent of total**
Texas	Negative ADI	**18.76**	**22.54**	1888	23.18
	Positive ADI	**21.92**	**11.62**	6257	76.82
Oklahoma	Negative ADI	**19.51**	**22.8**	634	19.44
	Positive ADI	**21.91**	**11.86**	2627	80.56
Kansas	Negative ADI	**19.22**	**22.67**	1711	25.60
	Positive ADI	**21.61**	**13.17**	4973	74.40
Nebraska	Negative ADI	**18.85**	**22.31**	1005	21.83
	Positive ADI	**21.42**	**13.42**	3599	78.17
South Dakota	Negative ADI	**18.71**	**22.39**	1183	19.25
	Positive ADI	**21.64**	**13.13**	4963	80.75
North Dakota	Negative ADI	**18.19**	**22.14**	1093	22.75
	Positive ADI	**21.74**	**14.28**	3711	77.25

The bolded information is the average day (for daily method) or week (for weekly method) of the maximum of temp/prec. This was used to show the difference between the average date of each for negative ADI and positive ADI observations.

To determine the cause of this shift in maximum temperature within the two different ADI regimes, several features that influence surface temperatures over the GP were investigated. First, the influence of precipitation on ADI is investigated due to links between latent/sensible heat flux and surface moisture heterogeneities caused by precipitation (e.g., Berg et al. 2014; Seneviratne et al. 2010). Results from this analysis show no significant correlations between ADI and any of the precipitation totals computed from the station data. Next, correlations between noted teleconnection patterns that influence North American temperature patterns (Ropelewski and Halpert 1986) and the ADI are analyzed. For this study, the Pacific-North American Pattern (PNA), El Niño Southern Oscillation (ENSO), North American Oscillation (NAO), Pacific Decadal Oscillation (PDO) and the Atlantic Multidecadal Oscillation (AMO) are chosen. Using monthly ADI values derived from the monthly climate division GHCN dataset (nClimDiv) to compute correlations with these teleconnection patters, results from this analysis again showed little to no correlations between any of the teleconnection patterns and the ADI. Lastly, the role of the climatological 500 mb ridge that develops during the summer season (Illston et al. 2004; Bluestein 1993) over the GP was investigated. Using NOAA-CIRES 20th Century Reanalysis Version 2 (Compo et al. 2011) monthly average 500 mb geopotential heights are correlated with gridded yearly ADI (gridded using an iterative improvement type objective analysis within the NCAR Command Language (NCL)). Results from this analysis showed more utility in describing the causes of the differences between the positive and negative ADI regimes (correlations of ~0.3 with July 500mb heights), however no significant correlations were found during this analysis. Thus, no direct causation of the negative and positive ADI regimes could be found from the analysis performed within this study. Further investigation into this feature of the ADI is warranted

given the physical difference between the two regimes and the impacts they impart on the ecosystems of the GP.

2.4.3 Daily ADI

Statewide decadal mean values of Daily ADI (Fig. 2.11) reveal a number of results across the GP. Mean ADI values were positive and show a systematic difference (~30 to 45 days) between temperature and precipitation maxima throughout the historical record. Texas and Oklahoma have larger mean ADI values, which is expected as they show the earliest precipitation peak of the GP states. The other 4 states are considerably lower, with no mean ADI value analyzed above 50 compared to 60 for Texas and Oklahoma. However, this difference appears to be changing with time over the length of the observational record. Linear trend analysis shows that each state is incurring a trend on its decadal mean ADI. For example, Texas, Oklahoma and North Dakota are incurring positive trends. However, using 1890-1949 data as the population statistic for the t-test, only North Dakota is showing a statistically significant difference (90% confidence level). Conversely, Kansas, Nebraska and South Dakota yielded negative trends in ADI with Kansas and Nebraska showing a statistically significant difference (95% confidence level) using 1890-1949 as the population statistic for the t-test. Thus, from the Daily ADI analysis a significant shift in ADI is analyzed in Kansas, Nebraska and North Dakota using a Student's t-test for significance between the 1890-1949 and 1950-2015 periods. This is confirmed with the linear regression lines for each of the three states. The results for Oklahoma displays a linear regression line with a strong (~14 days) positive trend, however the t-test does not show that the two periods were significantly different. This is likely due to the pattern of high and low mean ADI values that are seen throughout

the time series, which would overwhelm the comparatively smaller signal of the overall increase for this statistical test.

Daily ADI variability analysis (Fig. 2.12) also show significant differences between the two periods. The average standard deviation of Daily ADI across the region ranges from approximately 40 to 55 days, with the southern portion of the domain having higher variability than the northern states. Linear increases are noted in Texas, South Dakota and North Dakota that were statistically significant (95% confidence level) with the other three states also having slight (<4 days) positive standard deviation trends. It is evident in analysis of the ADI standard deviation time series that after the 1940 decadal period an increasing trend can be seen in many states (Texas, Oklahoma, Nebraska, and North Dakota) even though a strong overall trend is not determined through the linear regression analysis. Thus, the analysis shows that ADI variability is increasing over the GP, with significant increases in three of the states at the 95% confidence level.

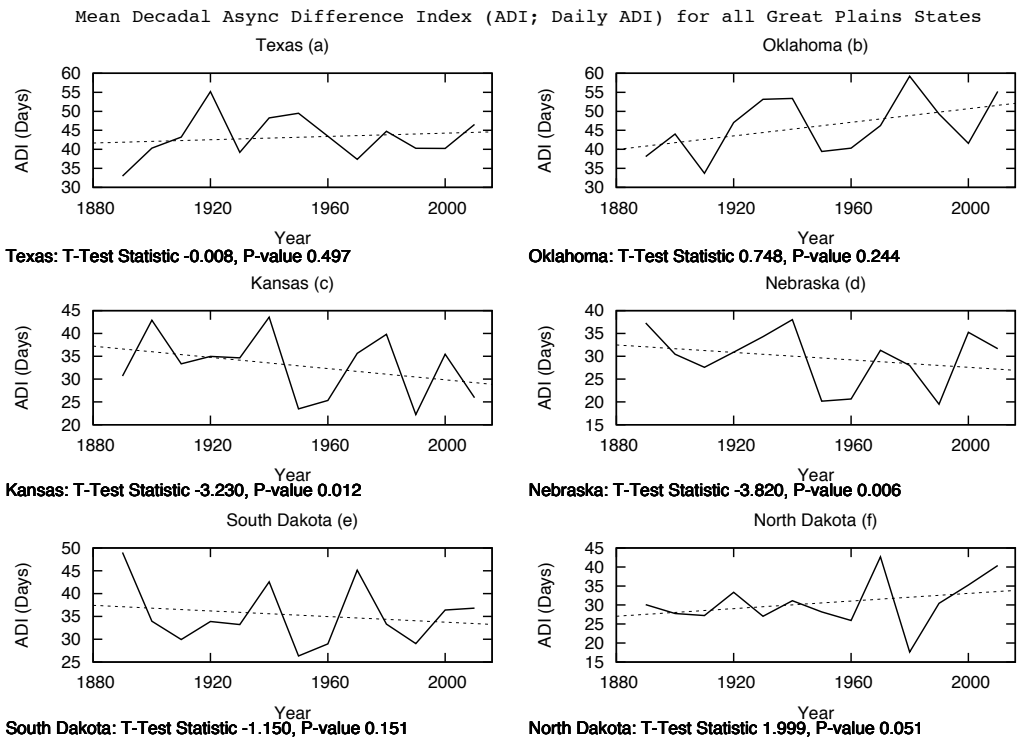

Figure 2.11: Decadal average Daily ADI for each state in the study domain. Solid line shows the decadal average, while the dashed line is the linear regression line created from the ADI data. Texas is plot (a), Oklahoma is plot (b), Kansas is plot (c), Nebraska is plot (d), South Dakota is plot (e) and North Dakota is plot (f).

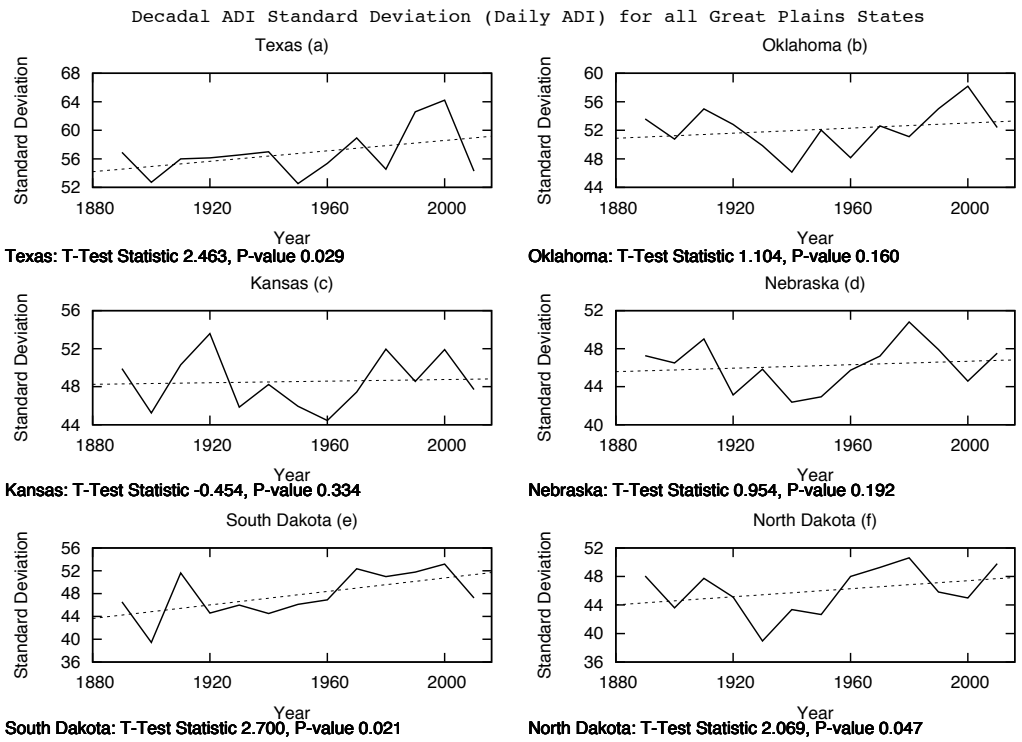

Figure 2.12: Same as figure 2.11, except for Daily ADI standard deviation.

2.4.4 Weekly ADI

Analysis of the Weekly ADI statewide decadal means (Fig. 2.13) shows similar results as Daily ADI. Weekly ADI continues to show systematic positive ADI of approximately 30-45 days throughout the dataset record. This shows that the methodology does not affect the overall results of obtaining a climatologically positive ADI, but the actual value of ADI in the Weekly ADI analysis is higher when compared to Daily ADI for the same state. Thus, the change of methodology does not change the overall nature of ADI, but it changes the decadal mean magnitudes, which affected the linear trends. Near zero trends in Texas, Nebraska and South Dakota are seen with stronger trends in Oklahoma, Kansas and North Dakota. The negative trend in Kansas is slightly higher in the Weekly ADI results (~8 day increase) compared to the Daily ADI (~7 day increase), with the trend in North Dakota showing a similar change (Weekly ADI ~10 day increase, Daily ADI ~7 day increase). The trend in Oklahoma, however, shows a slightly weaker increase in the Weekly ADI (~8 day increase) compared to the Daily ADI (~13 day increase). At the same time, the statistical significance did change. Kansas and North Dakota still reveals significant differences between the two-subset periods, however Nebraska no longer showed statistically significant results. This implies that the methodology (Daily ADI) likely results in the statistical significance for Nebraska rather than the results seen in the Daily ADI analysis being a physically meaningful result.

`

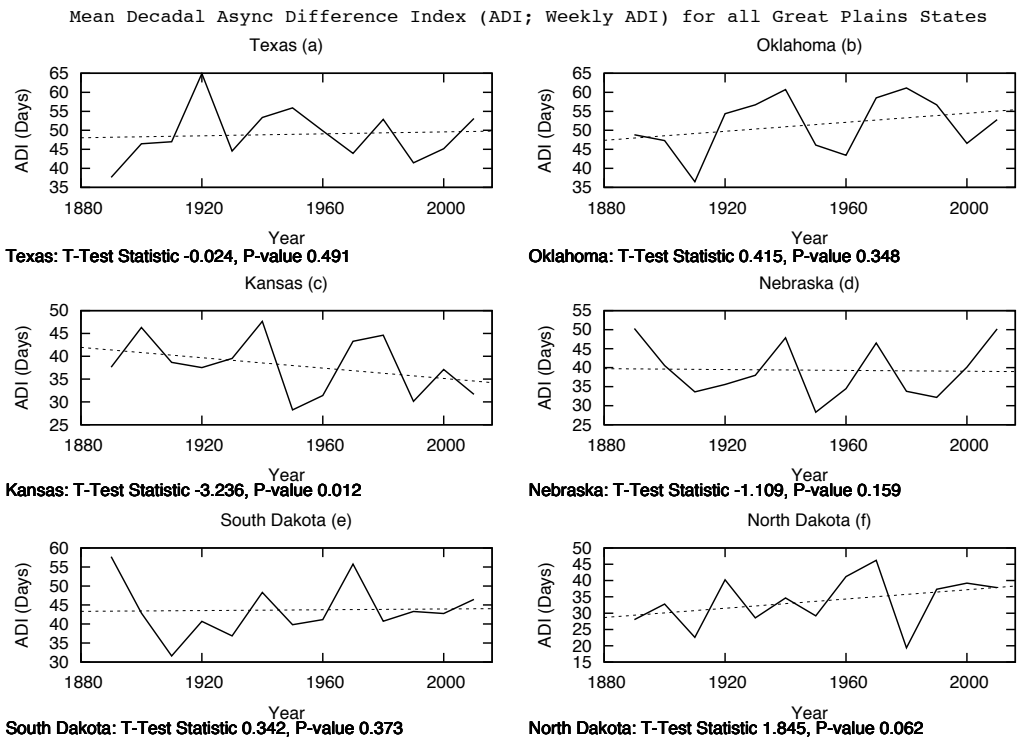

Figure 2.13: Same as figure 2.11, except for Weekly ADI decadal averages.

Variability in the Weekly ADI (Fig. 2.14) shows similar features to the Daily ADI as well, however with a decreased magnitude owing to the averaging of the daily data. The average value of variability in the region was approximately 40 to 50 days, with a majority of the values in the 40s. Further, the trends align with the Daily ADI variability, with Nebraska being the main difference. In the Daily ADI analysis, Nebraska yields a non-statistically significant increase in variability. However, with the Weekly ADI analysis, it shows a decreasing trend in variability, showing that no trend in ADI variability is occurring within Nebraska. Further, the five other states show very similar signals as the Daily ADI analysis whereby increasing trends are observed in all five states, with South and North Dakota being statistically significant at the 95% level (note - Texas, Oklahoma and Kansas were statistically significant at the 85% confidence level). The difference in these five states is Kansas, which analyzed the Weekly ADI analysis to have a much stronger (~ 7 day) increasing trend compared to the Daily ADI (~1 day increase) variability analysis. The other four states have close to the same trend in variability (~same number of day increases), compared to the Daily ADI analysis, from 1890 to 2015 analyzed through a linear regression analysis.

`

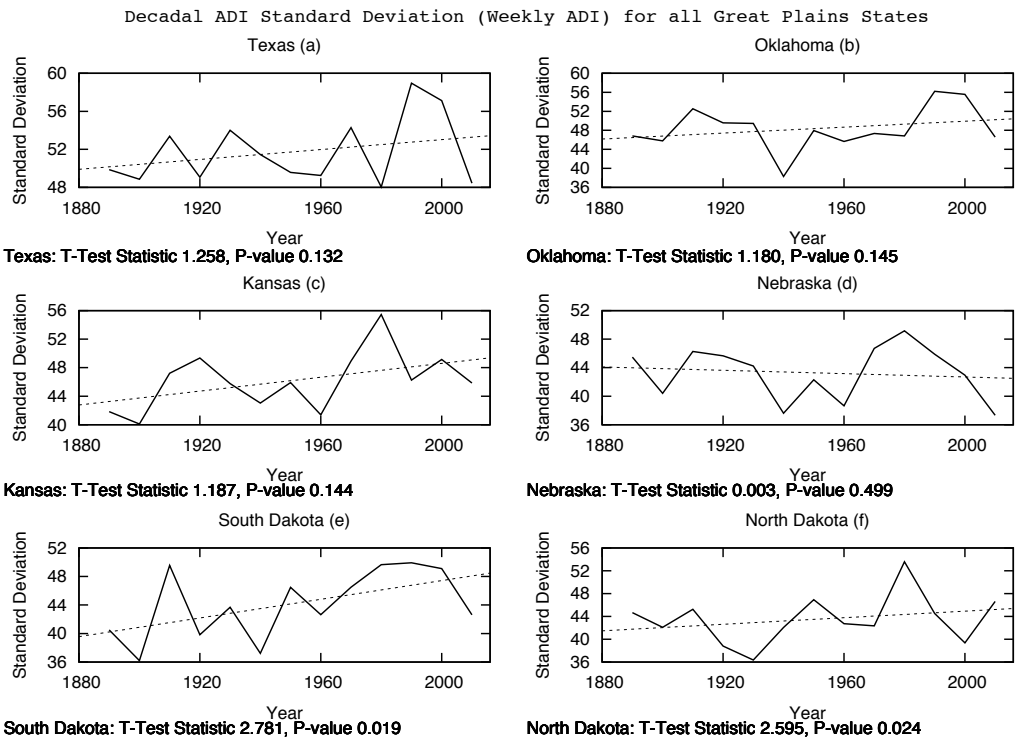

Figure 2.14: Same as Figure 2.11, except for Weekly ADI standard deviation.

2.5 Discussion

The goal of this study was to analyze the long-term trends in the AS between the date of maximum temperature and precipitation (Fig. 2.4) across the GP. To accomplish this task, long-term data gathered from the GHCN-Daily database for maximum temperature and precipitation was utilized and an Asynchronous Difference Index (ADI) was developed by computing the day of each relevant maxima and further computing the temporal span between the date of maximum temperature and precipitation. This was also completed for the week of maximum by averaging the data into weekly values and determining the week of each maximum before computing the difference between the weeks of each maximum. These ADI values were then averaged into decadal means, and multiple statistical analyses were utilized in the analysis.

Overall, the results show that ADI is changing throughout the 1890 to 2015 period for various states in the GP. Daily (Fig. 2.11) and Weekly (Fig. 2.13) ADI analyses yielded a statistically significant decreasing trend in Kansas (95% confidence level for both analyses) with a statistically significant increase in North Dakota (90% confidence level for both analyses). Trends in other states show significance for one analysis or the other, with Nebraska showing a significant decrease (95% confidence level) in the Daily ADI analysis, but not the Weekly analysis. Linear regression analysis on the Oklahoma data shows a strong increasing trend in both ADI analyses, however significance testing on the difference between the 1890-1949 and 1950-2015 periods show no statistically significant difference. This is likely because of the variable pattern exhibited within both the Daily and Weekly ADI decadal means, which caused the overall mean of both decades (the test statistics for the student's t-test) to be similar even though an overall increasing trend is seen.

Analysis of ADI standard deviation shows an increasing trend (linear regression lines) for both analyses and most states (Figs. 2.12 and 2.14). The only state to not show an increasing linear trend was Nebraska for the Weekly ADI analysis, which resulted in a slight decreasing trend. Statistical significance (95% confidence level) was seen in both analyses for South and North Dakota, with the Daily ADI analysis showing a significant increase in variability for Texas (95% confidence level). Although statistical significance may not have been noted, a difference was seen between the prior to 1950 and after 1950 decadal variability for several states. It appears as though a relative minimum in ADI variability occurred in the 1940's and then it increased from the 1950's onward in the central and southern Great Plain states (Texas, Oklahoma, Kansas and Nebraska). This result was observed in both ADI analyses.

Determining the drivers of the trends seen in ADI is difficult as the timing of maxima during a particular season is rarely studied. However, an analysis into which variable (temperature or precipitation) is driving the changes in ADI can be completed within the purview of this study. Daily analysis showing the decadal average day of maximum temperature (Fig. 2.15) and precipitation (Fig. 2.16) for Oklahoma, Kansas, Nebraska and North Dakota (states with notable linear trends or significant differences between periods) demonstrated that changes in the date of maximum temperature are the likely cause of the shift in ADI for North Dakota and Nebraska while a shift in the date of maximum precipitation being the cause for Oklahoma. The Kansas analysis displayed statistically significant differences (90% confidence level or above) for both the date of maximum temperature and precipitation. Weekly analysis of decadal average day of maximum temperature (Fig. 2.17) and precipitation (Fig. 2.18) demonstrated that only the trend in ADI for Oklahoma can be partially attributed to shifts in the date of maximum precipitation (90% confidence level) with Kansas and Oklahoma both yielding significant shifts (95% confidence

level) in their date of maximum temperature. Because all of these shifts in the date of maximum temperature and precipitation impact the decadal mean ADI, a positive shift in ADI represents either a positive shift in temperature, a negative shift in precipitation or both. Conversely, a negative shift in ADI reflects either a positive shift in precipitation, a negative shift in temperature or both. Overall, the shifts in the date of the occurrence of March to August maximum temperature show more significance in regards to the overall shifts in the ADI for both methodologies. However, it is important to note that using the Students t-test for this data may introduce errors, but because simple bootstrap significant tests showed similar results as those detailed above, the same methodology was used for all analyses in the study.

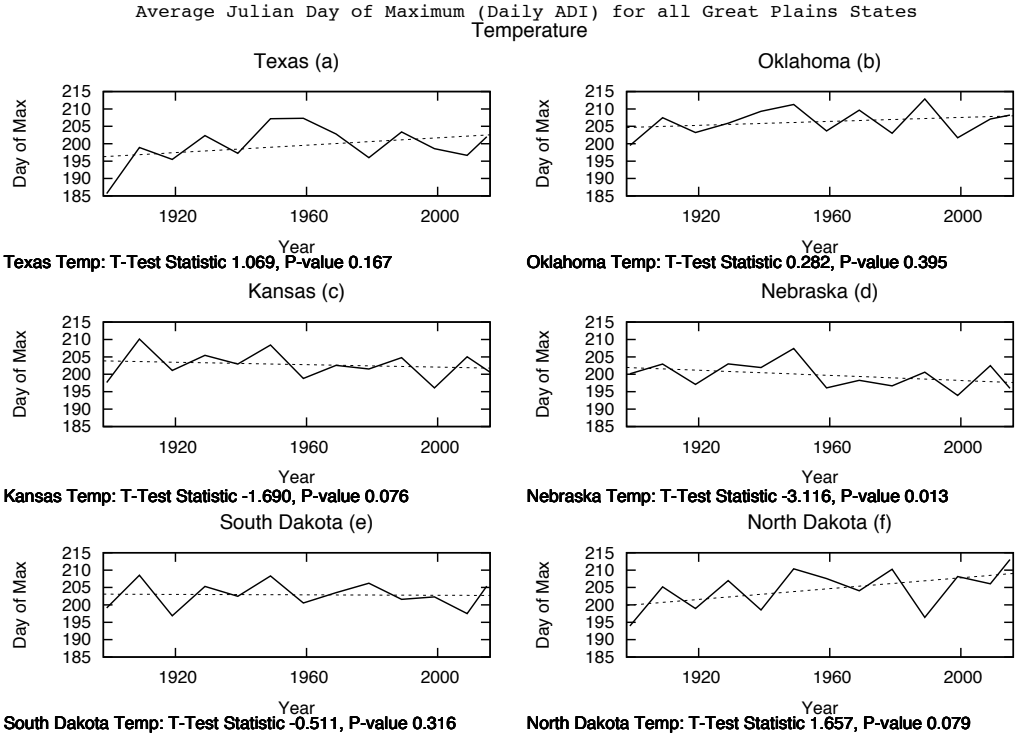

Figure 2.15: Decadal average date of maximum temperature for Daily ADI method. Solid line is the decadal average and the dashed line is a linear regression line created from the decadal average data.

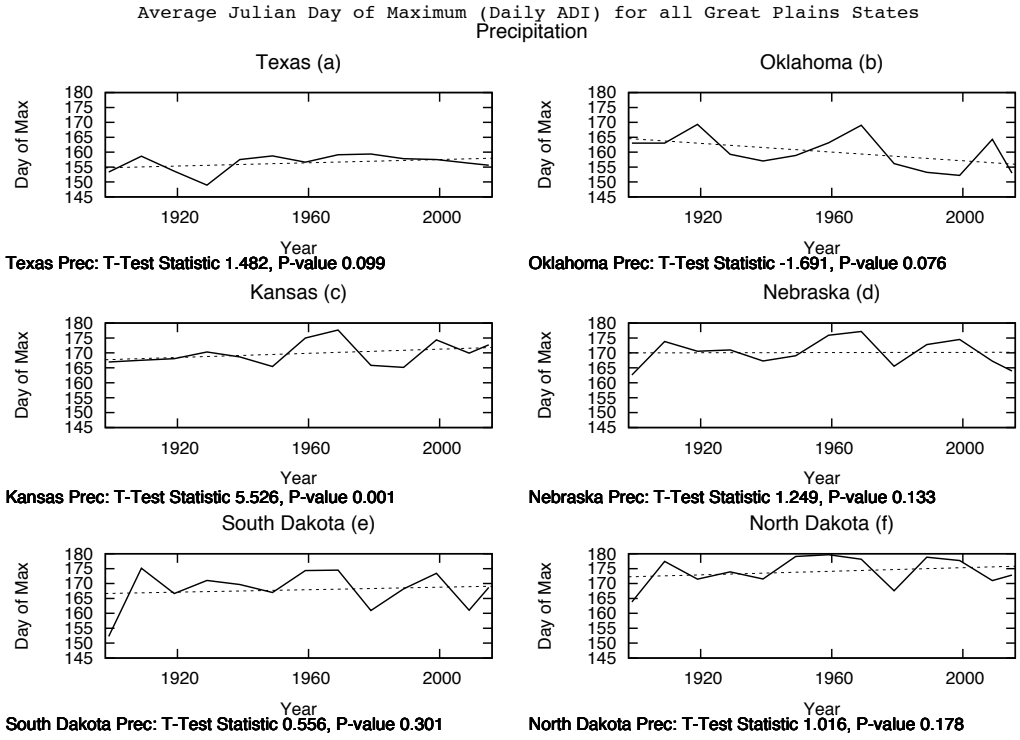

Figure 2.16: Same as figure 2.15, except for precipitation.

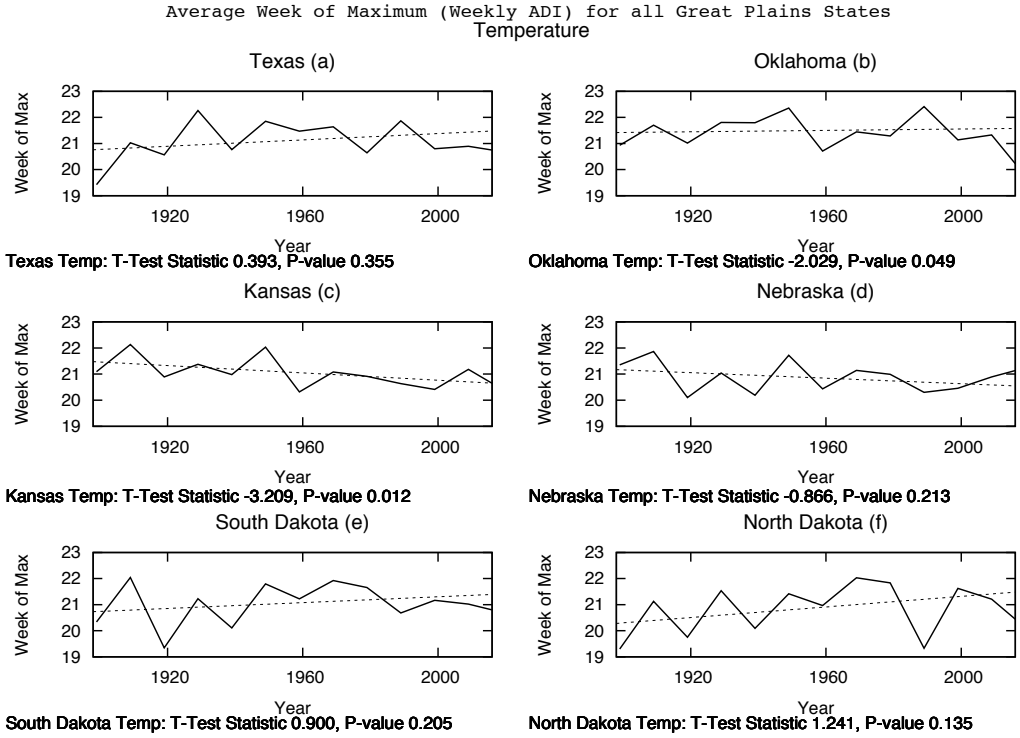

Figure 2.17: Same as figure 2.15, except for Weekly ADI method.

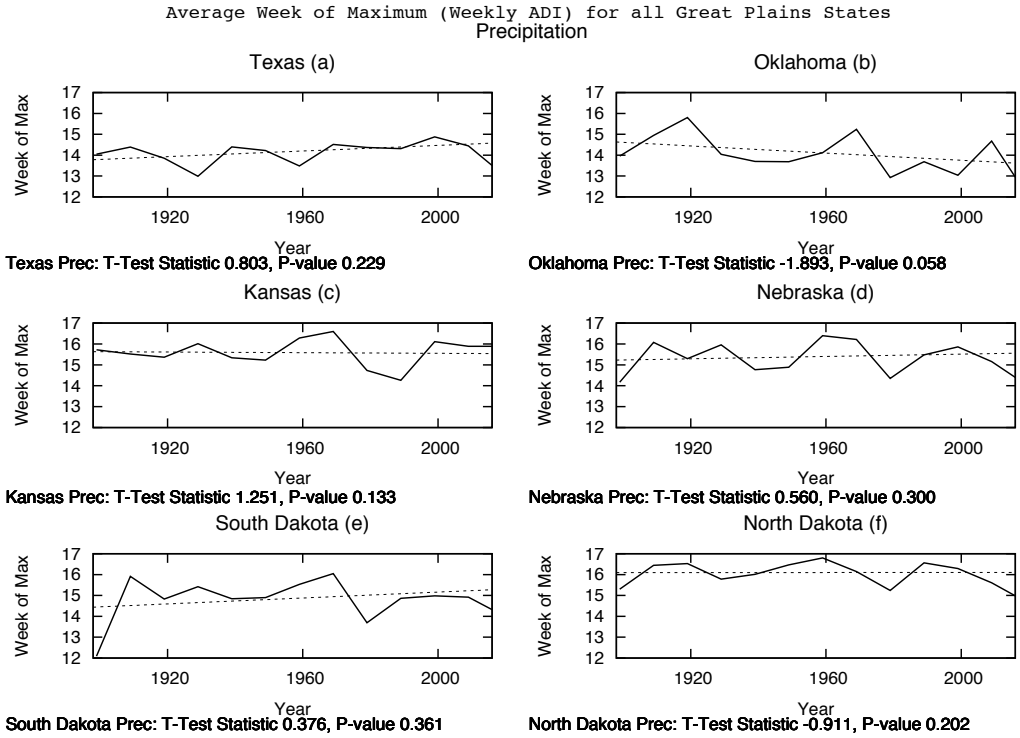

Figure 2.18: Same as figure 2.15, except for Weekly ADI method precipitation.

Chapter 3

Primary Atmospheric Drivers of Pluvial Years in the United States Great Plains

(Flanagan et al. 2018a)

3.1 Introduction

With the noted shifts in the climate over the GP seen in Chapter 2, being able to physically explain the causes behind these shifts is important, While the changes in temperature are likely linked to shifts in the global climate regime, changes in the timing of precipitation is harder to understand, yet crucial as precipitation is a critical asset for extensive agriculture across the Great Plains (GP) of the United States (Fisher et al. 2007). The GP of the United States (herein defined as the states of Texas, Oklahoma, Kansas, Nebraska, South Dakota and North Dakota) possess a unique precipitation climatology in that the climatological maxima of rainfall and temperature are asynchronous and occur at different times of the plant growing season (Chapter 2). Thus, if a precipitation deficit occurs during the time of year in which temperatures are climatologically at their maximum, the water stress on crops and the surface is dramatically increased. While irrigation can offset the impact of this water stress, conditions that bring about precipitation deficits typically cause abnormal temperature patterns and further crop damage can still occur (e.g., Wilhite 2000; Wilhelmi and Wilhite 2002; Hoerling et al. 2014; Yin et al. 2014; Livneh and Hoerling 2016). Thus, precipitation deficits and excesses are critically important for the GP.

The GP is also a region of high precipitation variability across multiple spatial and temporal scales (e.g., Ting and Wang 1997; Ruiz-Barradas and Nigam 2005). Droughts occur with enough frequency that numerous studies have investigated the drivers of such events within the GP region (Basara et al. 2013). A majority of these studies focused on the connections between various sea

surface temperature (SST) patterns and their influence on anomalous synoptic flow patterns and consequently GP precipitation (e.g., Trenberth and Branstator 1992; Schubert et al. 2004; Seager et al. 2005; Cook et al. 2008; Seager and Hoerling 2014). Aside from SST patterns, other forcing mechanisms contributing to drought in the GP region include internal atmospheric variability (Seager et al. 2014) and land-atmosphere coupling (Mo et al. 1997; Koster et al. 2000; Schubert et al. 2004).

Conversely, periods of enhanced precipitation (i.e., pluvials) have been less examined despite similar (or even worse) negative socioeconomic impacts of such events such as mismanagement of water resources (Cook et al. 2011; Pederson et al. 2013), increased risk of floods or increased flood intensity (Pal and Eltahir 2002; Illston et al. 2004) and increased risk of wildfire in later years through buildup of biomass during the pluvial year (Westerling et al. 2003, 2006). Yet, to gain a full understanding of precipitation variability across the GP, both pluvial and drought periods must be examined and quantified. Most investigations into pluvial periods have assumed that they are driven by conditions opposite that of drought and thus focused on the influence of global SSTs on synoptic flow patterns similar to drought events (Yang et al. 2007; Hu and Huang 2009; Schubert et al. 2009; Cook et al. 2011). Hu and Huang (2009) found that GP precipitation anomalies are modified when phase alignment occurred between the Pacific Decadal Oscillation (PDO) and El Niño-Southern Oscillation (ENSO). Conversely, Cook et al. (2011) determined that tropical Pacific SST anomalies had little explanatory power during the central and western United States 1905-1917 pluvial period and instead attributed the pluvial period to internal atmospheric variability. Moreover, Mo et al. (1997) illustrated the non-linearity in the associated precursor patterns associated with pluvial and drought events over the GP during the summertime. They found that differences in eddy activity and subsequent moisture transport over the GP was

key to the pluvial event. Trenberth and Guillemot (1996) found that differences in the North Pacific jet stream, eddy activity along the Pacific-North American storm track and moisture transport into the GP were the key differences between the 1993 floods and 1988 drought over the central United States. These past studies on pluvial events have focused primarily on single events, and a more comprehensive analysis of many events spanning multiple decades remains to be done.

An objective of this study is to use long-period (i.e., spanning the 20th and 21st centuries) climatological reanalysis datasets to examine past pluvial periods in the GP of the United States and describe qualitatively and quantitatively the primary atmospheric drivers of such events. Along with filling a gap in the climate literature, this work will also contribute to emerging studies on the changing nature of GP precipitation both in the recent past (e.g., Christian et al. 2015 Weaver et al. 2016) and under future climate change (e.g., Rosenzweig et al. 2001; Dore 2005; Wuebbles et al. 2014).

3.2 Data and Methods

3.2.1 Datasets

Long-term datasets are required for a comprehensive analysis of GP precipitation and relevant atmospheric variables. Precipitation data are from the Parameter-elevation Regressions on Independent Slopes Model (PRISM; Daly et al. 2000), which provides monthly precipitation from 1895 to present on a 4 km horizontal resolution. For atmospheric variables, I first consider two monthly reanalysis products: the National Oceanic and Atmospheric Administration-Cooperative Institute for Research in Environmental Research (NOAA-CIRES) 20th Century Reanalysis (20CR; Compo et al. 2011) and the European Center for Medium-Range Weather Forecasts (ECMWF) 20th Century Reanalysis (ERA-20C; Poli et al. 2016). Among these two

reanalysis products, the ERA-20C dataset better reproduces the observed annual climatology of precipitation over the GP as depicted by PRISM (Figure 3.1). In addition, ERA-20C produces a larger dataset of pluvial years for each composite compared to 20CR, especially when the Northern Great Plains (NGP; i.e., North Dakota, South Dakota, and Nebraska) and Southern Great Plains (SGP; i.e., Kansas, Oklahoma, and Texas) sub-regions are considered, which provides a more robust subset of the data to calculate the composite atmospheric fields. Thus, the 2°x 2° ERA-20C reanalysis dataset is selected to produce composites of atmospheric variables for this study and provides global coverage of all relevant atmospheric variables from 1926-2010 at various spatial resolutions, as precipitation data from ERA-20C is poor before 1926 (Poli et al. 2016). Mirroring previous pluvial studies, the analysis focuses on 500 mb geopotential heights and 250 mb *u* and *v* wind components to identify specific atmospheric patterns found within pluvial years in the NGP and SGP. Anomalies of these fields are derived by removing the mean of the 1926-2010 period. The inclusion of the NCEP-NCAR version 2 reanalysis (NCEP; Kalnay et al. 1996), 20CR and the Japanese 55-year Reanalysis (JRA55; Onogi et al. 2007) serves to test the robustness of the results. All datasets are bilinearly interpolated to the same 2° x 2° grid as ERA-20C for direct comparisons of the results.

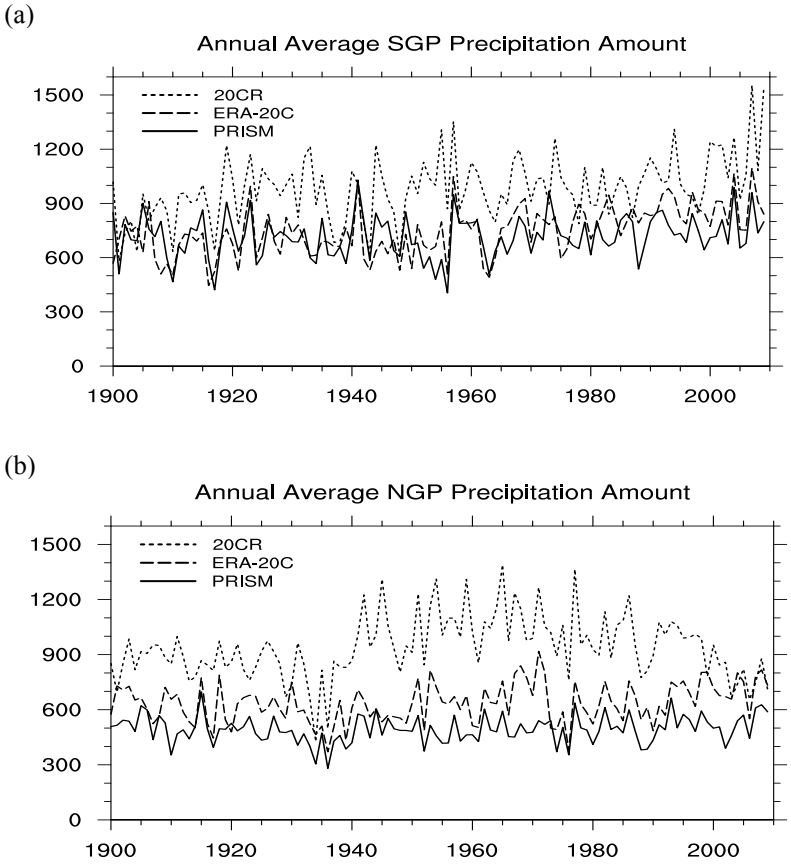

Figure 3.1: The annual grid point average of the (a) SGP and (b) NGP precipitation amount from PRISM (solid line), ERA-20C (long-dashed line) and 20CR (short-dashed line) datasets. The correlation between PRISM and ERA-20C in the SGP is 0.56 and 0.47 for 20CR. For the NGP, the correlation between PRISM and ERA-20C is 0.62 and for 20CR it is 0.38.

3.2.2 Definition of Pluvial Periods

To determine GP pluvial events, the GP was divided into two sub-regions – the NGP and the SGP. This division is completed because of distinct differences in precipitation variability

between the SGP and NGP (Figure 3.2; e.g., Christian et al. 2015; Weaver et al. 2016). Variability in the SGP is larger than that seen in the NGP, with a positive precipitation trend visible in ERA-20C more so than with PRISM (Fig. 3.2). For the NGP, both datasets have comparable trends and variance. Moreover, precipitation amounts are significantly higher for the SGP than the NGP, meaning that studying pluvial events for the entire GP would be unduly biased by SGP variability and totals. Therefore, pluvial events and their drivers in these two specific regions were examined separately.

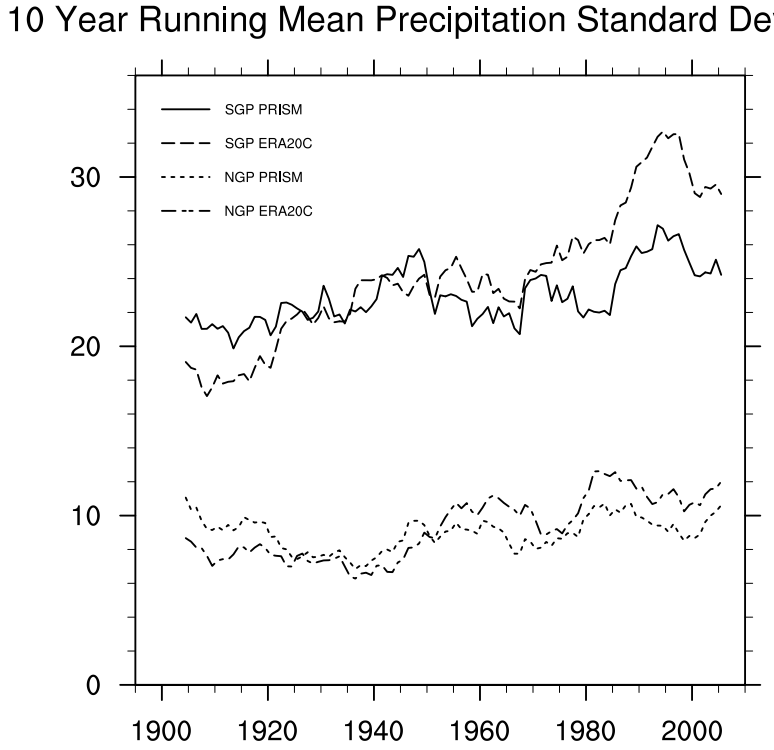

Figure 3.2: 10 year running mean standard deviation for the PRISM and ERA-20C datasets. The solid (PRISM) and long dashed (ERA20C) lines represent the SGP and the short dashed (PRISM) and long/short dashed line (ERA-20C) represent the NGP. Units are in precipitation (mm month^{-1}) standard deviation.

`

Next, a pluvial year for each sub-region is identified if the calendar-year total precipitation is 10% greater than the climatological annual total precipitation in that sub-region, i.e.,

$$\frac{P_x}{P_y} \geq 1.1 \qquad \text{(Eqn. 3.1)}$$

where P_x is the total annual precipitation amount of the given year and P_y is the average annual total precipitation from all (1926-2010) years. This definition is applied to all precipitation datasets, and a list of all identified pluvial years is found in Appendix 1, only years meeting the criterion in both PRISM and reanalysis products are used for composites analysis (Table 3.1). Sensitivity tests to other thresholds (e.g., 15%) yielded qualitatively similar results to those presented in this study (not shown).

Table 3.1 List of years for each composite category that were defined as pluvial within the study for the ERA-20C dataset.

	SGP	NGP
Total	1926, 1941, 1957, 1968, 1974, 1979, 1987, 1990, 1991, 1992, 1997, 2002, 2004, 2007, 2009	1941, 1951, 1962, 1965, 1977, 1982, 1986, 1993, 1995, 1998, 2005, 2007, 2008, 2009, 2010
Pattern	1926, 1941, 1987, 1991, 1992, 1997, 2002, 2004	1951, 1982, 1998, 2008, 2010
Break	1926, 1941, 1957, 1959, 1961, 1968, 1974, 1979, 1992, 1997, 2004, 2007	1941, 1951, 1962, 1965, 1971, 1977, 1982, 1986, 1993, 1995, 1998, 2005, 2007, 2008, 2010

Daily ERA-20C precipitation totals (i.e., accumulations from initialization 0600 UTC until 0000 UTC) and atmospheric fields (i.e., geopotential height, zonal (u) and meridional (v) winds, and specific humidity (q)) taken at 0000 UTC were analyzed to determine the drivers of significant

precipitation events during pluvial years. The 0000 UTC atmospheric fields are used rather than a daily-mean for comparison with actual soundings (not shown). Due to the non-normality of daily precipitation values, the 95th percentile of all precipitation events during pluvial years was used for defining a daily heavy precipitation event in each region. This methodology identified 275 events for the SGP and 274 events for the NGP.

3.2.3 Statistical Methods

To facilitate the statistical analysis of the identified pluvial years for each region, composites were created using three primary atmospheric variables from ERA-20C: the 500 mb eddy geopotential height (EGH; i.e., removal of the zonal mean from the geopotential height field), *u*, and *v*. The EGH anomaly field represents the transient zonal inhomogeneities which distinguishes wave features from the zonal-mean flow pattern (e.g., Randall 2014). Thus, EGH is a tool used to discern, separate, and analyze synoptic patterns that are responsible for weather events.

Several types of composites were explored. First, *Total* composites were defined as those composites resulting from using *all* pluvial years. However, such composite maps inherently hold a couple of limitations and caveats. The composites may be unduly influenced by a small subset of extreme events within the total population and, owing to the impacts of climate change, both the mean and variance of GP precipitation have changed over the 20th century (e.g., Fig. 3.1) introducing non-stationarity concerns into the data record. To address these issues, two additional composites were employed in this study:

- *Pattern* Composites: These composites were created by selecting specific pluvial years that have spatial *atmospheric* patterns that closely match the spatial pattern in the *Total*

composite (i.e., the "pattern" matches). To choose these specific pluvial years, an index of the *EGH anomaly field* was computed by projecting the EGH anomaly field for each year onto that obtained from the *Total* composite analysis. This index was computed for the two sub-regions in the study (10-50°N, 230-270°W for the SGP; 30-50°N, 230-270°W for the NGP). The EGH anomaly field was specifically chosen rather than the precipitation field itself because of the focus on atmospheric drivers responsible for pluvial years, not the specific precipitation spatial pattern. Years when the EGH anomaly index exceeded 0.5σ were designated *Pattern* years and subsequently used for the *Pattern* composites. Using this methodology, 8 (5) pluvial years were used for the *Pattern* composites in the SGP (NGP) region. Additionally, 19 (17) non-pluvial years also featured EGH anomaly years that matched the atmospheric forcing patterns in the SGP (NGP). As such, the *Pattern* compositing method highlights those years that influence strongly the *Total* composite results along with identifying other years that deviate from the *Total* composites.

- *Break* Composites: To examine the influence of nonstationarity on my results, the annual precipitation record was split into two distinct periods. The break point was objectively found by identifying the longest period (in years) where the standard deviations between the two were statistically significantly different ($p < 0.05$). Then, new means were computed for each of the two periods. These means form the basis for defining pluvial years in each *Break* period from (1). The *Break* pluvial years then form the basis for the *Break* composites of the atmospheric fields.

Figure 3.3 provides a flow diagram detailing the construction of these composite fields.

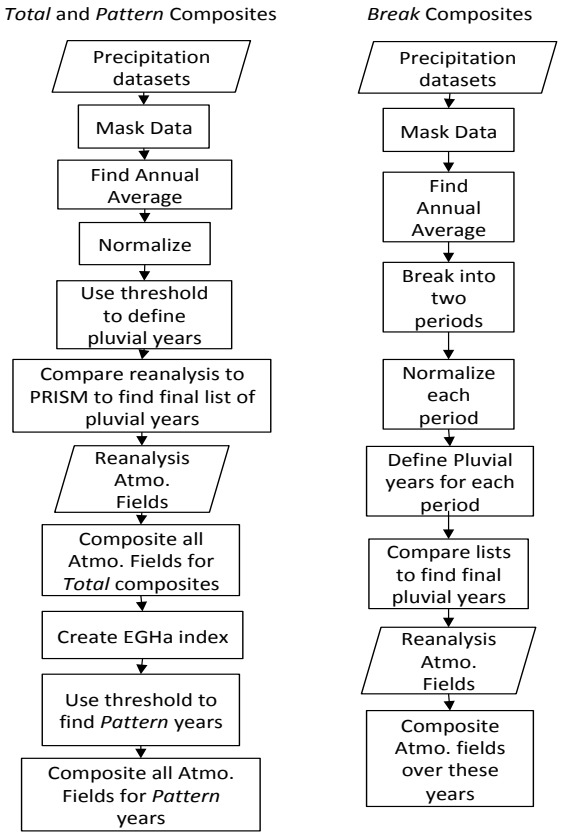

Composites for the heavy precipitation event analysis were created by averaging the 0000 UTC atmospheric fields over all days within pluvial years in which the daily precipitation amount crossed the 95th percentile. For the heavy precipitation event analyses, moisture fluxes (i.e., $u'q'$ and $v'q'$, where the prime notation indicates deviations from the time mean) were analyzed. This additional metric was included to identify both source regions of moisture for the heavy precipitation events and the actual transport path. Furthermore, the moisture fluxes complement the EGH anomaly spatial patterns by explicitly showing how the synoptic-scale waves depicted in the EGH anomaly fields contribute to the heavy precipitation events.

`

Significance testing of all composites was completed by taking 1000 random samples of the composited field (by grid point), with the same number of years as the composite and deriving 1000 resultant composites. The resulting 1000 bootstrapped composites were then used to define the two-tailed significance 90% threshold (e.g., Grotjahn and Faure, 2008; Klingaman et al. 2008; Guo et al. 2017; Seo et al. 2017; Bukovsky et al. 2017) used to determine if the composite-mean value of the field at a specific grid point (chosen for pluvial analysis) is significantly different from choosing values at random. Because of the relatively small sample size of pluvial years, particularly for the *Pattern* composites, the 90% significance threshold was used for all significance testing.

3.3 Results

3.3.1 Southern Great Plains Pluvial Analysis

The initial step in understanding the primary drivers of GP pluvial years was understanding the synoptic- and larger-scale pattern that drives the excess precipitation. Here, "synoptic" refers to the spatial scale of the atmospheric fields and patterns studied – that is, structures and phenomena that are at least 1000 km in scale (i.e., the size of extratropical cyclones). The *Total* SGP EGH anomaly composites (Fig. 3.4a) depict a Rossby wave pattern over North America, with negative anomalies centered over the southwestern portion of the United States and south of Greenland with an area of positive anomalies over the northeastern United States. To better diagnose these patterns, years in which the 500 mb EGH anomaly field matched the *Total* composite anomaly height field across the SW portion of North America are also investigated. The *Pattern* composite (Fig. 3.4c) depicts a stronger negative anomaly signal occurs in the SW extending further to the northwest over the North Pacific Ocean. To further diagnose the

`

differences in the wave structure for the *Pattern* years, the *v* (Fig. 3.5) and *u* (Fig. 3.6) anomaly fields were investigated. The 250 mb *v* wind component anomaly *Pattern* composite (Fig. 5a) exhibits a series of statistically-significant (denoted by stippling in Fig. 3.5) couplets across Asia and North America, representing synoptic-scale waves, as synoptic wave patterns cause the flow to become anomalously meridional on their peripheries. The 250 mb *u* wind component anomaly *Pattern* composites (Fig. 3.6a) depict a southward displacement of the North Pacific jet during those years, with the center of the positive anomalies starting over eastern central Asia and stretching across the Pacific and negative anomalies to the north. This southward displacement of the jet facilitates more wave activity further southward than climatologically normal, increasing the chances for heavy rainfall over the southern United States (Figs. 3.4a and 3.4c).

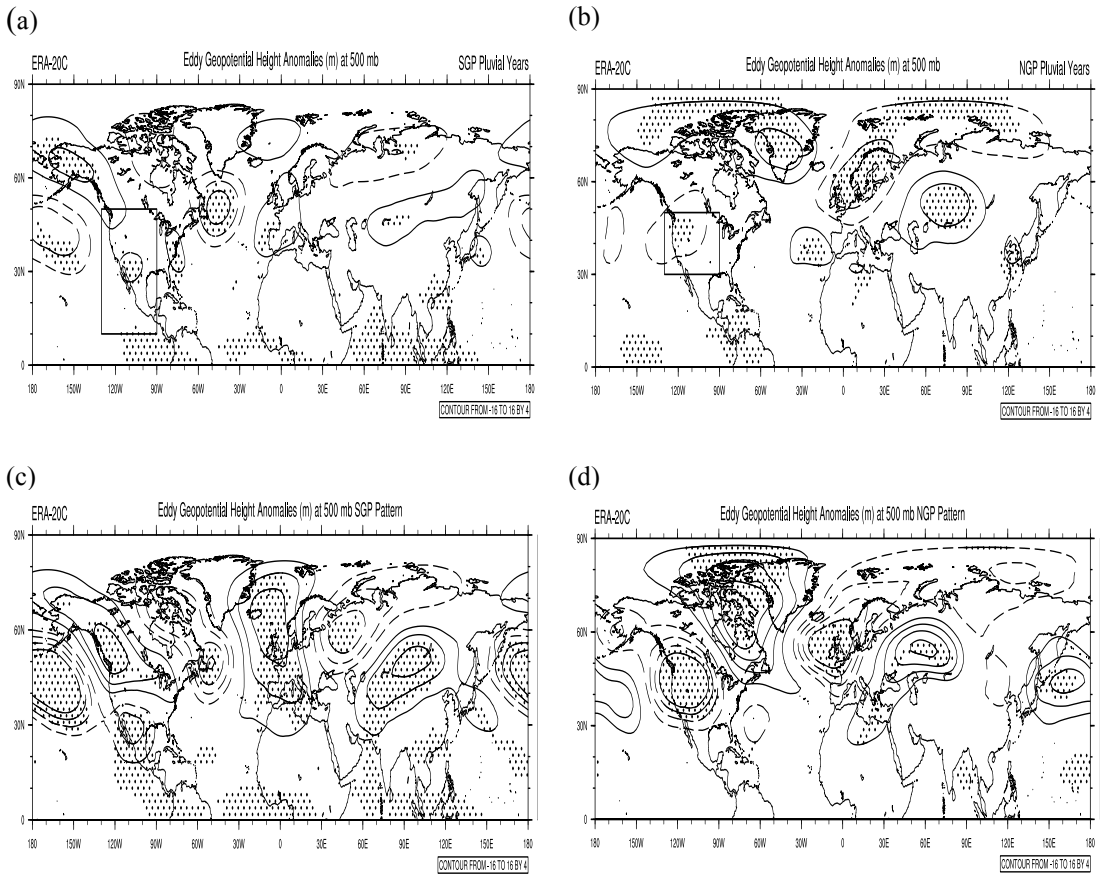

Figure 3.4: The (a), (b) *Total* (all *Total* pluvial years) and (c), (d) *Pattern* (*Pattern* pluvial years) composites for the (a), (c) SGP and (b), (d) NGP. Contours are plotted from 16 to -16 meters in intervals of 4 meters without the 0 meter contour. Statistically significant values at the 90% level are stippled. Negative contours are dashed and solid contours represent positive values. The boxed regions in (a) and (b) represent the areas used to create the eddy geopotential height anomaly index noted in Fig. 3.3.

3.3.2 Northern Great Plains Pluvial Analysis

Similar to the SGP analysis, the NGP investigation into the primary atmospheric patterns for NGP pluvial years with analysis of the EGH anomalies was completed. The *Total* annual NGP EGH anomaly composite (Fig. 3.4b) shows an area of negative height anomalies over the northwestern United States. The NGP *Pattern* composites of EGH (Fig. 3.4d) show larger negative anomalies over the northwestern United States with an enlarged area of negative EGH anomalies extending northwestward towards the Aleutian Islands. Though not statistically significant, the

negative EGH anomalies in the North Pacific suggest that storm systems originating from the North Pacific near the Aleutian Low produce the negative height anomalies in the northwestern United States. Analyses of NGP anomalous wind components (Figs. 3.5b and 3.6b) depict a much different pattern than that seen in the SGP composites. Statistically-significant 250 mb *v* wind component anomalies are located further northward and are less coherent in terms of a wave structure or pattern in the *Pattern* composites compared to the SGP *Pattern* composites (compare Fig. 3.5b with Fig. 3.5a). Moreover, the 250 mb *u* anomalies exhibit positive anomalies over the central western coast of the United States extending up over the Aleutian Islands, representing with an extension of the North Pacific jet stream over the United States and thus facilitating more storm systems to traverse the NGP along this extended storm track (e.g., Griffin and Martin 2017).

(a)

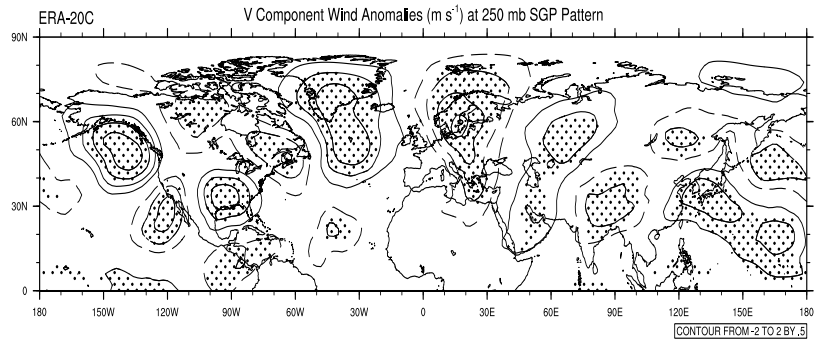

(b)

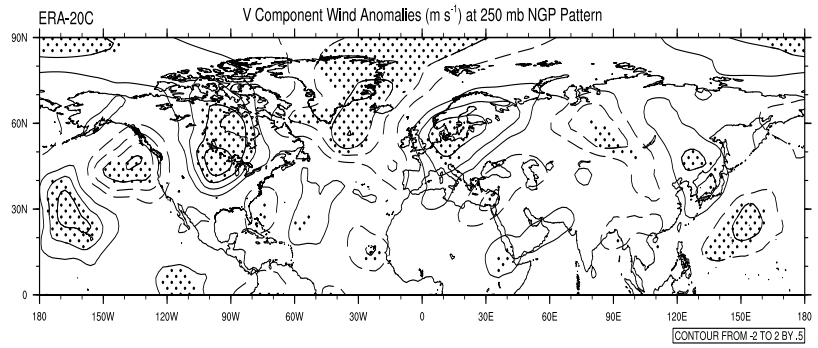

Figure 3.5: 250 mb *v* wind component anomalies for (a) SGP and (b) NGP *Pattern* years. Contours are plotted from 2 to -2 m s^{-1} in intervals of 0.5 m s^{-1}. Statistically significant values at the 90% level are stippled. Negative contours are dashed while positive contours are solid.

(a)

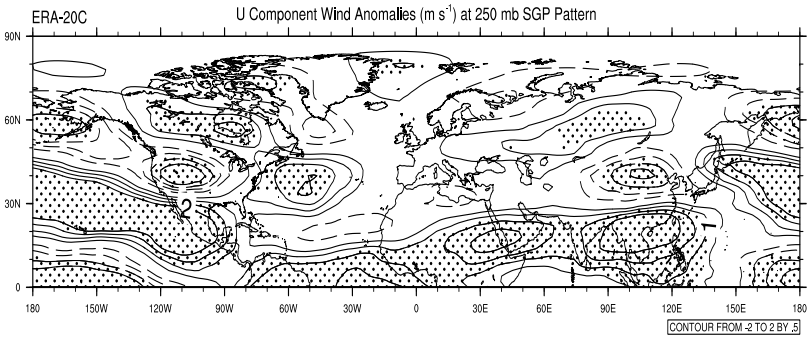

(b)

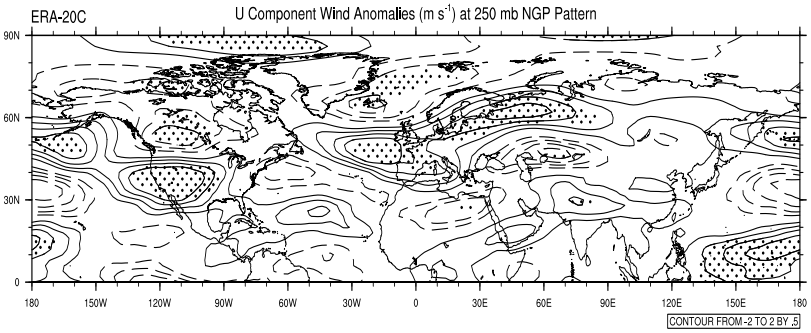

Figure 3.6: 250 mb *u* wind component anomalies for (a) SGP and (b) NGP *Pattern* years. Contours are plotted from 2 to -2 m s^{-1} in intervals of 0.5 m s^{-1}. Statistically significant values at the 90% level are stippled. Negative contours are dashed while positive contours are solid.

3.3.3 Robustness of the Pattern Composite Results

Because each reanalysis used a different dynamical core, parameterization configuration, vertical and horizontal resolution, etc., testing the results in other reanalysis datasets was utilized to test the robustness of the conclusions. For brevity, the *Pattern* composites from ERA-20C was compared with those from several other reanalysis datasets. For the SGP region (Figure 3.7), the *Pattern* composites for each different reanalysis dataset depict a center of negative height anomalies over the southwestern United States. Despite small differences in the details of the negative anomalies, the different reanalyses largely agree on the general EGH anomaly pattern shown for ERA-20C (i.e., Fig. 3.4). This is generally true for the NGP as well (not shown), except for the JRA55 dataset. For JRA-55, not a single year emerged for analysis in the *Pattern* composite. This lack of samples arises because of the scarcity of pluvial years identified within the JRA55 dataset for the NGP in particular. Curiously, the JRA55 reanalysis capably supplied years for the *Pattern* composites for the SGP, suggesting that this reanalysis may not depict salient features of NGP precipitation variability. Despite this one discrepancy, the results remain robust and statistically significant independent of the reanalysis product chosen.

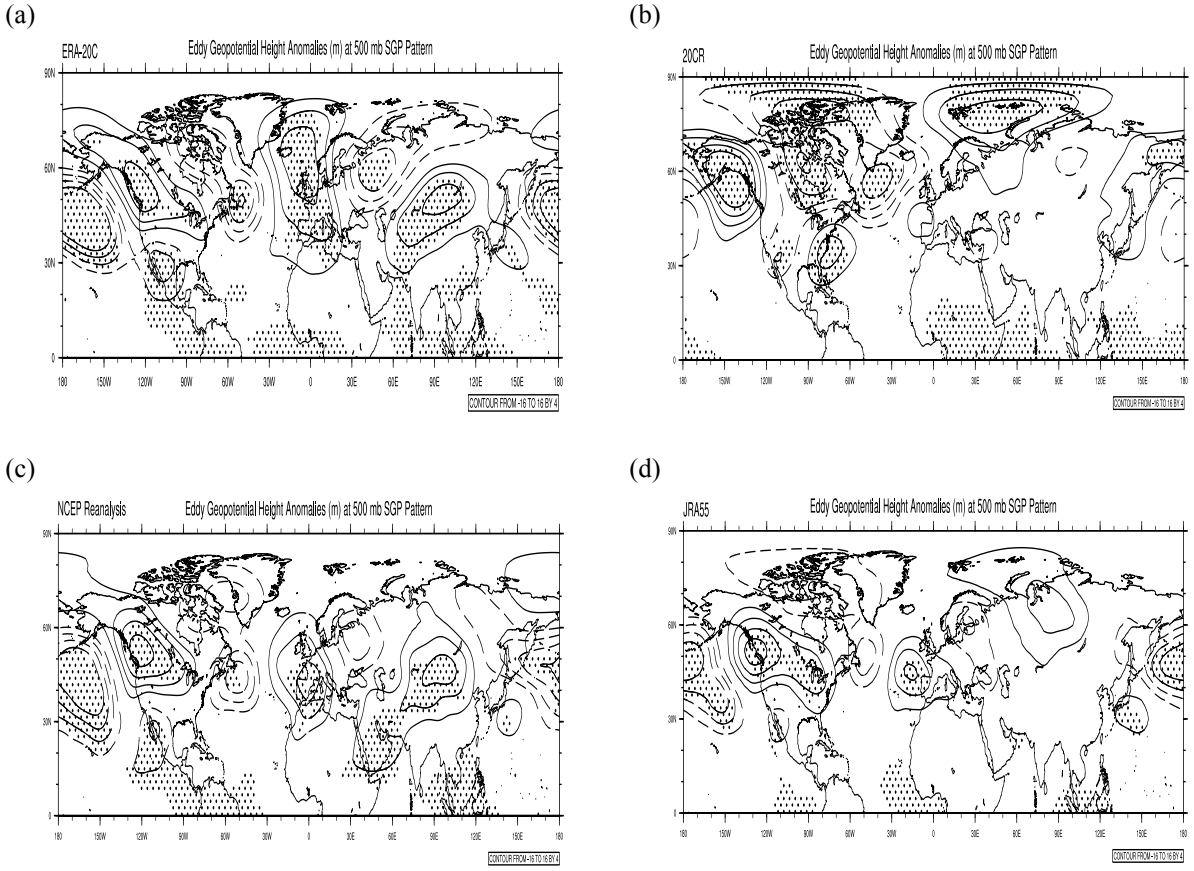

Figure 3.7: Eddy Geopotential Height Anomaly SGP *Pattern* composites for (a) ERA-20C, (b) 20CR, (c) NCEP-NCAR and (d) JRA55. Contours are plotted from 16 to -16 meters in intervals of 4 meters and statistically significant values at 90% are stippled. Negative contours are dashed and solid contours represent positive values. All datasets were analyzed on a 2° x 2° grid.

3.3.4 Heavy Precipitation Event Analysis

To determine the drivers of heavy precipitation during pluvial years, composites of daily heavy precipitation events during pluvial years are examined. The EGH anomalies for the SGP (Fig. 3.8a) and NGP (Fig. 3.8b) show a significant height dipole across the United States with negative (positive) height anomalies in the west (east). Differences between the two subregions emerge in terms of location and strength of the negative dipole. In particular, the SGP composite indicates weaker negative anomalies centered over SE New Mexico versus a strong negative node over NW Colorado in the NGP composite (Fig. 3.8). More importantly, the EGH anomaly patterns also elude to differences in moisture fluxes (*u'q', v'q'*) between these two regions (Fig. 3.9). The magnitude differences in these fluxes is particularly important for NGP heavy precipitation events due to the distance between the primary moisture source (e.g., Gulf of Mexico) and the northern extent of the GP. To show this, analysis of the 925 mb net moisture flux averaged over the GP (24-50°N, 254-276°W) during each region's heavy precipitation events was calculated and compared. Moisture flux anomaly values for the NGP (963.3 m s^{-1} g kg^{-1}) were 14% higher compared to the SGP (840.7 m s^{-1} g kg^{-1}) net flux anomalies during the pluvial year heavy precipitation events and 15% higher than the climatological value of the moisture flux anomalies over the GP (831.2 m s^{-1} g kg^{-1}). However, the moisture flux anomalies are still largely positive during SGP heavy precipitation events showing that enhanced moisture fluxes play a role in heavy precipitation events across the entire GP.

`

(a)

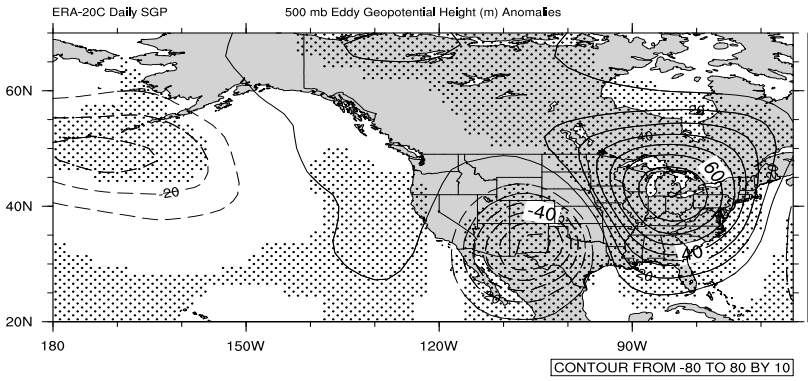

(b)

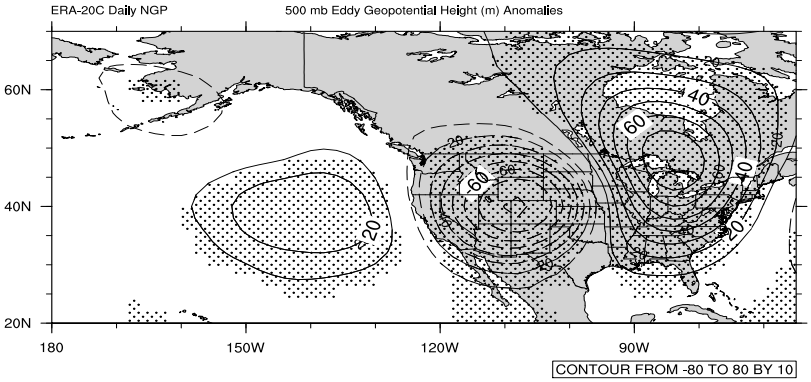

Figure 3.8: Composite 500 mb eddy geopotential height anomalies for daily heavy rain events for the (a) SGP and (b) NGP. Units are in meters, contours from -80 to 80 with intervals of 10 and values that are statistically significant at the 90% level are stippled. Negative contours are dashed and solid contours represent positive values.

(a)

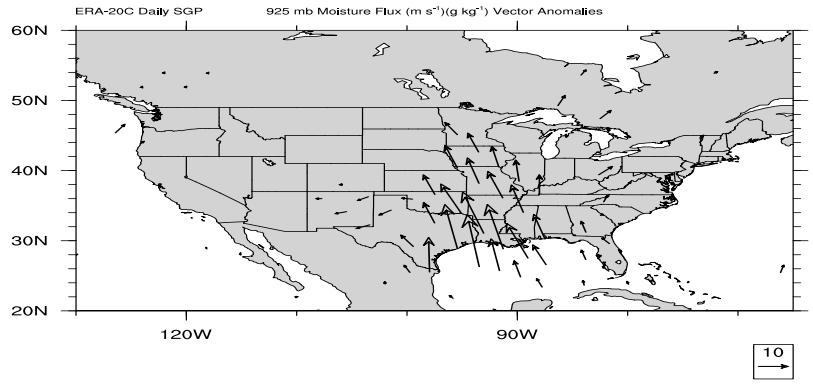

(b)

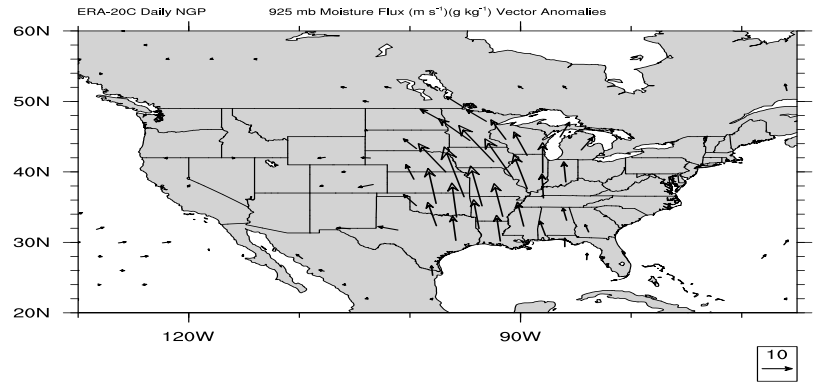

Figure 3.9: Composite 925mb moisture flux (*u'q', v'q'*) anomaly vectors for daily heavy rain events for the (a) SGP and (b) NGP. Units are in m s^{-1} g kg^{-1}, the standard vector length was used for a vector magnitude of 10 m s^{-1} g kg^{-1} and vectors that are statistically significant at the 90% level are plotted.

3.3.5 Break Composites

Finally, the role that nonstationarity in precipitation statistics may be playing in the pluvial year composites was investigated. As described in Section 3.2, the standard deviation of SGP and NGP precipitation was analyzed separately to determine if different regimes of variability exist within the long data region. A statistically-significant difference in standard deviations in both regions appears in 1980, and so 1980 is considered a "break point" or regime shift point for the pluvial analyses. The subsequent results of the *Break* composites (Fig. 3.10) reveal highly similar EGH anomaly patterns observed for the *Total* composites (Figs. 3.4a and 3.4b) for the SGP and the NGP. While small differences in the location and size of the important anomaly centers are apparent, differences are statistically insignificant via Monte Carlo simulations. Additionally, analysis of 250 mb *u* and *v* anomalies for the *Break* composites (not shown) are also similar to those in the *Total* composites. These similarities are somewhat expected - there are overlapping years included within the *Total* and *Break* composites (Table 3.1). More specifically, two years (1961 and 1974) are added to the SGP *Break* composite compared to the *Total* composite years used but five years (1987, 1990, 1991, 2002 and 2009) are removed, Likewise, one year (2009) is removed and one (1971) added to the NGP *Break* composite sample versus the NGP *Total* composite sample. Taken together, non-stationarity in the GP precipitation time series has minimal impact on the results of this analysis.

(a)

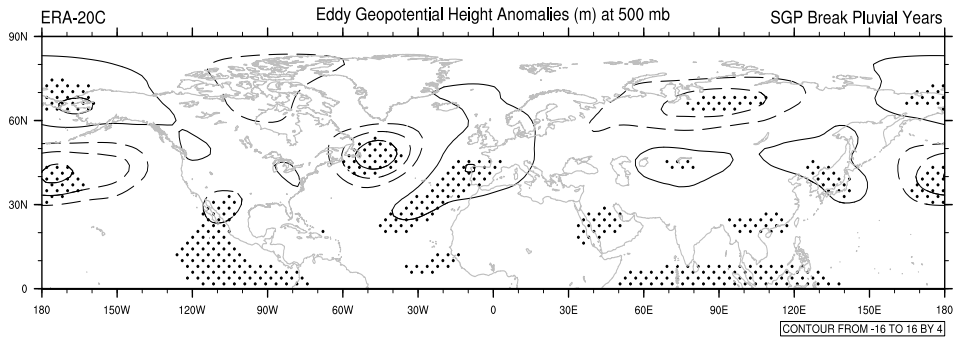

(b)

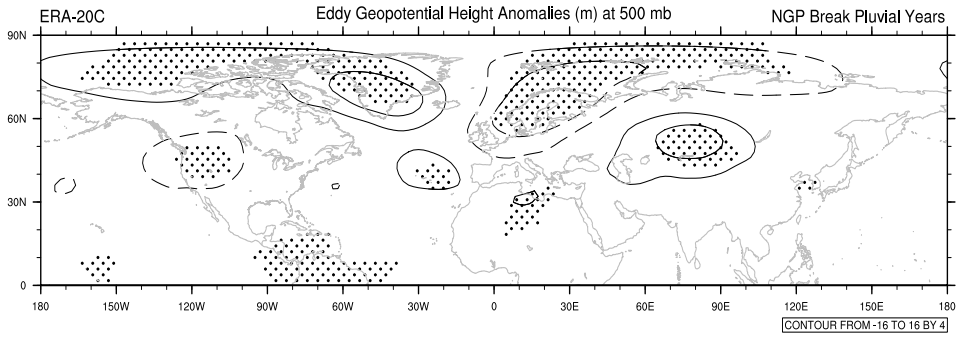

Figure 3.10: *Break* (all *Break* pluvial years) composites for 500 mb eddy geopotential height anomalies for the (a) SGP and (b) NGP. Units are in meters, contours are from -20 to 20 with intervals of 4 and values that are statistically significant at the 90% are stippled. Negative contours are dashed and solid contours represent positive values.

3.4 Discussion

The results highlight the primary atmospheric drivers responsible high rainfall years over the NGP and SGP separately. However, several other key conclusions arise when considering all composites collectively. Starting in the SGP, *u* anomalies associated with pluvial years (Fig. 3.6a) suggest that the Pacific waveguide is displaced equatorward more frequently than during non-pluvial years. This waveguide is an important feature of the atmosphere over the Pacific and North America region as it facilitates the passage of eastward-traveling synoptic waves towards North America (Branstator and Teng 2017; see also Figs. 3.4a and 3.4c). The southward shift of the storm track would also allow for enhanced moisture transport into the SGP as the storms can more readily tap into moisture-rich sources in the lower mid-latitudes of the Pacific. This anomalous southward shift of the Pacific waveguide is further supported by the uniformity of the *v* anomalies and strongly negative EGH anomalies seen in the daily heavy precipitation event analysis (Fig. 3.8a). Thus, enhanced synoptic activity over the SW United States is a hallmark trait for pluvial periods in the SGP. Furthermore, the SW United States is also a climatological hotspot for cutoff lows – i.e., persistent areas of low pressure / geopotential heights displaced from the main jet stream and thus "stuck" or "cutoff" from the large-scale zonal flow pattern – especially during the warm season (April – September). These systems typically induce instability and therefore precipitation and even severe convective events (Nieto et al. 2005). The "closed contour" nature of the negative height anomalies over the SW United States seen in the *Total* and *Pattern* composites (Figs. 3.4a and 3.4c) are suggestive of these cutoff low features.

While the *frequency* of synoptic waves and precipitation events appears important for SGP pluvial years, the *intensity* of the synoptic waves are the important factor for NGP pluvial years. Evidence for this conclusion includes larger negative height anomalies EGH anomalies in the NGP

Total and *Pattern* composites (Figs. 3.4b and 3.4d) and the daily heavy precipitation analysis composites (Fig. 3.8b) compared to the counterpart SGP composites (Figs. 3.4a, 3.4c, and 3.8a) Moreover, the magnitude of the NGP moisture flux anomalies during heavy precipitation events correlate with stronger extraropical cyclone activity, as deeper and more intense storms have stronger cyclonic flow that can transport more moisture further inland. Indeed, because the NGP is located much further away from the key source of moisture for heavy precipitation events than areas of the SGP, these stronger fluxes are necessary. Without these deep troughs over the north central United States, moisture transport would be insufficient to provide the necessary precipitable water necessary for such heavy rainfall events. Additionally, the EGH anomalies analyzed for NGP pluvial years (Figs. 3.4b and 3.4d) influence the atmospheric pattern in other ways, including acting as an eastward extension of the Pacific jet stream. As the jet stream is the main waveguide or pathway for synoptic storms to travel, a jet extension toward North America favors more propagation of synoptic waves over central North America, resulting in the EGH anomalies in the *Total* and *Pattern* composites. Feedbacks between the waves and the large-scale flow are also important to consider for jet extension regimes. For example, while an extended jet allows for more synoptic wave activity, that enhanced wave activity both extracts *and* returns kinetic energy to the large-scale mean flow. Therefore, the more intense extratropical cyclones could reinforce the extended jet regime and thus contribute positively to the extreme rainfall events in the NGP. This feedback aspect is beyond the scope of this work but is interesting to consider.

Lastly, the analysis focused on extratropical midlatitude variability and its impact on heavy rainfall in the GP on an annual basis. However, other remote forcings from global SSTs (e.g., Hu and Huang 2009; Cook et al. 2011) and anomalous tropical convection in the West Pacific Warm Pool (e.g., Barsugli and Sardeshmukh 2002) are also contributors to pluvial rainfall patterns in the

`

GP. The Pacific jet stream, identified in this study as an important conduit for the extratropical cyclones impacting the GP rainfall, can also be modulated (in strength and position) from the Madden-Julian Oscillation (MJO; e.g., Moore et al. 2010). Moreover, these remote impacts are also seasonally-dependent, and thus the seasonality of GP pluvial events remains an open question for future work.

Chapter 4

Role of Pacific Sea Surface Temperatures in United States Great Plains Pluvial Years

(Flanagan et al. 2018b)

4.1 Introduction

With the results seen in Chapter 3 into the atmospheric anomalies associated with GP *Pattern* pluvial years, further analysis of these pluvial years will aid in discriminating these pluvial years from non-*Pattern* pluvial years. As the primary source of global climate variability, the role of sea surface temperatures (SSTs) in weather and climate has been well studied and documented. From the most dominant mode of SST variability, the El Niño-Southern Oscillation (ENSO; e.g., Rasmusson and Carpenter 1982; Hoerling et al. 1997; Trenberth 1997; Harrison and Larkin 1998; Larkin and Harrison 2005a,b; Chiodi and Harrison 2013; Chen et al. 2014; L'Heureux et al. 2015; Yu et al. 2015; Guo et al. 2017) to the regional influences of western boundary currents (e.g., Nakamura et al. 2004; Wallace and Hobbs 2006; Kwon et al. 2010), a focus has been placed on explaining climate signals through modes of SST variability. This is especially true for North American climate, owing to the proximity to both the Pacific and Atlantic Oceans (e.g., Sanders 1986; Kuo et al. 1991; Reed et al. 1993, Findell and Delworth 2010). Primarily, efforts have utilized global to regional model simulations to categorize these teleconnections (e.g., Bates et al. 2001; Barsugli and Sardeshmukh 2002; Chen 2002; Ruiz-Barradas and Nigam 2005; Schubert et al. 2009; Wang et al. 2010) along with observational studies (e.g., Deser and Wallace 1990; Hu and Feng 2001; Lau and Weng 2002; Lau et al. 2004; Ding and Wang 2005; Frankignoul and Sennéchael 2007; Hu and Huang 2009; Ding et al. 2011; Ciancarelli et al. 2013; Seager and Hoerling 2014; Guo et al. 2017) that utilize advanced statistical methodologies to link modes of SST variability to North American climate.

`

However, most studies have primarily focused on the impacts of SST variability on North American precipitation deficits (e.g., Schubert et al. 2009; Findell and Delworth 2010; Hunt 2011; Wang et al. 2010; Seager and Hoerling 2014; Schubert et al. 2016). Further, many of the studies that have investigated the influences of SST on precipitation excesses (e.g., Ting and Wang 1997; Yang et al. 2007; Hu and Huang 2009; Findell and Delworth 2010; Hunt 2011; Cook et al. 2011) concluded that processes driving North American precipitation excesses are mirror images of the processes that drive precipitation deficits – i.e., they are mostly linear in their dynamics.

Hu and Huang (2009) investigated the links between different phases of ENSO and the Pacific Decadal Oscillation (PDO) and wet and dry periods over the GP. They found that (1) when ENSO and PDO are in their warm (positive) phase there is a higher occurrence of excessive precipitation over the GP and (2) when both are in their cold (negative) phase, the occurrence of precipitation deficits is higher over the region. They further found that the link between precipitation and the ENSO-PDO relationship is strongest during spring and weakest during the fall. Yang et al. (2007) used wavelet and cross-covariance function analysis to show that warm SSTs in the tropical Pacific (during the boreal spring and summer) weaken the easterly trade winds which can lead to strengthened southerly winds and thus moisture transport from Central America and the Gulf of Mexico to the GP. That moisture transport from the Gulf of California also aids in the occurrence of higher precipitation totals. Lastly, Guo et al. (2017) applied self-organizing maps to investigate different patterns of Pacific SST variability and their associated impacts on North American climate. They found that the precipitation response over North American during both canonical (i.e., maximum positive SST anomalies in the eastern tropical Pacific) and central Pacific (i.e., maximum positive SST anomalies in the central tropical Pacific) El Niño events is a north to south dipole, with precipitation during the central Pacific El Niño events showing smaller

areal coverage of wet anomalies over the southern United States compared to the canonical El Niño events. While these studies have primarily investigated the links between SST variability and total GP precipitation, few studies have investigated the connections between SST anomaly signals and longer periods of excessive precipitation over the GP.

While previous research linking SST and central United States precipitation variability has focused on the occurrence of concurrent or time lagged SST anomalies on precipitation patterns, few have focused specifically on the *synoptic scale drivers* of these precipitation anomalies. Chapter 3 documented distinct atmospheric patterns linked to above-normal precipitation over the GP region (Figs. 4.1a,b). Synoptic wave frequency over the southwestern United States showed signs of being crucial to SGP above average precipitation (i.e., pluvial) years while northwestern United States synoptic wave intensity and its subsequent impact on atmospheric flow patterns were crucial to the occurrence of NGP pluvial years. While the distinct atmospheric signals during *Pattern* pluvial years (years that were found to be strongly linked to an atmospheric anomaly pattern) were diagnosed in Chapter 3 they did not determine the sources of the atmospheric anomalies. Further, it was noted in Chapter 3 that a subset of the pluvial years in the NGP and SGP did not occur concurrently with a distinct atmospheric anomaly signal. Thus, while the atmospheric response to tropical Pacific SST anomalies (i.e., an induced Rossby wave train over the Pacific Ocean Basin and North America) and resultant latent heat release is well known (Hoskins and Karoly 1981), the connections between SSTs, the associated atmospheric signal, and GP excessive precipitation has not been investigated.

While previous studies have investigated the link between SSTs and GP precipitation, a gap between these SST anomaly signals and the *synoptic* drivers of excessive precipitation over the GP remains. Hence, the purpose of this study is to bridge the gap between the current

understanding of the influence of SST anomalies on GP precipitation and the primary atmospheric drivers associated with GP pluvial years. To achieve this, this study will (1) build on the findings of Chapter 3 and link the identified atmospheric patterns identified in that study with larger scale modes of climate variability, namely SSTs and (2) establish the fundamental pathways for these interactions which can be used to improve the prediction of when these atmospheric patterns will produce a pluvial year in the GP.

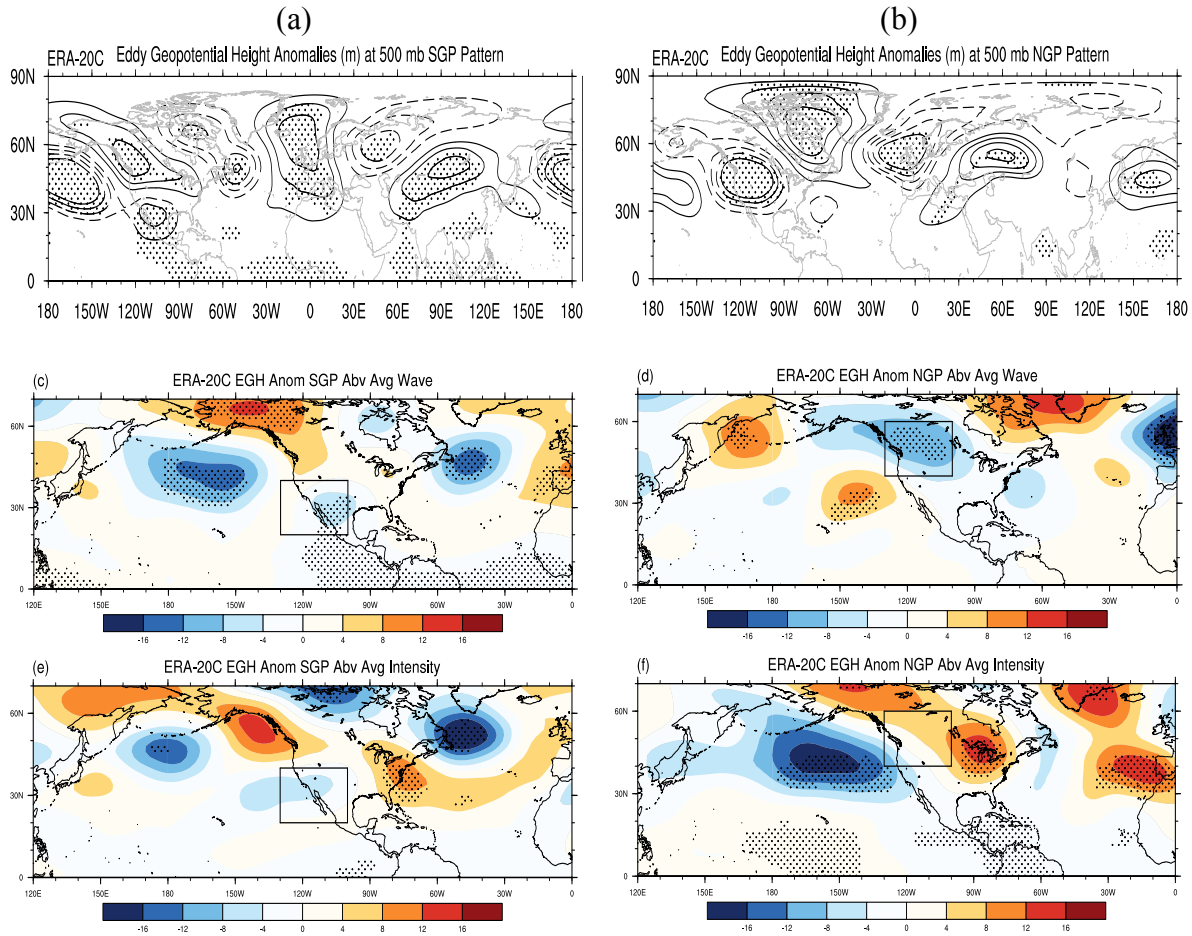

Figure 4.1: ERA-20C 500 mb Eddy Geopotential Height (EGH) anomalies for (a) from Chapter 3 for SGP *Pattern* pluvial years, (b) from Chapter 3 for NGP *Pattern* pluvial years, (c) SGP above average synoptic wave event years, (d) NGP above average synoptic event years, (e) SGP above average intensity synoptic wave years, (f) NGP above average intensity synoptic wave years. Contours are from -16 to 16 by 4 m, with stippling represented grid-points that are statistically significant at the 90% level. Black boxes on figures c,d,e,f represent the areas used to identify synoptic waves for the event classification scheme for the (c,e) SGP and (d,f) NGP.

4.2 Data and Methods

4.2.1 Datasets

Pluvial years are defined using the same methodology as in Chapter 3, with a year being identified as a pluvial if the annual precipitation amount over either the Southern Great Plains (SGP; Texas, Oklahoma, Kansas) or Northern Great Plains (NGP; Nebraska, South Dakota and North Dakota) is 10% above the annual climatological (1926-2010) mean. The pluvial years identified in the European Centre for Medium-Range Weather Forecasts (ECMWF) 20th Century Reanalysis (ERA-20C; Poli et al. 2016) dataset are compared to pluvial years identified in Parameter-elevation Regressions on Independent Slopes Model (PRISM; Daly et al. 2000) observations and only years which are common to both lists are utilized as pluvial years in this study.

To facilitate the diagnosis of GP pluvial years, monthly-mean fields from the ERA-20C monthly and daily datasets are chosen to represent atmospheric fields. This reanalysis product assimilates surface-based observations from 1900 to 2010 using a 4D-Var assimilation system to reanalyze historical weather signals and provide spatially continuous atmospheric and surface fields across the globe at a native resolution of 125 km. For this study, a 2° x 2° grid is used to maintain analysis consistency with Chapter 3 ERA-20C data also uses the Hadley Centre Sea Ice and Sea Surface Temperature version 2 (HadISSTv2; Rayner et al. 2003) dataset to initialize the ocean model used for the reanalysis product. Analyses done in this study are replicated with both ERA-20C and HadISSTv2 SST fields to test for robustness, and results are nearly identical. Fields from 1926-2010 are annually averaged, consistent with Chapter 3.

4.2.2 Calculating the Eddy Geopotential Height Index

Identification and descriptions of the primary atmospheric patterns associated with SGP and NGP pluvial years follow from Chapter 3. These patterns are key in describing the pluvial years that are primarily driven by synoptic signals. Through use of *Total* pluvial years, defined in Chapter 3, an index was created by projecting the EGH anomaly field for each year onto the *Total* EGH anomaly composite map for two different regions. Thus, this index represents when the NGP and SGP pluvial patterns identified in Chapter 3 are more active (higher value of the index) or quiescent (lower values of the index). *Pattern* pluvial years are defined as pluvial years which depict an EGH anomaly field which is similar to that of the Total EGH anomaly composite. As such, *Pattern* pluvial years were found by setting a threshold for the EGH index and identifying any pluvial year which crossed this threshold, thus gathering all years which display a stronger anomalous *atmospheric forcing* for a pluvial over either the NGP or SGP. For more details into the calculation and use of this index refer to Chapter 3

4.2.3 Synoptic Wave Event Classification Scheme

With the evidence found in Chapter 3 relating to the occurrence of GP *Pattern* pluvial years and synoptic wave features, a method was developed to identify synoptic waves and water vapor transport in the ERA-20C dataset. As synoptic wave features are distinguished by their curvature and influence on the flow pattern, relative vorticity and the geopotential height anomalies are chosen to identify synoptic wave events over two different regions, one for the SGP (20°-40°N, 130°-100°W; southwestern United States) and one for the NGP (40°-60°N, 130°-100°W; northwestern United States). The different regions are associated with the anomalous synoptic signals crucial to the occurrence of *Pattern* pluvial years found in Chapter 3 (i.e. southwestern United States for SGP and the northwestern United States for the NGP).

To identify synoptic waves, thresholds were set to classify events from the 0000 UTC daily ERA-20C fields. After utilizing a high-pass 10-day filter to isolate the synoptic timescale features at each grid-point, the data was detrended, the annual cycles removed and the data standardized. To identify synoptic waves, the average geopotential height anomaly within the region was required to be at least -0.5σ or below, with at least one grid-point with a relative vorticity value of at least 1.5σ and at least one grid-point with a geopotential height value of at least -1.5σ. As the values were filtered and standardized, the +/-1.5σ values represent strong deviations from the typical flow pattern and given the sign of relative vorticity and geopotential height anomalies the events identified using these thresholds are Northern Hemisphere troughs. To investigate the intensity of the synoptic waves, the lowest grid-point standardized geopotential height anomaly value for each identified wave was found. Through an analysis of the synoptic wave events by varying the height and relative vorticity thresholds, the final thresholds for each variable were calibrated to remove the identification of ridge events from the scheme.

4.2.4 Composite and Regression Analysis

For this study, two different statistical methods were implemented: (1) the composite analysis of surface and atmospheric fields and (2) linear regression analysis using the EGH anomaly index. Composites were created for SSTs, 250 mb streamfunction and 500 mb EGH anomalies for *Pattern* pluvial years (Table 4.1). SSTs were investigated owing to their strong connection to global climate variability, while the streamfunction variable was chosen to illustrate the effect of SSTs on the stationary wave signal during pluvial years (AMS 2012). Seasonal composites (i.e., December, January, February (DJF), March, April, May (MAM), June, July, August (JJA) and September, October, November (SON)) of SST and streamfunction were also

analyzed to detail the seasonal persistence of the SST and atmospheric signals found during *Pattern* pluvial years. Further, composites were created for years with above average number of synoptic wave events and those with more intense synoptic waves. These were created to compare the atmospheric and surface fields during these years to the composites created from the list of *Pattern* pluvial years. In this way, these above average event composites were able to further show the connections between synoptic wave frequency and intensity and GP *Pattern* pluvial years that was stated in Chapter 3.

Table 4.1. List of years averaged over to derive each composite plot. *Pattern* years are found using the methodology defined within the Chapter 3. Also included is the list of all pluvial years from the ERA-20C dataset found in Chapter 3

	SGP	NGP
All Pluvial Years	1926, 1941, 1957, 1968, 1974, 1979, 1987, 1990, 1991, 1992, 1997, 2002, 2004, 2007, 2009	1941, 1951, 1962, 1965, 1977, 1982, 1986, 1993, 1995, 1998, 2005, 2007, 2008, 2009, 2010
Pattern	1926, 1941, 1987, 1991, 1992, 1997, 2002, 2004	1951, 1982, 1998, 2008, 2010
Event Composites (Intensity)	1941, 1957, 1974, 1991, 2009	1941, 1965, 1986, 1995, 1998, 2005
Event Composites (Synoptic Waves)	1926, 1957, 1968, 1979, 1987, 1992, 1997, 2002, 2004, 2007	1951, 1962, 1977, 1986, 2007, 2008, 2010

Linear regression analysis was used to diagnose the contemporaneous correlation between the EGH anomaly index and relevant surface (SST) and atmospheric (250 mb wind components and 250 mb streamfunction) fields. The EGH index and all ERA-20C fields were standardized and detrended prior to linear regression. Significance testing for statistical relationships was completed using a 1000 iteration bootstrap test (by grid-point) and using a 90% two-tailed threshold.

4.3 Diagnosis of Synoptic Waves during Great Plains *Pattern* Pluvial Years

4.3.1 Synoptic Wave Event Statistics

Owing to the importance of synoptic waves with regard to the occurrence of *Pattern* pluvial years Chapter 3, the frequency and intensity of synoptic waves over the southwestern and northwestern United States was investigated for the SGP and NGP, respectively. For all years within the ERA-20C dataset, an average of 52 (62) synoptic wave events per year occurred over the southwestern (northwestern) United States as defined by the classification scheme. When the average number of events per year during pluvial years was compared with all years, the results were nearly identical for both regions (Table 4.2). However, when only *Pattern* years for both regions were considered, the results yielded increased totals with 63 (81) events on average per *Pattern* year for the SGP (NGP). The difference in means between all years and *Pattern* years was statistically significant for both regions, consistent with the findings in Chapter 3.

Table 2. Average number of synoptic wave events (troughs) per year and intensity of those waves. Rounding was completed to represent events rather than the decimal average; the actual average is in parenthesis below the rounded number.

Synoptic Wave Events		SGP	NGP
	All	52 *(51.7)*	62 *(61.5)*
	Pluvial	52 *(52)*	60 *(60.4)*
	Pattern	63* *(62.5)*	81* *(81.2)*
Synoptic Wave Intensity			
	All	-3.3σ *(-3.32 σ)*	-2.7σ *(-2.65 σ)*
	Pluvial	-3.4σ* *(-3.42 σ)*	-2.7σ *(-2.68 σ)*
	Pattern	3.5σ* *(-3.46 σ)*	-2.7σ *(-2.72 σ)*

* Statistically significantly different from the annual mean using a 90% one-tailed bootstrap significance test.

When the intensity of synoptic waves during pluvial years was considered, the results were different to the frequency of these waves. Overall, the average of the minimum value in the SGP (NGP) was approximately -3.3σ (-2.7σ) (Table 4.2). For all pluvial years, this average did not significantly change for the NGP or the SGP. For *Pattern* pluvial years, the mean intensity for all waves for the SGP increased to approximately -3.5σ and for the NGP no change was seen between all pluvial years and *Pattern* pluvial years. However, only the results for the SGP were statistically significant. These statistics represent a first step in determining if key results pertaining to synoptic waves for SGP and NGP *Pattern* pluvial years were valid. Results show that the frequency and intensity of these waves are important to the occurrence of SGP *Pattern* pluvial years, while for

NGP *Pattern* pluvial years the results are less conclusive, with the statistics showing little changes and no statistical significance. Thus, it was not possible to conclude if the statement about synoptic wave intensity during NGP *Pattern* pluvial years over the northwestern United States was crucial to a NGP *Pattern* pluvial year.

4.3.2 Event Classification Composites

While the statistics of the synoptic wave and intensity provide information about the dynamic atmospheric contributors to pluvial years, it does not wholly answer the question into the importance of either. Investigating the relationships between various surface and atmospheric variables during years with above average synoptic waves or synoptic wave intensity are critical to determining the importance these features on *Pattern* pluvial years. While the statistical relationship may not show a strong linkage between *Pattern* pluvial years and these synoptic wave features, investigating the atmospheric anomaly signals during years with above average synoptic waves or wave intensity could reveal further information about the importance of these features on *Pattern* pluvial years. First, composites of EGH were compared to the results of Chapter 3 to show the relative importance of either above average intensity or synoptic wave events on the occurrence of a *Pattern* pluvial year. For above average synoptic wave years, the negative EGH anomaly signals (Fig. 4.1c) were similar to that of the *Pattern* composites from Chapter 3 (Fig. 4.1a). An area of negative EGH anomalies exists over the southwestern United States with a larger magnitude negative anomaly over the North Pacific Ocean. This shows the relative importance of more frequent synoptic waves, as years identified through this methodology show nearly the same anomaly signal as the EGH *Pattern* composites from Chapter 3 (Fig. 4.1a). The SGP EGH anomaly composite during above average synoptic wave intensity years (Fig. 4.1e) shows a statistically

insignificant negative EGH signal over the southwestern United States and eastern Pacific Ocean, and no statistically significant signals over the northern Pacific. Thus, for SGP *Pattern* pluvial years, more frequent synoptic waves over the southwestern United States appear to be crucial for the occurrence of a *Pattern* pluvial year.

For above average synoptic wave years, a significant SST anomaly (Fig. 4.2a) signal exists across the central tropical Pacific. Previous studies have shown a link between enhanced southern United States precipitation and El Niño events (e.g., Ropelewski and Halpert 1986,1987,1989; Gershunov and Barnett 1998; Dai and Wigley 2000; Larkin and Harrison 2005). However, this composite SST feature of warm anomalies resembles more of a Central Pacific (CP) ENSO event (e.g., Larkin and Harrison 2005; Ashok et al. 2007; Yu and Kao 2007; Kao and Yu 2009; Kug et al. 2009; Fang and Mu 2018), with a maximum SST anomaly located in the central tropical Pacific Ocean. Thus, the atmospheric response was also different from canonical ENSO events (e.g., Barsugli and Sardeshmukh 2002). Indeed, Garfinkel et al. (2013) showed that during CP warm ENSO events, the North Pacific low is located further south compared to a typical El Niño event. As such, this southward shift in the low center would also induce a southward shift in the Pacific jet stream, thus impacting the synoptic wave signal over the southern United States. Note that the SST composites likely contain both CP and canonical (Eastern Pacific) ENSO warm events. However, because of the relative magnitude of the anomalies in the central Pacific, CP warm ENSO events likely dominate the atmospheric anomalies and synoptic wave frequency. Fig. 4.2a also presents the streamfunction composite for the SGP above average synoptic wave activity years. The composite illustrates a large area of negative anomalies across the Northern Hemisphere, with the largest negative anomalies over the North Pacific and the southwestern United States. The anomaly gradient over the central North Pacific shows that the jet stream was

shifted anomalously southward, facilitating an increase in the occurrence of synoptic waves over the southern United States. (e.g., Trenberth 1998; Neelin 2011; Wang et al. 2013; Wirth et al. 2018).

Figure 4.2c details SST and streamfunction anomalies during SGP pluvial years with above average intensity synoptic waves. The anomalies during above average intensity pluvial years are similar to the features seen in the above average synoptic wave pluvial years, yet the major streamfunction anomaly regions were shifted to the west and not as significant as in the above average synoptic wave pluvial composite. Further, the SST anomalies were weakened and not as robust as during the above average synoptic wave pluvial years. Thus, while from the statistical analysis the intensity and frequency are important for SGP *Pattern* pluvial years, the frequency of synoptic waves over the southwestern United States appears to be more important for SGP *Pattern* pluvial years owing to the strong similarities between the above average synoptic wave composites and the results seen in Chapter 3.

For the NGP, pluvial years with an above average number of synoptic waves (Fig. 4.1d) show a similar signal as that seen in Chapter 3 for NGP *Pattern* pluvial years (Fig. 4.1b). A large area of negative EGH anomalies was located further to the north compared to EGH anomalies during NGP *Pattern* pluvial years, over northwestern North America. As for SST and streamfunction, no distinct signal in either field was seen during years with an above average number of synoptic waves (Fig. 4.2b). Results from the pluvial years with above average intensity synoptic waves are no more conclusive. EGH anomalies during above average intensity years (Fig. 4.1f), shows little similarity to the EGH composite during *Pattern* pluvial years (Fig. 4.1b), with the area of negative EGH anomalies shifted far to the west with positive EGH anomalies to the east. SST anomalies (Fig. 4.2d) during these years show a large area of positive SST anomalies

across the tropical Pacific resembling an ENSO event, with stream anomalies across the Pacific Ocean basin resembling that of the SGP above average synoptic wave streamfunction composite (Fig. 4.2a). Positive streamfunction anomalies were seen just north of the tropical Pacific with negative anomalies over the north Pacific. These atmospheric anomalies are counter to that seen in Chapter 3 during NGP *Pattern* pluvial years, as this signal depicts the major height anomalies further to the west of the region noted in Chapter 3 (Fig. 4.1b). This analysis indicates that neither frequency of synoptic waves nor their intensity is related to the occurrence of NGP *Pattern* pluvial years. Thus, the results within this portion of the study show that the argument made in Chapter 3 were not valid.

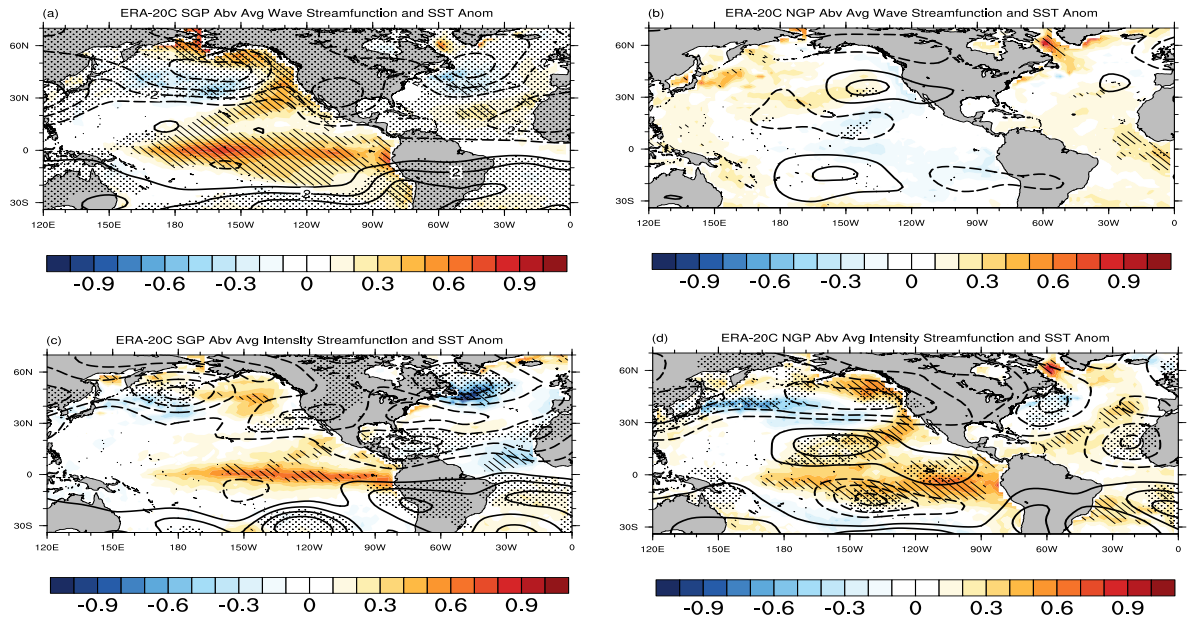

Figure 4.2: SST (°C); shaded contours) and 250 mb streamfunction (10^{-6} m^2s^{-1}) anomalies for (a) SGP above average synoptic wave pluvial years, (b) NGP above average synoptic wave pluvial years, (c) SGP above average intensity synoptic wave pluvial years and (d) NGP above average intensity synoptic wave pluvial years. Contour interval 0.1°C for SST anomalies and 1 x 10^{-6} m^2s^{-1} for streamfunction anomalies. Solid (dashed) contours represent positive (negative) streamfunction anomalies; zero contour omitted. Statistical significance at the 90% level is noted by stippling for the streamfunction anomalies and dashed areas for the sea surface temperature anomalies.

4.4 Diagnosis of Great Plains *Pattern* Pluvial Years

4.4.1 SST and Streamfunction Composites

Through an investigation into the frequency and intensity of synoptic waves, results show a connection between wave frequency and key features of *Pattern* pluvial years, i.e., confirming that synoptic wave frequency is crucial for the occurrence of GP *Pattern* pluvial years, with intensity being important for the SGP. However, these results do not show the state of the ocean or atmosphere during *Pattern* years specifically. Thus, analysis detailing the state of the ocean surface and atmosphere is still needed to definitively show the links between *Pattern* pluvial years and SST signals.

The composite of SST anomalies during SGP *Pattern* years show a large area of positive SST anomalies across the tropical Pacific (Fig. 4.3). Similar to the SGP above average synoptic wave event SST composite, the center of largest magnitude anomalies was located over the central tropical Pacific. When the SGP analysis was broken into seasonal composites of SST (Fig. 4.3b,c,d,e), the same general signal appears in each season; SST anomalies in DJF (Fig. 4.3b) occurred mainly over the central tropical Pacific without any signal over the eastern tropical Pacific while MAM SST anomalies (Fig. 4.3c) show that the center of warm SST anomalies shift eastward. This composite anomaly signal continues during JJA (Fig. 4.3d) and SON (Fig. 4.3e). However, by SON, the SST composite signal resembles more of a canonical El Niño event. Thus, the seasonality of SSTs during *Pattern* pluvial years is important, given the seasonality of precipitation within these pluvial years. Results from Christian et al. (2015) into the seasonality of pluvial months during pluvial years found a higher probability of excessive rain later in the year (October and November) and early spring (February and March) compared to the rest of the year. From the seasonal analysis of SST and streamfunction, the results yield that the spring (MAM), fall (SON)

and winter (DJF) seasons correspond to the times of year in which you see the largest SST anomalies coincident with the strongest atmospheric anomalies, although the atmospheric signal during fall (SON) isn't as strong as seen in the spring or winter. Thus, while the seasonal signal of SST and streamfunction anomalies are persistent throughout the year, they are likely impacting SGP precipitation in different ways during different seasons.

During SGP *Pattern* pluvial years (Fig. 4.3), negative streamfunction anomalies cover most of the Northern Hemisphere, with the largest magnitudes over the northern Pacific and across the southwestern and south central North America (Fig. 4.3a). A positive anomaly area in the tropical Pacific, with a gradient between negative anomalies across the northern Pacific, show that the Pacific jet stream is located further south of its climatological position. As the jet stream is predominantly a zone of strong westerly winds, these westerly propagating waves will be concentrated along this narrow band of strong winds. Thus, these results agree with the event composite results. Both analyses show a shift in the North Pacific jet stream resulting from anomalies in the atmospheric height regime.

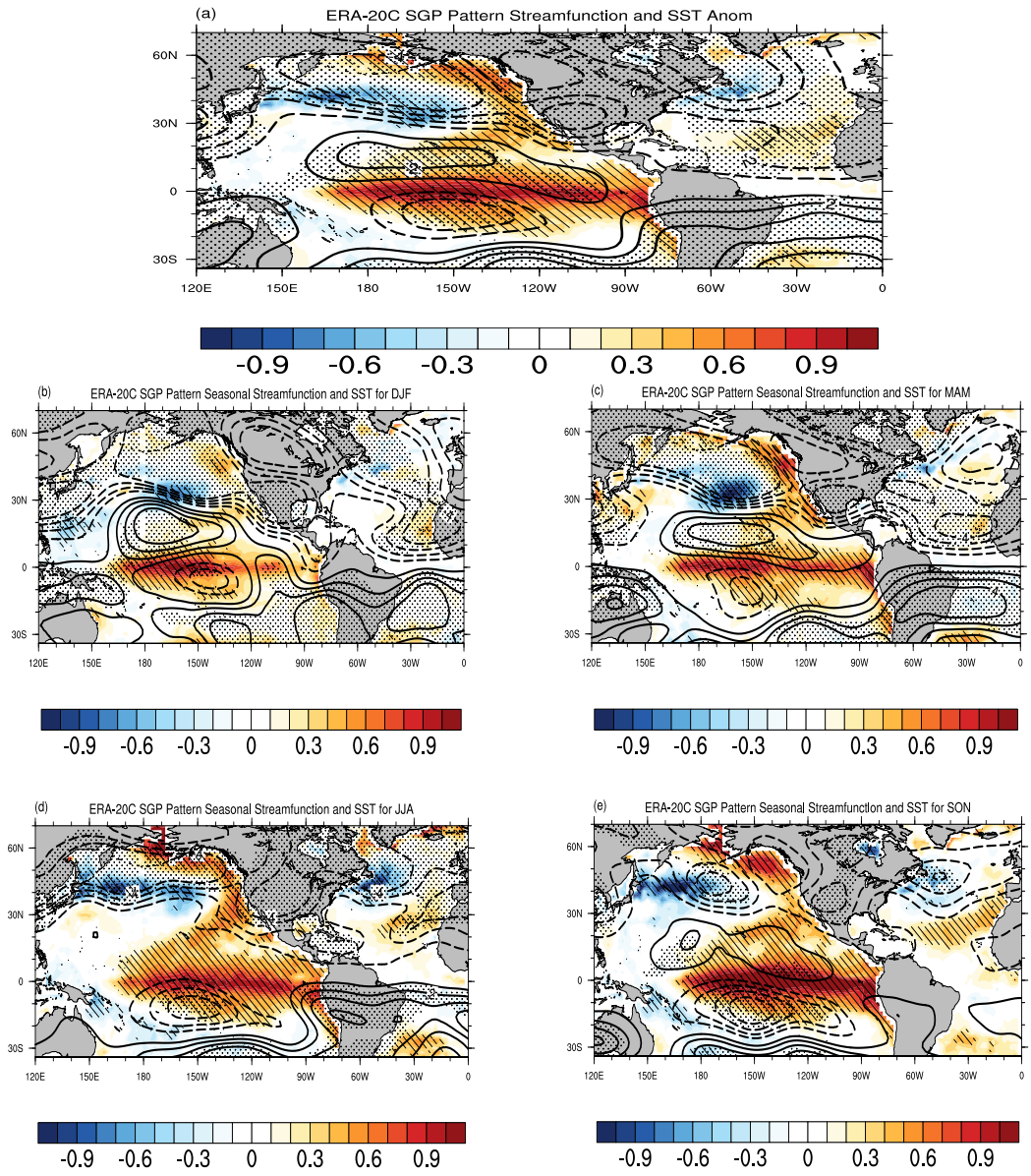

Figure 4.3: SGP *Pattern* pluvial year SST and 250 mb streamfunction anomalies (a) annual composite and seasonal composites during *Pattern* pluvial years for (b) DJF, (c) MAM, (d) JJA and (c) SON. Color shading is used for the sea surface temperature anomalies (°C), contoured from -1 to 1 by 0.1 and contours are used for the streamfunction anomalies (m), contoured from -4 to 4 by 1. Statistical significance at the 90% level is noted by stippling for the streamfunction anomalies and dashed areas for the sea surface temperature anomalies.

Seasonal composites of streamfunction anomalies during SGP *Pattern* pluvial years yield the same overall signal during all 4 seasons with minor differences, especially during DJF (Fig. 4.3b) and MAM (Fig. 4.3c). During JJA (Fig. 4.3d), the negative anomalies over the tropical Pacific and the North Pacific exist, however positive anomalies between the two regions are no longer present. During SON (Fig. 4.3e), a signal resembling that of the DJF and MAM anomalies exists, with reduced magnitudes of the positive anomalies in the lower latitudes over the Pacific Ocean being the main difference. Even with all 4 seasons showing some atmospheric anomaly signal over the Pacific basin, the strongest atmospheric influence from the SST warm signal is likely during the boreal winter and spring.

During NGP *Pattern* pluvial years, an area of positive SST anomalies (Figure 4.4) appears off the western coast of tropical South America (Fig. 4.4a). Additionally, positive anomalies off the coast of Japan show that the Kuroshio-Oyashio Extension (KOE) SST region could be involved in NGP pluvial years. These KOE SST anomalies may work to increase the baroclinicity across the North Pacific, increasing cyclogenesis, and maintaining the storm-track (jet stream) location over the North Pacific (Kwon et al. 2010; Ma et al. 2015, 2017). However, with the lack of a strong SST signal over the KOE region, these anomalies appear to have more of a tertiary impact on the precipitation variability of the NGP region.

`

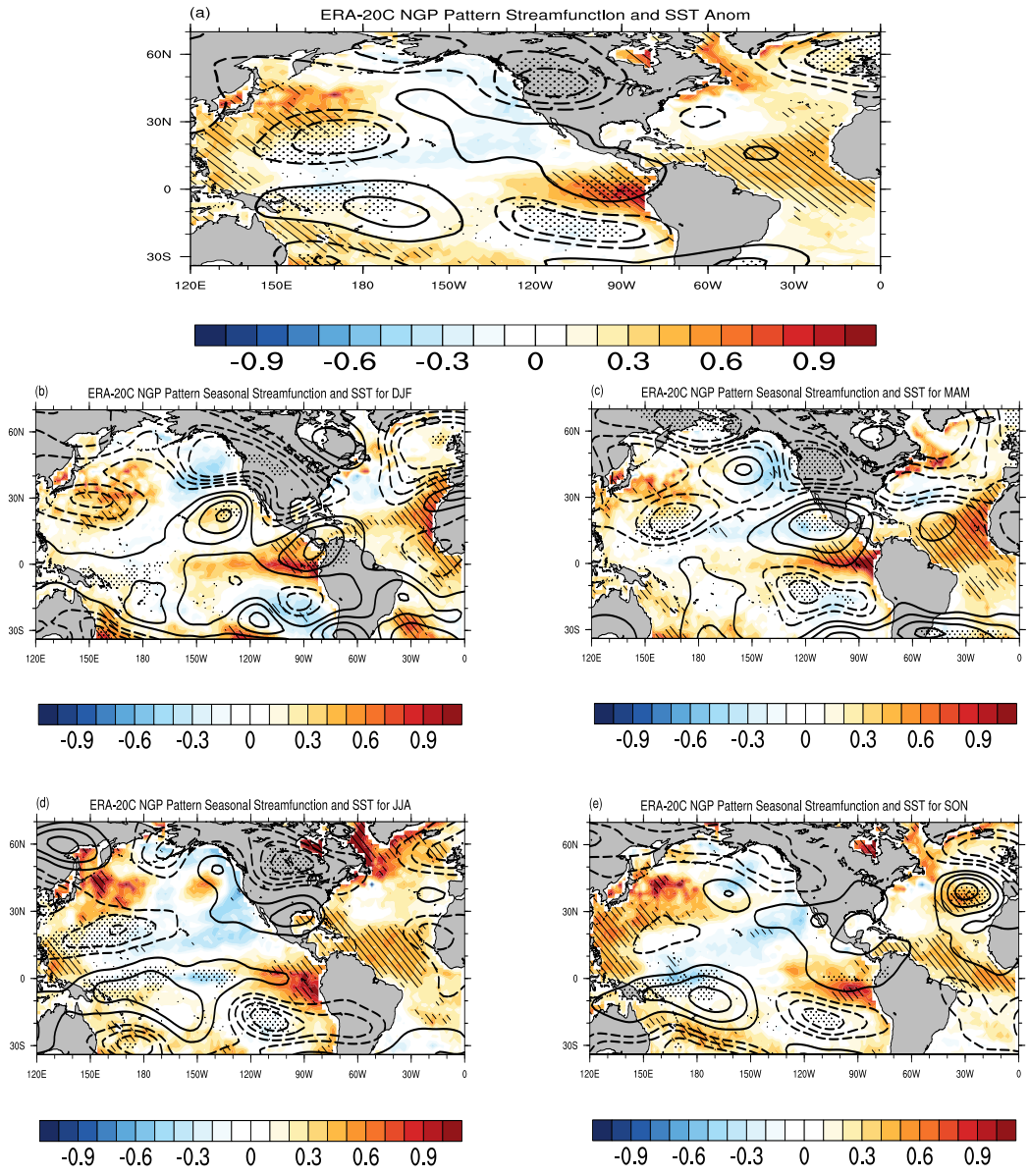

Figure 4.4: NGP *Pattern* pluvial year SST and 250 mb streamfunction anomalies (a) annual composite and seasonal composites during *Pattern* pluvial years for (b) DJF, (c) MAM, (d) JJA and (c) SON. Color shading is used for the sea surface temperature anomalies (°C), contoured from -1 to 1 by 0.1 and contours are used for the streamfunction anomalies (m), contoured from -4 to 4 by 1. Statistical significance at the 90% level is noted by stippling for the streamfunction anomalies and dashed areas for the sea surface temperature anomalies.

The seasonal composites of SST anomalies for NGP *Pattern* years yield statistically significant SST anomalies in the west central Pacific and KOE regions during DJF (Fig. 4.4b), JJA (Fig. 4.4d) and SON (Fig. 4.4e) and an eastern tropical Pacific warm signal during MAM (Fig. 4.4c). The most persistent and significant anomalies in the NGP SST composite, however, appear in the tropical Atlantic during all seasons, along with a positive anomaly signal over the Caribbean during JJA (Fig. 4.4d). Christian et al. (2015) shows that a majority of the excessive rainfall occurs during the warm or convective season of the NGP. Thus, given the lack of a consistent atmospheric or SST signal linked to the occurrence of excessive rainfall, it is likely that the occurrence of NGP pluvial years is likely related to anomalous convective activity, scales which are too small for this study. Yet, the western tropical Atlantic SST warm anomalies seen in JJA (Fig. 4.4d) likely have an influence on moisture transport through the low-level jet and thus could provide a secondary impact on precipitation amounts in the NGP (e.g., Oglesby et al. 1989; Schubert et al. 2008; Knippertz and Wernli 2010).

During NGP *Pattern* pluvial years (Fig. 4.4a), an area of negative anomalies lies across northern North America, representative of the negative height anomalies that define this pattern in Chapter 3, but there is a lack of defined anomalies across most of the Northern Hemisphere during these years. Further, the seasonal streamfunction anomalies show a more variable signal. During DJF (Fig. 4.4b) and MAM (Fig. 4.4c) negative anomalies are seen over the northwestern United States, during JJA (Fig. 4.4d) these anomalies shift further to the east and are broader, and during SON (Fig. 4.4e) no significant streamfunction anomaly feature is noted. While negative heights are seen over the northwestern United States during DJF, MAM and JJA, the signals are quite different during each season.

4.4.2 Eddy Geopotential Height Index Linear Regression Analysis

While composite analyses detailed the linkages between Pacific SSTs, the atmospheric state, and the occurrence of excess rainfall over the GP during *Pattern* pluvial years, the linear facets of these connections are also investigated. A linear regression and correlation analysis was conducted using annually averaged upper tropospheric wind fields and SSTs along with the Chapter 3 standardized EGH anomaly indices (one for NGP and one for SGP) as the base indices. Regression of SST anomalies onto the standardized SGP EGH index (Figure 4.5a) illustrated positive SST anomalies across the tropical Pacific, with the largest anomalies in the central tropical Pacific. Statistically significant negative SST anomalies also exist in the North Pacific. The regression signal closely resembles the *Pattern* composite (Fig. 4.3a) and the SGP above average synoptic wave event SST composite (Fig. 4.2a), but with higher magnitude. The Pacific Ocean signal as a whole resembles that of the PDO, a feature that has been linked in its warm phase to GP precipitation (Hu and Huang 2009). However, as the PDO is a low-frequency oceanic signal (e.g., Mantua et al. 1997; Newman et la. 2003; Schneider and Cornuelle 2005; Mills and Walsh 2013; Newman et al. 2016), the linear regression methodology may mask the comparatively higher-frequency ENSO signal, which would not emerge strongly in annual-mean fields.

The regression of 250 mb streamfunction onto the SGP EGH index (Fig. 4.5b) shows a signal resembling that seen in the in the above average synoptic wave event and *Pattern* streamfunction composites (i.e., Figs. 4.2a and 4.3a). The SGP streamfunction regression plot shows that during years in which the SGP EGH index is higher, streamfunction across the tropical Pacific will be lower, south of Hawaii will see stronger ridges and across the north Pacific Ocean basin troughs will be deeper, including across the southern United States. This consistent signal in the Pacific SST and streamfunction analyses suggests a link between SST and streamfunction

anomalies during SGP *Pattern* pluvial years. As seen in the streamfunction plots (Fig. 4.5b) the SST signal is coincident with a gradient in streamfunction anomalies, located near 30°N over the Pacific Ocean, signifying the shift in the jet stream. Further, the 250 mb zonal wind anomalies (Fig. 4.5c) are analyzed to determine if a consistent shift in the jet occurs. The zonal wind anomaly regressions shows that during years with an enhanced SGP EGH index higher zonal winds would be analyzed across the north Pacific Ocean basin and the southern United States. Thus, the *u* wind field shows a corresponding shift in the location of the jet stream during years in which the EGH anomaly index is higher.

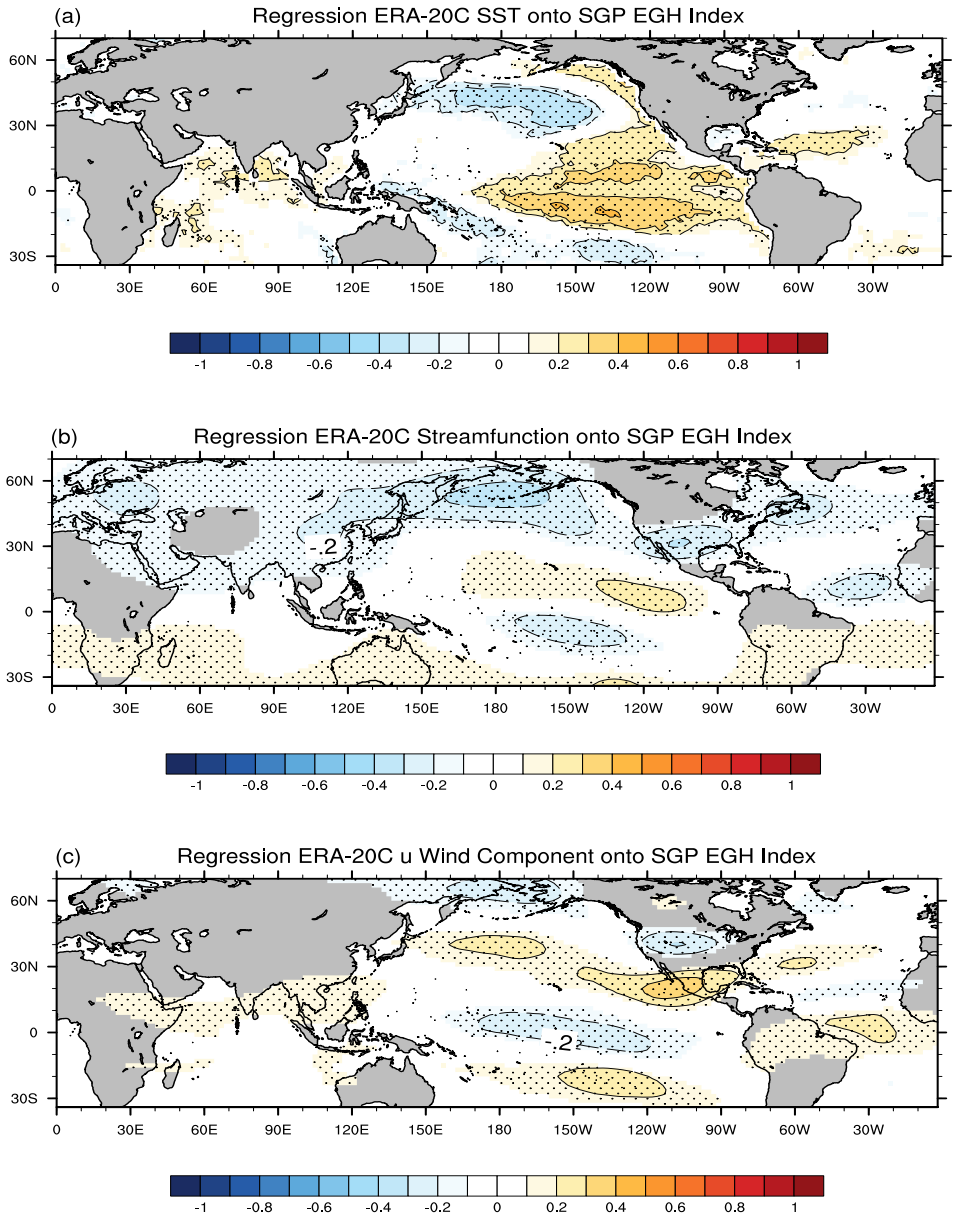

Figure 4.5: Regression of (a) SST (°C), (b) 250 mb streamfunction (m^2s^{-1} *10^{-6}), and (c) 250 mb *u* wind component (ms^{-1}) onto the standardized SGP EGH index, contour interval 0.1°C; zero contour omitted. Stippled regions indicate regression coefficients which are statistically significant at the 90% level.

The NGP SST regression coefficient plot (Fig. 4.6a) resembles the NGP *Pattern* SST composites (Fig. 4.4a) with higher NGP EGH index years having warmer SSTs over the western north Pacific and lower SSTs across the eastern west Pacific. Unlike the SGP, the tropical Pacific is devoid of significant SST anomalies. Thus, the NGP atmospheric signal is not (linearly) linked with the tropical Pacific or Atlantic. During higher NGP EGH index years, decreased streamfunction (Fig. 4.6b) over the northwestern United States depicts a height anomaly signal matching that of the NGP pattern in Chapter 3, with stronger troughs over the northwestern United States. Unlike the SGP, the regression of 250 mb zonal wind anomalies on the NGP EGH index yields no significant features (not shown). However, regressions with the 250 mb *v* wind anomalies (Fig. 4.6c) depicts a negative to positive couplet over the northwestern United States, a key feature of NGP *Pattern* pluvial years in which the troughs over the northwestern United States induce a southerly flow to the east and a northerly flow to the west of the trough. These wind anomalies indicate that height anomalies over the northwestern United States alter the flow pattern during NGP *Pattern* pluvial years, again agreeing with the results of Chapter 3 about the importance of the intensity of northwestern United States synoptic waves.

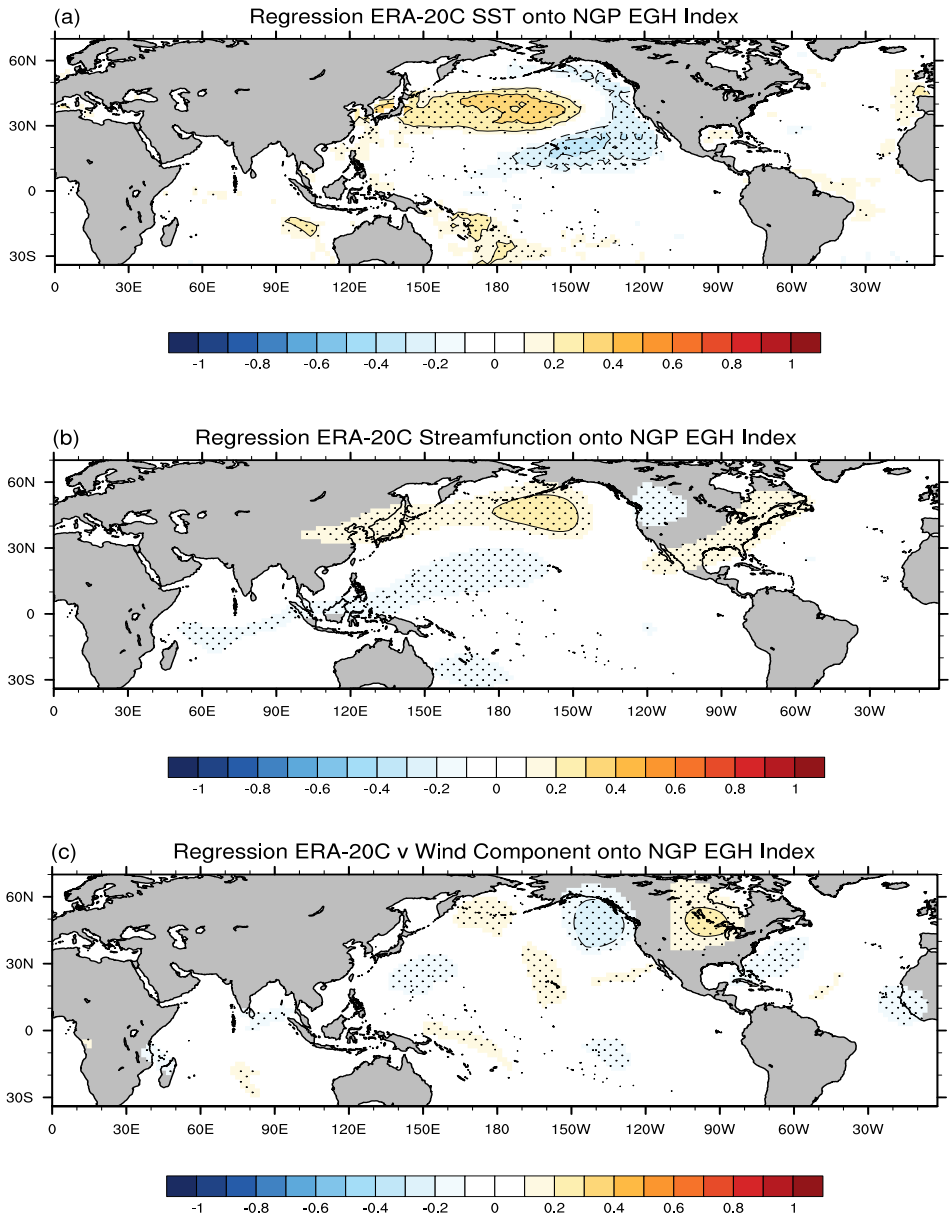

Figure 4.6: Regression of (a) SST (°C), (b) 250 mb streamfunction (m^2s^{-1} *10^{-6}), and (c) 250 mb *u* wind component (ms^{-1}) onto the standardized NGP EGH index, contour interval 0.1°C; zero contour omitted. Stippled regions indicate regression coefficients which are statistically significant at the 90% level.

4.5 Discussion

The diagnosis of GP pluvial years was completed using composite analysis of various atmospheric and surface fields from the ERA-20C dataset. In the SGP, pluvial years were characterized by significant SST anomalies in the tropical Pacific (Fig. 4.2a,3,5a). However, while previous work showed links between *eastern* tropical Pacific SST anomalies (canonical ENSO signal) and precipitation variability in the GP (Ting and Wang 1997; Yang et al. 2007; Hu and Huang 2009; Findell and Delworth 2010; Hunt 2010; Cook et al. 2011), the results suggest a link between excess precipitation on annual time scales and *central tropical Pacific* SST anomalies.

Streamfunction anomalies (Fig. 4.3) detail an "atmospheric bridge" (Lau 1997; Alexander et al. 2002) which connects the warm SST anomalies to North Pacific climate anomalies, including a southward shift in the jet stream and the subsequent enhancement of the frequency of GP synoptic waves during *Pattern* pluvial years. However, the atmospheric response to a warm ENSO event is a stationary wave pattern that is directed to the east as it goes higher in latitude, whereas the response seen during *Pattern* pluvial years is located directly north of the main anomaly center analyzed in the SST composites. This atmospheric response is typically associated with CP warm SST periods (Livezey et al. 1997; Ashok et al. 2007; Fu et al. 2013).

The magnitude and structure of the streamfunction anomalies in the results compare well with previous works on CP ENSO teleconnections with NH atmospheric regimes (e.g., Livezey et al. 1997; Ashok et al. 2007; Graf and Zanchettin, 2012; Fu et al. 2013). Indeed, SGP *Pattern* pluvial year streamfunction anomalies and those streamfunction anomalies linearly related to variability in the Niño 4 index (a proxy for central tropical Pacific SST anomalies) are markedly similar to one another (Figure 4.7; spatial correlation of the two patterns is $r = 0.96$). Further, the response in the atmosphere to the CP SST anomalies is a ridge to the north of the tropical Pacific

and a trough over the north Pacific as noted in the SGP *Pattern* pluvial results. These anomalous atmospheric height patterns cause an anomalous shift of the Pacific jet stream to the south. This shift in the jet stream shifts synoptic wave activity towards the southern United States, as the jet stream acts as the primary guide for synoptic waves across the Pacific Ocean basin (Branstator and Teng 2017). Hence, the results suggest a link between the atmospheric anomalies seen in the SGP *Pattern* pluvial year analysis and the SST anomalies seen in the central tropical Pacific during SGP *Pattern* pluvial years.

During NGP pluvial years, no clear Pacific SST anomaly signal emerges in all of the analyses. The NGP SST *Pattern* composites (Fig. 4.4) and the regression coefficient plot (Fig. 4.6a) both showed positive signals over the north central Pacific, the KOE region and the eastern-tropical Pacific, while the above average synoptic wave intensity pluvial years composite showed negative anomalies over the KOE region with more significant warm anomalies over the tropical Pacific. While previous studies have shown a possible connection between the tropical Pacific and NGP precipitation, the results do not show a clear pathway for such a connection. Instead, the seasonally-persistent NGP *Pattern* pluvial year tropical *Atlantic* SST signal is the unique feature seen during these NGP pluvial years. SST anomalies in the Caribbean and Gulf of Mexico contribute positively to moisture transport into the central United States via an amplified LLJ (e.g., Wang 2007; Wang and Lee 2007; Martin and Schumacher 2011). However, connections between those SST anomalies and tropical Atlantic are less clear. For example, Kushnir et al. (2010) found that tropical north Atlantic positive SST anomalies reduce the strength of the north Atlantic subtropical high and thus *weaken* moisture flow into the United States. Thus, while the statistical analysis indicates that the tropical Atlantic SST anomalies could be playing a role, building a physical connection between the tropical Atlantic and the NGP requires further analysis.

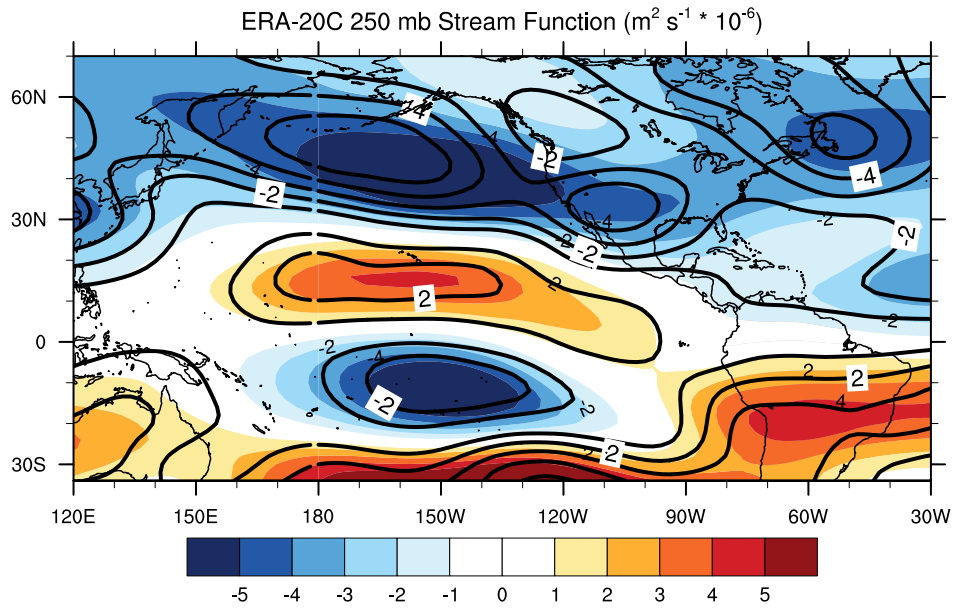

Figure 4.7: 250 mb Streamfunction contours for SGP *Pattern* pluvial years and color shading for the linear regression of the global streamfunction field onto the Niño 4 Index. Contours and color shading was plotted between -5 and 5 every 1 $m^2 s^{-1} * 10^{-6}$.

The NGP streamfunction analyses yield different atmospheric flow patterns during respective years. The annual NGP streamfunction anomaly *Pattern* composite (Fig. 4.4a) features only significant anomalies in the northwestern United States owing to the strong height anomalies that define the NGP pluvial pattern. A positive streamfunction anomaly (Fig. 4.6b) is seen over the North Pacific with a negative signal over the northwestern United States. These features link well with the North Central Pacific SST anomalies seen in the *Pattern* composite and regression plot. SST anomalies in the KOE region are known to anchor the Pacific jet stream further north and thus maintain a consistent synoptic wave signal over the region (Kwon et al. 2010; Ma et al. 2015, 2017). Thus, the SST anomalies could induce increased latent heat release, which would drive anomalously high heights across that region and force the jet stream northward, maintaining a Pacific jet that is located in the northern latitudes.

`

In the SGP, the Chapter 3 atmospheric pattern associated with pluvial years shows a distinct SST and teleconnection signal connected to the tropical Pacific, a schematic of which is shown in Figure 4.8. The most important features of pluvial years in the SGP driven by anomalous synoptic conditions are the increased frequency of synoptic waves over the southwestern United States in association with the location of the significant central tropical Pacific SST anomalies.

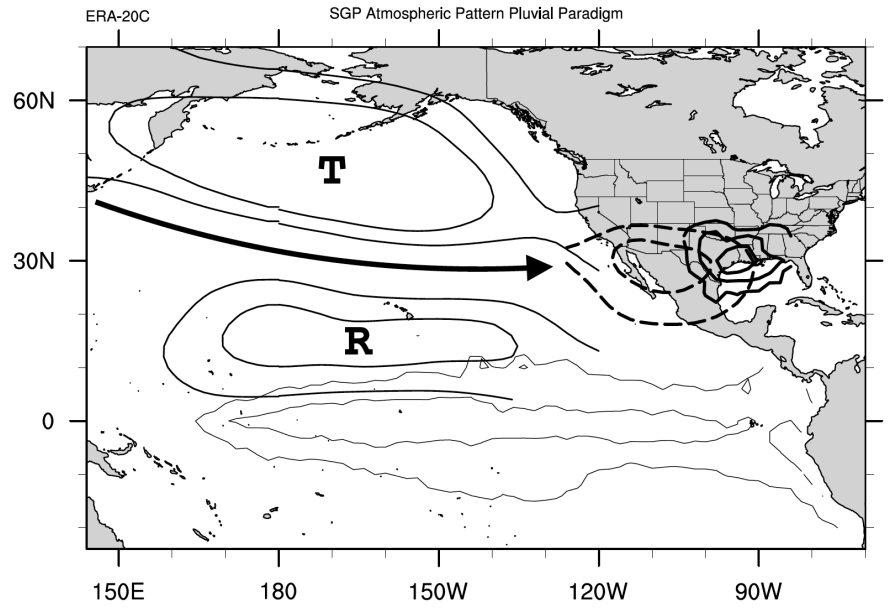

For the NGP it is difficult to synthesize the results into single paradigm given the results differ significantly for each different analysis method. The inconsistent results within the NGP *Pattern* pluvial year analysis show the lack of a link between *Pattern* pluvial years and large-scale signals. Given the seasonality of pluvial years in the NGP (Christian et al. 2015), the excessive

precipitation in this region may be more linked to anomalous convective events than large-scale low-frequency climate modes. Thus, further investigation into NGP pluvial years on shorter time scales using reanalysis datasets with spatial resolutions in which convection is better resolved would aid in diagnosing NGP pluvial years.

Finally, the atmospheric signals (namely the EGH and streamfunction anomaly signals) for NGP and SGP *Pattern* pluvial years found in Chapter 3 and this study can now be diagnosed within different datasets, namely global climate model simulations. Analysis of model simulations under present climate conditions can be used to validate the results reported here and in Chapter 3. Furthermore, using simulations of future climate change, one can determine the possible effects of climate variability and change on GP pluvial years and GP precipitation variability. Additionally, this work can be used for operational forecasting including an analysis of hindcast model simulations. Lastly, though the focus of this work is on longer time scales, it can be adapted for subseasonal to seasonal investigations of GP pluvial years. Being able to accurately simulate and forecast pluvial events in the GP would greatly improve the use of available water resources scenarios and aid in planning for future water use.

Chapter 5

Southern Great Plains Pluvial Year Case Study

5.1 Introduction

While an investigation of GP pluvial years from a climatological standpoint is useful to diagnose the instantaneous drivers and conditions during such years, an investigation of an independent pluvial year using the results from the climatological investigation will aid the validation of the results. Given the period of the ERA-20C data used in Chapters 3 and 4 spanned 1926 to 2010, there are limited years outside of this period to utilize. However, during 2015, the SGP was impacted by a strong pluvial (Fig. 5.1) which caused record-breaking rainfall over portions of the SGP region, especially during the month of May (Duchon et al. 2017). As a result, numerous flood events occurred across portions of Oklahoma and Texas, causing an estimated $2.5 billion in damages across the region (NOAA National Centers for Environmental Information "U.S. Billion-Dollar Weather and Climate Disasters 1980-2018" available at https://www.ncdc.noaa.gov/billions/events.pdf). Further, beyond May, precipitation accumulated throughout the year yielding record-breaking annual totals in Oklahoma (Fig. 5.2) whereby for the PRISM dataset, the annual total across the SGP was 52% above normal and via the methodology described in Chapter 3 for defining a pluvial (Eqn. 3.1), 2015 was the largest above average precipitation year within the PRISM dataset for the SGP.

Because 2015 is not contained within the ERA-20C dataset used to describe the climatological analysis of SGP pluvial years, 2015 is an excellent period to test the SGP *Pattern* pluvial year framework. To this end, this case study explored the same fields used in Chapters 3 and 4, namely EGH, *u* and *v* wind components, SSTs and stream function on an annual and

seasonal basis for 2015. In addition, an analysis of surface conditions during the year was completed to aid in the investigation of land-atmosphere coupling during 2015. Finally, an analysis of a non-Pattern pluvial year within the SGP domain (2007) was examined to contrast with the 2015 SGP pluvial year results. In all, the goal of this study was to investigate the 2015 SGP pluvial and validate the SGP *Pattern* pluvial framework.

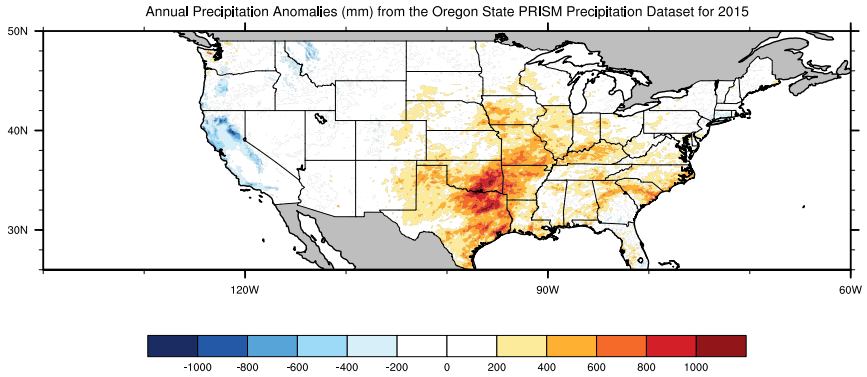

Figure. 5.1: Annual precipitation anomalies (mm) for 2015 from the Oregon State PRISM precipitation dataset.

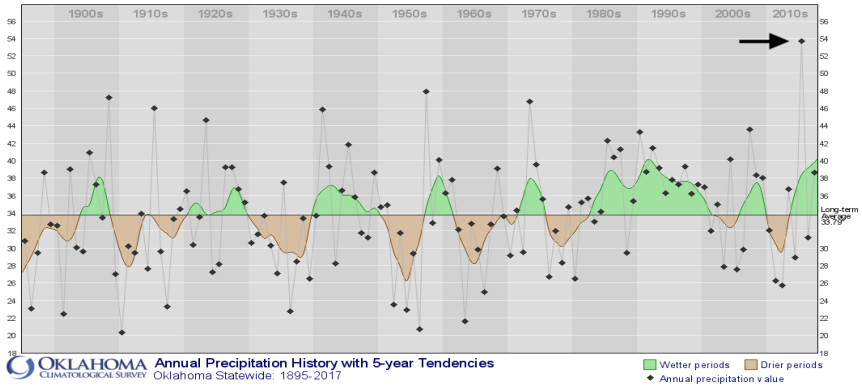

Figure 5.2: Statewide average annual precipitation record (in inches) for Oklahoma measured by Cooperative Observer Network (COOP) from 1895 to 2017. The solid black line represents the statewide climatological average, the dots represent the observation data points and the green/brown shaded regions are the 5-year running average of precipitation. The arrow indicates the 2015 precipitation statewide average for Oklahoma.

5.2 Atmospheric and surface datasets

The ECMWF Reanalysis Interim (ERA-Interim; Dee et al. 2011) dataset was chosen for this case study given it contains the same dynamical core, but with different assimilation observations and temporal scope. The ERA-Interim dataset has a temporal period from 1979 to present, utilizing a 4D-Variational assimilation system with a variety of observations described within Dee et al. 2011. While the ERA-20C and ERA-Interim utilize different versions of the dynamical core and assimilation system, they both utilize the ECMWF Integrated Forecast System (IFS) model as the backbone of the reanalysis system. All atmospheric analyses within this component of the study will be from the ERA-Interim dataset focused the same atmospheric and surface fields seen in Chapters 3 and 4.

5.3 Synoptic Diagnosis of the Excessive Precipitation During 2015

As was described in Chapter 3, EGH was used instead of Geopotential Height owing to EGH's "representation of transient zonal inhomogeneities which distinguish wave features from the zonal-mean flow pattern" (Randall 2014), which allows for an investigation of synoptic patterns that cause weather events. In 2015, EGH anomalies (Fig. 5.3a) depict an area of negative EGH anomalies over the southwestern United States with a larger area of negative anomalies over the northern Pacific Ocean basin, north of Hawaii. Positive EGH anomalies dominate over Alaska, northwestern Canada and China, with lesser magnitude positive anomalies across the southeastern United States. This pattern is reminiscent of the signals seen in the SGP *Pattern* pluvial year EGH composites (Fig. 3.4c). However, the geopotential height field (Fig. 5.3b) allows for an analysis of stationary wave features and during 2015 a large band of positive anomalies was seen across the entire northern hemisphere, with small areas of lower height anomalies across the central North Pacific Ocean and just off the coast of the southwestern United States. Thus, the pattern of a ridge

over the tropical Pacific, lowered heights north of Hawaii was evident, but weaker than expected given the fit of the EGH anomaly field (Fig. 5.3a) with the SGP *Pattern* pluvial year EGH anomaly field (Fig. 3.4c).

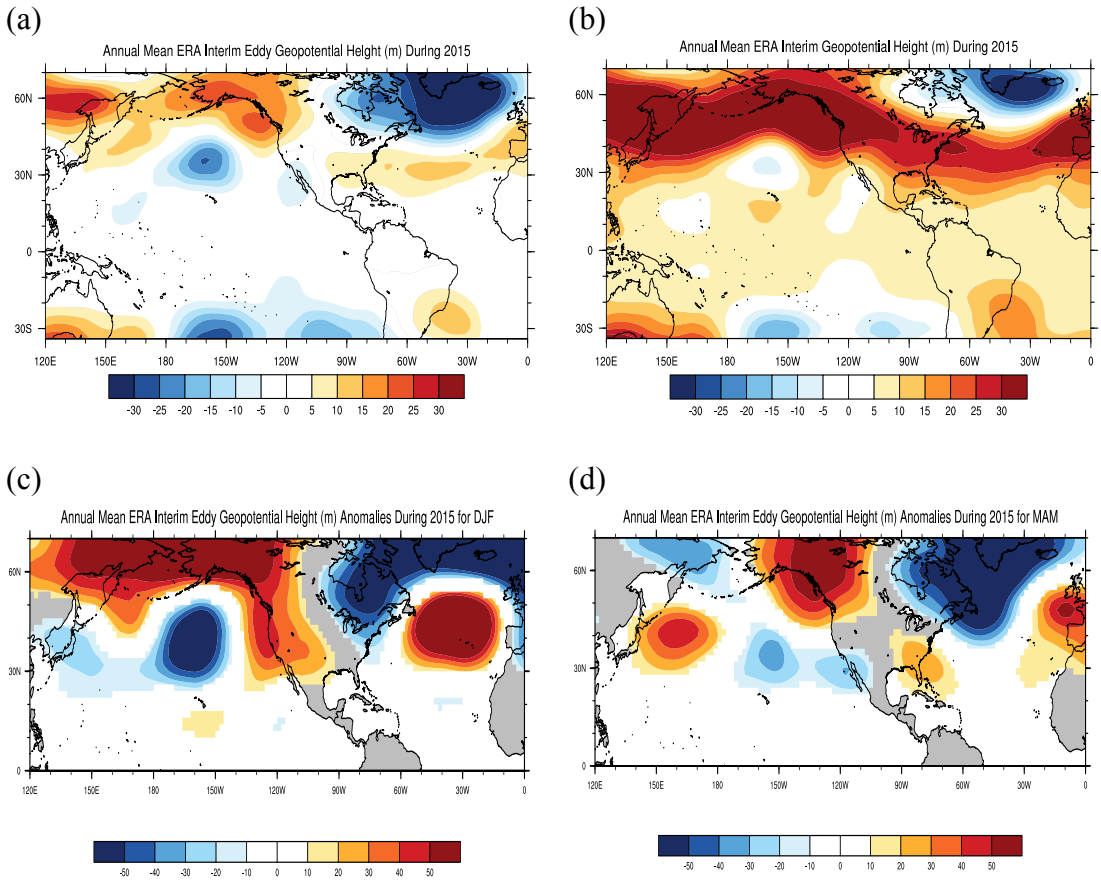

Figure 5.3: Height anomalies for 2015 measure in meters, (a) eddy (zonal mean removed) geoptential height (EGH) anomalies, (b) geoptential height anomalies, (c) EGH anomalies for winter (DJF) and (d) spring (MAM). Contoured from -50 to 50 every 10 meters.

During the winter of 2015, a large magnitude ridge occurred over the western coast of North America (Fig. 5.3c), largely blocking the synoptic waves over the North Pacific Ocean basin from impacting the United States. As such, the pattern appeared to be blocked during this season and had little influence on SGP precipitation. However, during the spring (Fig. 5.3d), the EGH anomaly pattern suggests that a Rex block (Rex 1950) was in place over western North America given the positive EGH anomalies over the northeastern Pacific and the negative EGH anomalies

`

over the east central North Pacific. This stagnated the atmospheric flow pattern and locked the trough over the southern United States providing ample, persistent forcing for precipitation observed during May 2015.

The *u* wind component anomalies (Fig. 5.4a), detail a different picture compared to the findings from SGP *Pattern* pluvial years in Chapter 3 (Fig. 3.6a). Negative *u* wind component anomalies were analyzed over the North Pacific Ocean that stretch across the southwestern and southern United States. Positive *u* wind component anomalies occurred across the central North Pacific Ocean, however, the spatial extent of the anomalies were not as large compared to the *u* wind component anomalies from the composite of all SGP *Pattern* pluvial years (Fig. 3.6a). The *v* wind component anomalies (Fig. 5.4b) differ from the signal seen during *Pattern* pluvial years as well (Fig. 3.5a). Positive *v* wind component anomalies are analyzed across most of the globe, with an area of increased positive anomalies seen over the central United States. This area of positive anomalies matches well with the center of positive anomalies over the United States during SGP *Pattern* pluvial years (Fig. 3.5a), however, the lack of negative anomalies during 2015 within this analysis denotes the lack of a strong influence on the background flow by the synoptic wave regime.

To further investigate these patterns of wind anomalies, the zonal mean of each anomaly field was removed from the time mean anomalies. These eddy wind component anomalies detail the influence of the transient eddies on the background flow during 2015. While the eddy *u* wind component anomalies (Fig. 5.4c) were similar to the *u* wind component anomalies seen in Figure 5.4a, the eddy *v* wind component anomalies (Fig. 5.4d) do not remain the same. While the positive area of *v* wind anomalies remained over the central United States, negative eddy *v* wind anomalies occurred to the west over the eastern Pacific Ocean. Thus, from the eddy wind component analyses,

these transient synoptic waves did influence the background flow during this year, however, the flow perturbation did not occur on time scales long enough to influence the annual mean fields. Further, it does not appear that the *u* wind field was influenced by these transient eddies, as the two analyses were largely the same. As such the main influence on the *u* wind field was likely the stationary wave pattern more evident in the annual mean anomaly composites shown in Figure 5.3b. The lack of a strong negative anomaly evident in the stationary wave pattern would facilitate the lack of a strong response in the *u* wind component anomaly field, as the anomaly created by the enhanced ridge was dampened by the lack of a strong gradient of height anomalies owing to the lack of strong negative height anomalies to the north. Thus, the spatial extent of the positive *u* wind component anomalies during 2015 were diminished compared to those seen during SGP *Pattern* pluvial years (Fig. 3.6a).

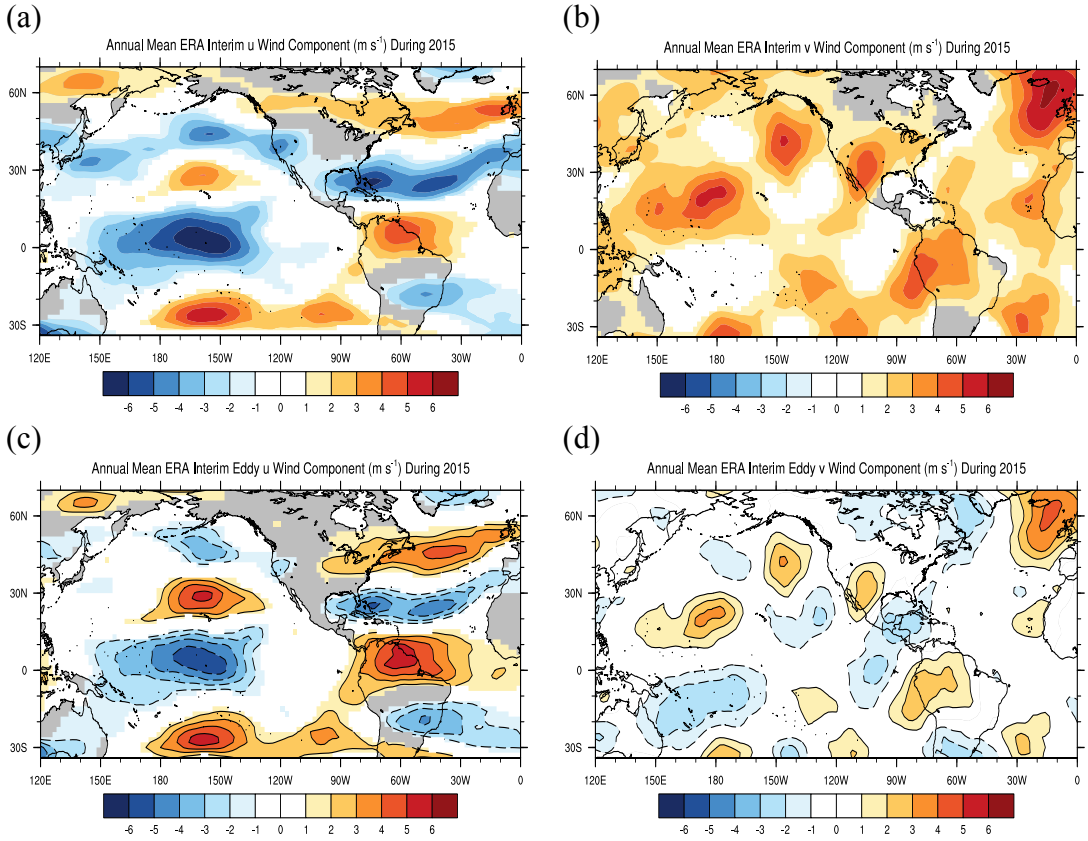

Figure 5.4: Wind component anomalies for 2015 measure in m s^{-1}, (a) *u* wind component anomalies, (b) *v* wind component anomalies, (c) eddy (zonal mean removed) *u* wind component anomalies and (d) eddy (zonal mean removed) *v* wind component anomalies. Contoured from -6 to 6 every 1 m s^{-1}.

5.4 Climate Scale Diagnosis of the 2015 Southern Great Plains Pluvial

To further investigate the stationary wave field, an investigation into SSTs and stream function during 2015 was completed, similar to the analysis of Chapter 4. This was completed to diagnose the impacts of the SSTs on the atmospheric signals observed from the synoptic analysis. During 2015, SSTs (Fig. 5.5a) were anomalously warm across the tropical Pacific and the eastern north Pacific along the western North American coastline. However, the strong canonical El Niño during 2015 did not develop until later that year after the month of May. This can be seen via the seasonal SST analyses, as during winter (DJF; Fig. 5.5b) and spring (MAM; Fig. 5.5c) warm SST

`

anomalies were mostly contained in the central Pacific. Conversely, during the summer (JJA; Fig. 5.5d) and fall (SON; Fig. 5.5e), warm anomalies were analyzed in the eastern tropical Pacific Ocean which denote the strong 2015 canonical El Niño event.

Annual mean stream function anomalies during 2015 (Fig. 5.5) show a deeper ridge north of the tropical Pacific with a slight strengthening of the North Pacific trough. The negative stream function anomalies across the north Pacific were not as large in magnitude as within the SGP *Pattern* pluvial year composites (Fig. 4.3a), but the signal was present during 2015 in the North Pacific. In the seasonal analyses, the southern ridge to northern trough signal was observed during the winter (Fig. 5.5b) and spring (Fig. 5.5c), when SST anomalies are more supportive of the CP/atmospheric teleconnection described in Chapter 4 (Fig. 4.8). Again, however, the stream function anomaly signals seen during the summer (Fig. 5.5d) and fall (Fig. 5.5e) were not consistent with the *Pattern* signal.

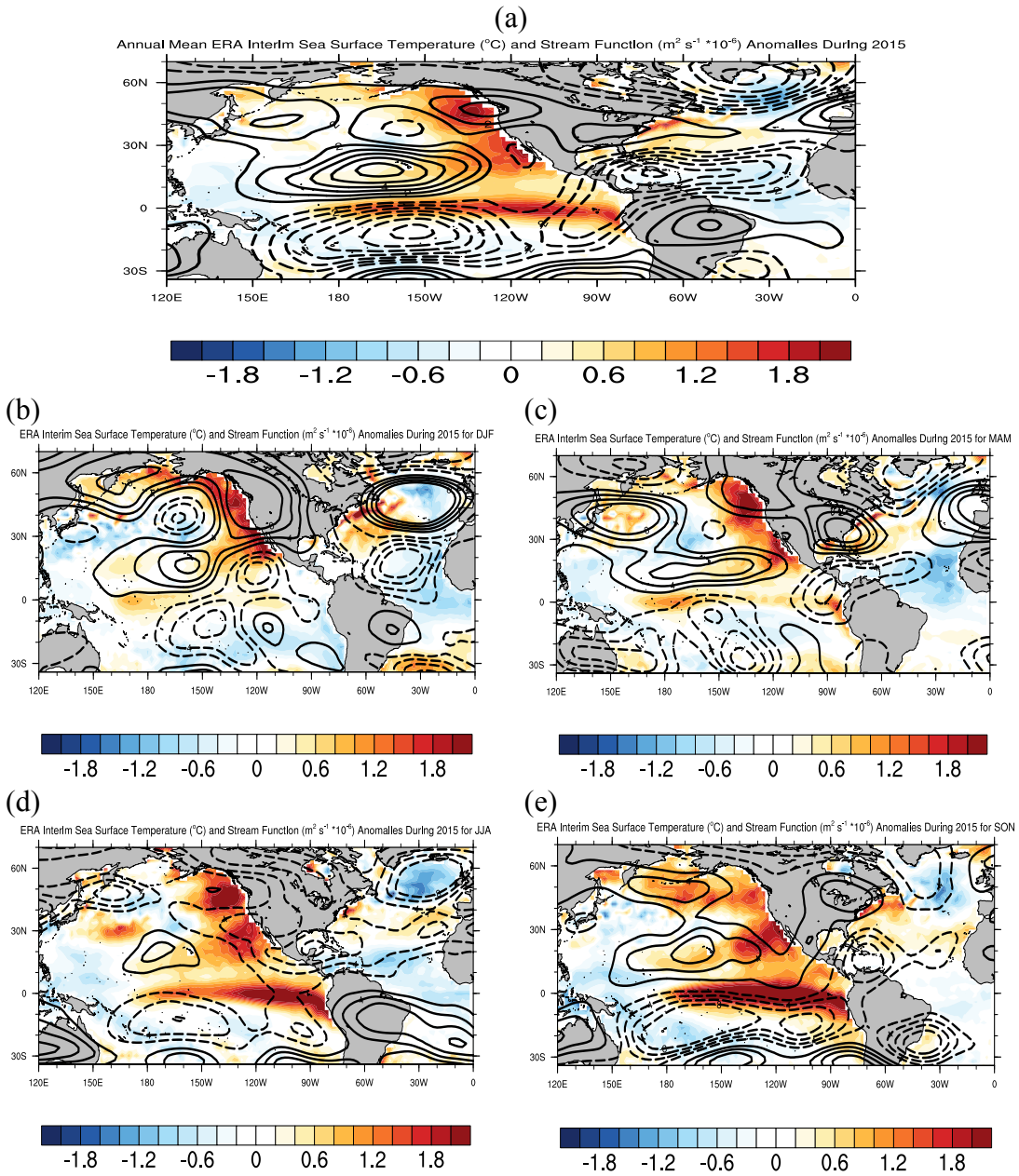

Figure 5.5: Sea surface temperature (°C) and stream function ($m^2\ s^{-1} * 10^{-6}$) anomalies during 2015 for (a) annual mean, (b) winter (DJF) mean, (c) spring (MAM) mean, (d) summer (JJA) mean, and (e) fall (SON) mean. Sea surface temperature is plotted from -2 to 2 every 0.2 (°C) and stream function is contoured from -8 to 8 every 1 $m^2\ s^{-1} * 10^{-6}$.

5.5 Discussion

This study demonstrated via the ERA-Interim dataset that 2015 fits the SGP *Pattern* pluvial year framework described in Chapters 3 and 4. Through analysis of EGH, SST, streamfunction and wind components, the anomaly signals observed in these fields display key features that describe the average anomaly fields across all SGP *Pattern* pluvial years. Conversely, while 2007 was also a pluvial year, it does not fit into the SGP *Pattern* pluvial year framework. Anomalous precipitation (Fig. 5.6a) during 2007 fell across much of the GP, with larger positive anomalies across Oklahoma and Texas. The 2007 EGH anomaly field (Fig. 5.6b) yielded a large area of negative EGH anomalies across the central Pacific, with a negative EGH signal over the Bay of California. Positive EGH anomaly signals stretched across most of the north hemisphere, with an area of higher magnitude positive EGH anomalies over the northwestern United States. With neutral to slightly higher EGHs over the SGP, specific atmospheric signatures associated with enhanced precipitation over the SGP and the key feature of a SGP *Pattern* pluvial year, the closed negative EGH anomaly area over the southwestern United States, did not occur. In terms of a climate signal, the 2007 SST and streamfunction anomalies (Fig. 5.6c) were very different when compared to 2015 and the SGP *Pattern* pluvial year framework. Instead of positive SST anomalies across the tropical Pacific, negative SST anomalies occurred across the tropical Pacific in a pattern consistent of a canonical La Niña. This feature is typically associated with drought conditions across the GP (e.g., Schubert et al. 2009; Findell and Delworth 2010; Wang et al. 2010; Seager and Hoerling 2014; Schubert et al. 2016). However the La Niña episode did not develop until later in the year and the typical atmospheric conditions forced by La Niña periods were not prevalent during the period when the majority of the precipitation occurred. Thus, the EGH, SST and streamfunction anomalies demonstrated that the excessive rainfall over the SGP in 2007 did not

occur owing to large-scale dynamic atmospheric flow anomalies. Overall, these results detail why 2007 was not included in the SGP *Pattern* pluvial year analysis while 2015 fits into that categorization. However, this does not explain the processes that describe why an above average precipitation regime existed in 2007. While this research focuses on the anomalous atmospheric component of pluvial years in the GP, focus on these non-*Pattern* pluvial years and their drivers should be completed to detail the causation of all GP pluvial years.

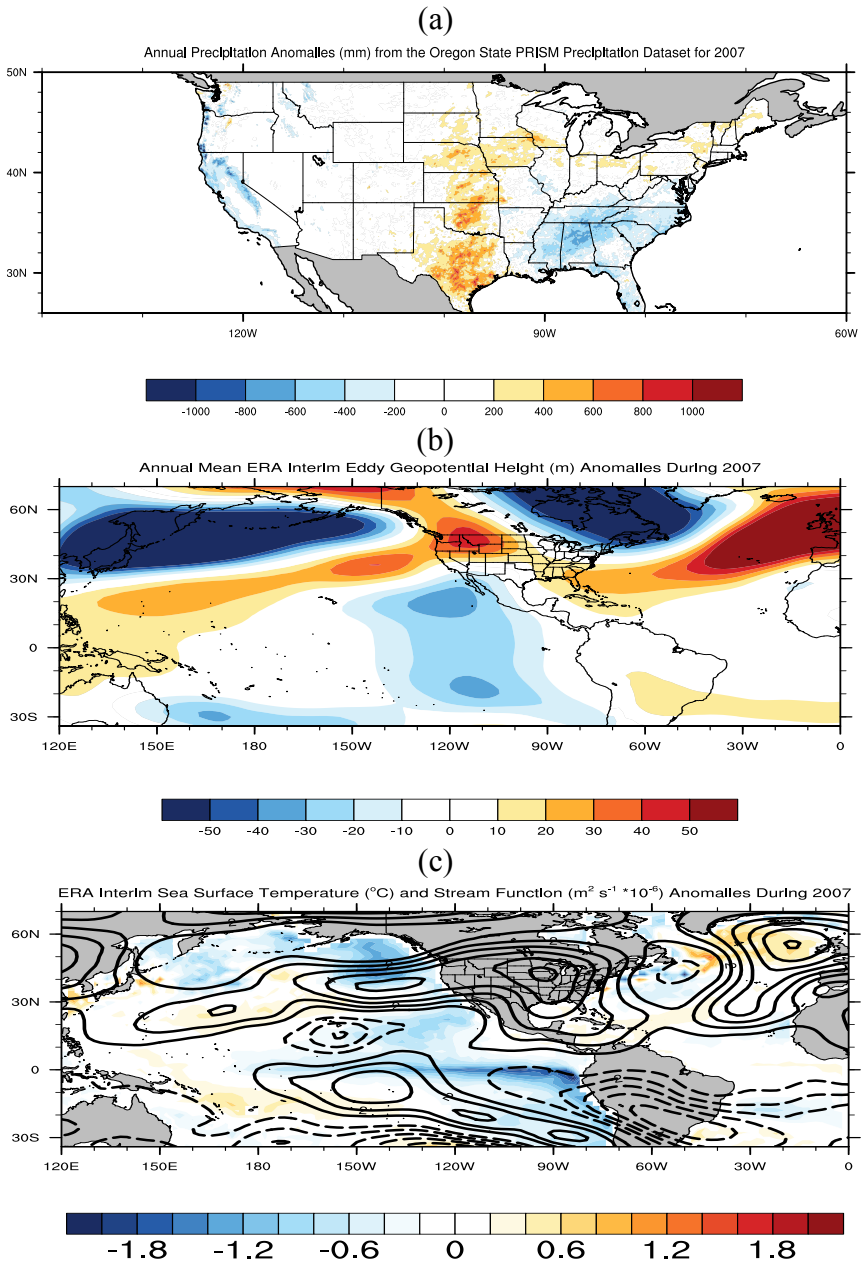

Figure 5.6: Analyses for 2007. (a) Annual precipitation anomalies (mm) for 2007 form the Oregon State PRISM precipitation dataset, (b) eddy geopotential height (m) anomalies for 2007, contoured from -50 to 50 every 10 meters, (c) annual mean sea surface temperature (°C) and stream function ($m^2\ s^{-1} * 10^{-6}$) anomalies for 2007 with sea surface temperature plotted from -2 to 2 every 0.2 (°C) and stream function contoured from -8 to 8 every 1 $m^2\ s^{-1} * 10^{-6}$.

Chapter 6

Summary and Conclusions

6.1 Introduction

Whether for agriculture, society, ecosystem services, or weather, water is crucial to the sustainability of the GP region. Thus, it is critical to understand the variability of water within the region to be able to adapt to changing water availability. Yet, without a complete understanding of the GP climate addressing these changes is not possible. Thus, the goal of this work was to develop a more complete understanding of the GP climate from a local to global standpoint to understand the implications on water availability in the GP into the future. This study addressed the knowledge gap in three parts;

1. Analyze the annual climate of the GP,
2. Developing an understanding of the drivers of the anomalous excessive precipitation during NGP and SGP pluvial years,
3. Diagnosing the anomaly signals found in (2) to quantify the predictive (climate) anomaly signals associated with NGP or SGP pluvial years.

6.2 Analysis of the Great Plains Annual Climate

The impact of the shifts between temperature and precipitation maxima is critical to the climate of the GP region. Changes to the growing season of the region impact ecosystem health, water resources, and socioeconomic viability and sustainability. For example, small shifts in the timing of maximum temperature (e.g., Bertin 2008; Menzel et al. 2006; Hughes 2000; Menzel 2003; Cleland et al. 2007; Badeck et al. 2004) and precipitation (Méndez-Barroso et al. 2009;

Vivoni et al. 2008; Di et al. 1994; Fay 2009) incur significant changes to plant and crop phenology. This results in changes in water resource management (i.e., irrigation, land management, etc.) along with the timing of seeding and harvesting (Terjung et al. 1984; Rosenzweig 1990) to maintain the current ecosystem and level of agricultural production. However, not all shifts in ADI could impact the ecosystem negatively. Lower values of ADI could indicate higher soil moisture values during the peak time of water stress, or when temperatures begin to peak, thus mitigating the impact of the peak temperatures on the ecosystem (Schlenker and Roberts 2009).

These results provide an insight into the changes that are occurring to the regional climate system within the GP. While the synoptic patterns for precipitation and temperature over the region are better understood, the influences of other critical features that drive climatological processes such as land-atmosphere interactions are less so, especially for precipitation (Alfieri et al. 2008; Haugland and Crawford 2005; André et al. 1990; Pielke et al. 1991; Koster et al. 2004). Future work is likely to be directed into two different areas: 1) investigating the ADI in terms of reanalysis and model output and 2) investigating the connection between plant vigor and health (Vegetation indices (e.g., NDVI, EVI), Net Primary Productivity (NPP) or Gross Primary Productivity (GPP)) of terrestrial ecosystems (Zhang et al., 2016). Analysis of model and reanalysis output of ADI values and trends will allow for further quantification of the causes of ADI variability and the changes this feature could incur in the future. Further the analysis of modeled ADI across the GP would allow for features seen in the observational dataset identified within this study to be investigated in more detail, specifically the differences observed between positive and negative ADI regimes and the causes of the increased variability of ADI. Additionally, while the link between this feature of the GP climate and the ecosystem is intuitive and supported by literature,

quantifying it using vegetation indices or vegetation health statistics could provide insights into the direct effect the shifts in the ADI detailed by this study are having on the ecosystem.

Whether the noted shifts in the ADI are being caused by human influences or natural variability cannot be determined within the scope of this study. However, the duration of these trends along with the specific signals noted after 1950 in the variability of ADI yield evidence that a change has occurred within the natural variability likely impacted by anthropogenic influences. Further, the results are consistent with Christian et al. (2015) and Weaver et al. (2016) which both demonstrated increased variability of precipitation in the GP domain.

6.3 Primary Atmospheric Drivers of Great Plain Pluvial Years

The primary large-scale atmospheric drivers of pluvial years over the Southern Great Plains (SGP) and Northern Great Plains (NGP) were investigated via composite analysis of atmospheric reanalysis products. The goal of this study was to generalize previous works on GP pluvial periods, which focused on specific pluvial events, and develop a more meteorological framework of understanding of GP precipitation variability. Subsetting the pluvial years into the *Pattern* and *Break* composite analyses illustrated that (a) the associated atmospheric patterns are indeed features of the pluvial years and not an artifact of extreme events in the *Total* composites and (b) changing statistics of GP precipitation have minimal impact on the atmospheric driving patterns identified in this study. The results were tested with several atmospheric datasets and found to be robust findings, adding confidence to the conclusions drawn from this work (e.g., Fig. 3.7).

The study yielded two distinct annual-mean atmospheric patterns that are linked to pluvial events in the subregions of the GP. The SGP pluvial pattern consists of a closed area of negative height anomalies across the SW United States with the wind anomalies showing a coherent

hemispheric wavetrain pattern and an enhanced southward shift in the jet stream associated with the passage of storm systems (Fig. 3.4a and 3.4c). This pattern would lead to enhanced moisture flow from the south within the boundary layer leading to a higher chance of heavy precipitation (Fig. 3.8a). However, enhanced moisture transport is not *necessary* to drive pluvial years, but rather an increase in the number of precipitation events themselves. The lack of a relevant intensity signal in moisture fluxes in the SGP is likely due to the larger variability in precipitation in the SGP (Fig. 3.2) and thus the propensity for heavy precipitation events in the SGP from year to year. The pattern of EGH anomalies analyzed through the *Pattern* composite analysis is a common feature in daily heavy precipitation events over the SGP (Zhao et al. 2017) and is seen in the daily heavy precipitation event results as well.

The NGP pattern features negative height anomalies over the NW United States and Southern Canada with an eastward extension of the North Pacific jet (Figs. 3.4b and 3.4d). The NGP EGH pattern is consistent with enhanced moisture advection into the NGP (Fig. 3.8b). This jet extension aids in the propagation of synoptic waves towards the NGP region. The NGP *v* wind anomalies (Fig. 3.5b) depict a pattern of couplets across the northern United States; however the pattern is less coherent than in the SGP composites and regionally confined. Thus, the passage of more amplified synoptic waves over the northern United States, rather than the occurrence of frequent synoptic events important to SGP pluvial years, likely drives the heavy precipitation during NGP pluvial years. These stronger storm systems also provide enhanced moisture transport from the Gulf of Mexico causing even more precipitation to occur during the year. The difference in synoptic activity can be seen in the daily heavy precipitation analysis, as comparisons between the SGP and NGP results (Fig. 3.8) show that the magnitude of the EGH anomalies in the NGP are higher than that of the SGP anomalies.

`

From a meteorological standpoint, the results presented in this work detail a complex atmospheric pattern that is the initial step in understanding the wet side of GP precipitation variability. From a water resources standpoint, the work details a pathway to understanding the processes that bring excess water to the region. Though the study represents an initial step in diagnosing these atmospheric patterns responsible for pluvial years over the GP, the results present a possible framework for predicting excess precipitation periods over the GP region. As of now, such long-range precipitation forecasts from the NOAA Climate Prediction Center, for example, rely on statistical models relating SST, trends and other long-time-scale signals over the United States (e.g., O'Lenic et al. 2008). The GP pluvial results present a new opportunity to explore predicting GP pluvial years, which will be explored in future work.

Understanding GP precipitation variability is a difficult challenge, from the lack of previous research into the wet side of precipitation variability (Cook et al. 2011), to the multifaceted drivers of precipitation over the region such as land-atmosphere interactions (Mo et al. 1997; Koster et al. 2000; Schubert et al. 2004), internal atmospheric variability (Ruiz-Barradas and Nigam 2005; Seager et al. 2014), and climate teleconnections (e.g., Trenberth and Branstator 1992; Schubert et al. 2004; Seager et al. 2005; Cook et al. 2008; Seager and Hoerling 2014). However, variability of water resources is important to the region as agriculture is a dominant component of the regional economy (Fisher et al. 2007). Thus, increasing the current understanding of the causes of GP precipitation variability is key to successfully managing and maintaining the socioeconomic and ecosystem success of the GP region.

The results presented in this study advance the current knowledge in understanding one facet of the GP precipitation variability that has largely gone unstudied. Previous studies have investigated pluvial/flood cases (Trenberth and Guillmot 1996; Cook et al. 2011) and pluvials on

seasonal time scales (Mo et al 1997; Hu and Huang 2009) with a focus on eddy frequency and intensity, moisture flux, flow patterns and associated climate patterns. My results largely agree with their findings – enhanced synoptic wave activity, either in terms of frequency (SGP) or intensity (NGP), enhanced moisture transport during precipitation events, and anomalous flow patterns over the northern Pacific Ocean all play a role in driving GP pluvial events. However, this study extends the validity of these results through analysis of annual reanalysis data spanning over 80 years, a feature lacking in all other studies. Thus, while similar results as the other studies were found, this work advances the understanding of pluvial events by providing a more robust analysis on their occurrences.

Some caveats for this study exist. First, this study relied on composite analyses for distinguishing the associated atmospheric patterns with the pluvial years. Other statistical tools such as empirical orthogonal functions (EOF) / principal component analysis (PCA) could offer insights into the data and the covariability between GP precipitation and geophysical fields that were not seen within this study. Further investigation using linear and nonlinear methods will be completed as part of future work in further diagnosing the patterns found in this study. Secondly, these results are mainly focused on a subset of pluvial years, and as such, the atmospheric patterns identified in these analyses cannot fully explain the occurrence of all pluvial events. The lack of any significant atmospheric signal in pluvial years not included within the *Pattern* composites highlights the complex nature of the variability of precipitation over the GP. Additionally, the non-pluvial years that were found to meet the criteria for the *Pattern* composite (EGH anomaly index value over 0.5) need to be further investigated and tested. Determining the reasons why these years matched the pattern found in the *Total* composite yet did not have excessive precipitation could further enhance the understanding of GP precipitation variability.

`

Overall, the results of this study bridge the gap between past studies by demonstrating the linkage between the atmospheric patterns contributing to heavy precipitation events and annual GP precipitation variability. Analysis into the causes of the SGP and NGP patterns is necessary to apply this work to predictability of pluvial years in the GP. This predictability aspect is tied to predicting both frequency and intensity of storm systems, as both play a role in different regions of the GP. Owing to the synoptic nature of these waves, this study also supports the need for more studies in subseasonal-to-seasonal (S2S) forecasting and predictions, an emerging area of importance in the weather and climate communities.

6.4 Links Between Great Plain Pluvial Years and Pacific Sea Surface Temperatures

The overall goal of this section was to (1) diagnose the atmospheric signals found in Chapter 3, (2) investigate the critical atmospheric and oceanic features seen during *Pattern* pluvial years, and (3) determine whether a robust, predictive SST signature existed for both the SGP and NGP domains. Through the analysis, it was demonstrated that:

- The frequency of synoptic waves over the southwestern United States is the defining feature for SGP *Pattern* pluvial years.
- Streamfunction composites during SGP *Pattern* pluvial years revealed that an anomalous stationary wave feature over the central and north Pacific Ocean basin explains the shift in the Pacific jet stream, which subsequently increases the frequency of synoptic waves in the southwestern United Sates during these years.
- Warm SST anomalies over the tropical Pacific Ocean were found during *Pattern* pluvial years, showing a link between *central* tropical Pacific warm SST anomalies and SGP excessive precipitation during *Pattern* pluvial years.

`

- Statistical analysis showed that the frequency of synoptic waves over the northwestern United States could be crucial for the occurrence of NGP *Pattern* pluvial years, counter to results from Chapter 3.
- Tropical Pacific and Atlantic SST signals were seen in some NGP pluvial year analyses.

Thus, from these results a framework for explaining the occurrence of SGP *Pattern* pluvial years was developed (Fig. 4.8) while it was not possible to do the same for NGP *Pattern* pluvial years.

Further, with the primary atmospheric drivers of pluvial years diagnosed along with their associated climate signals, comments on the future of GP pluvials can be made. While NGP pluvials are not associated with a known climate signal from this analysis, SGP *Pattern* pluvial years can be associated with CP SST warm anomalies. Thus, the frequency of CP warm SST events would theoretically impact the frequency of SGP *Pattern* pluvial years. With studies noting an increased frequency of CP warm SST events in recent decades (e.g., Ashok et al. 2007; Kao and Yu 2009; Yeh et al. 2009; Yu et al. 2010), this does appear to be the case. Owing to the noted increase in frequency of drought events seen in climate model simulation studies (e.g., Easterling et al. 2000, Dai 2011; Cook et al. 2015), excess precipitation years could become increasingly valuable to the region in terms of restoring water resources. This result fits in line with the noted increase in the variability of precipitation over the GP (Weaver et al. 2016; Chapter 2), which implies that the frequency of drought and pluvial events is increasing. Thus, the increase in pluvial years over the SGP owing to an increase in CP SST warm events could become invaluable for the SGP if the noted future drying prediction proves correct. For the NGP, the reasoning behind why this is occurring still is not answered. The research completed in this project did not provide a conclusive answer as to how NGP pluvial years occur. However, for the SGP, the links between CP SST anomalies, the stationary wave anomalies over the North Pacific Ocean basin, the shift of

the Pacific jet stream and excessive precipitation were more conclusive. Thus, from this work it can be theorized that SGP Pattern pluvial years are increasing in frequency owing to the increased frequency of CP SST anomaly events. However, further research is needed to show that the connection between the increased frequency of SGP pluvial events is valid.

6.5 Southern Great Plains Pluvial Year Case Study

The overall goal of this study was to diagnose the 2015 SGP pluvial year in terms of the results from Chapters 3 and 4, to see if the atmospheric conditions were such that the 2015 SGP pluvial could be fit into the SGP *Pattern* pluvial year framework. To this end, ERA-Interim data was used to analyze the atmospheric and surface conditions during 2015 using the EGH, SST, streamfunction and wind component fields. Results showed that 2015 fits into the SGP *Pattern* pluvial year framework, in terms of the EGH (Fig. 5.3), SST, and streamfunction (Fig. 5.5) anomaly fields. However, the wind component anomalies (Fig. 5.4) did not produce similar signals as those seen during SGP *Pattern* pluvial years. When eddy wind component anomalies were analyzed, eddy *v* wind component anomalies (Fig. 5.4d) showed a similar couplet as that seen during SGP *Pattern* pluvial years, in which the negative EGH anomalies impact the typical meridional flow regime. However, removing the zonal mean from the *u* wind component anomaly field (Fig. 5.4c) did not produce an analysis similar to that of SGP *Pattern* pluvial year *u* wind component anomalies. It was shown that during 2015, large positive height anomalies served to interrupt the anomalous westerly flow typical during these SGP *Pattern* pluvial years through a weakened enhancement of the North Pacific basin trough. However, EGH (Fig. 5.3), SST, and streamfunction anomalies (Fig. 5.5) during 2015 well represented the SGP *Pattern* pluvial year composites seen in Chapters 3 and 4 and thus 2015 is likely a SGP *Pattern* pluvial year. The pluvial

of 2015 was then compared to the SGP pluvial of 2007, a year which was not categorized as a *Pattern* pluvial year. An investigation into EGH (Fig. 5.6b) and SST and streamfunction (Fig. 5.6c) anomalies during 2007 detailed the differences between a SGP non-*Pattern* and SGP *Pattern* pluvial year, with the largest difference being in regards to the SST and streamfunction annual anomalies which were nearly complete opposites. While the drivers of *Pattern* pluvial years were discussed in this work, it is left for future work to further investigate these non-*Pattern* pluvial years to diagnose their drivers.

6.6 Final Remarks

The overall goal of this work was to investigate the GP hydroclimate to more thoroughly understand how changes in climate could impact water resources in the GP region. In accomplishing this task, two features of the GP hydroclimate were investigated: 1) the asynchronous nature between annual temperature and precipitation maxima over the region and 2) annual above average precipitation events (pluvials). The asynchronous nature of temperature and precipitation impacts water availability, especially related to plant physiology, and thus shifts in this feature can impact the growth, maintenance and overall health of the region's ecology. Pluvial events represent the possible recovery of water resources in drought stricken areas, and increased risk of flood events on multiple time-scales, thus they greatly impact the hydroclimate of the GP. This project set about to fill in these gaps in the literature and put these results in the context of the GP hydroclimate to show how local to global changes in the GP climate impact the region's hydroclimate. With the hypothesis of this work stating "shifts in GP and global climate variability will result in changes to the GP hydroclimate" the conclusions of this project have shown that

shifts in the GP and global climate variability impact the GP hydroclimate and thus the hypothesis is accepted.

While results for the analysis of the annual GP climate showed distinct changes in the statistical relationship between temperature and precipitation maxima, this analysis was completed on a larger spatial scale (statewide) and thus these results cannot be used to described smaller scale variability in the GP climate. Investigating ADI on a smaller scale (climate regions, station data, etc.) would provide further insight into the changes of the GP climate and hydroclimate owing to shifts in the ADI. However, the results still can be used to describe how the overall climate in the GP is affecting water availability and the ecology of the region, even with the caveat that these results should not be utilized to describe smaller scale climate without further analysis of ADI across the region.

Results from the second portion of this study identified an atmospheric anomaly pattern that is connected with the excessive precipitation that occurs during NGP and SGP pluvial years. In this, years in which the atmospheric anomaly pattern was identified were separated out to further diagnose this atmospheric signal. Although the investigation focused on these *Pattern* pluvial years, the remaining pluvial years for both the NGP and SGP are still important to diagnose as well. Further, the focus of the results in Chapter 4 and 5 pertained to SGP *Pattern* pluvial years, as the methodology utilized in this work could not provide conclusive results into NGP *Pattern* pluvial years. As precipitation in the NGP is closely linked to nocturnal convective events (Wallace 1975), along with the seasonality of pluvial events showing higher chances of pluvial months during the warm season (Christian et al. 2015), an investigation into the role of anomalous convective events and their drivers is needed to further diagnose NGP pluvial years. Lastly, an investigation into the nature of precipitation in the GP (Fig. 3.2) revealed that processes within the

GP are shifting the variability in precipitation, especially in the SGP, which leads to changes in the hydroclimate of the GP. This result supports the hypothesis stated in Chapter 1 in that shifts in the GP climate is leading to changes in water over the GP.

Finally, it would be remise not to note the small sample size of pluvial years, especially *Pattern* pluvial years, identified using the PRISM and ERA-20C datasets in concert. While the sample size is limited not by the methodology but by the temporal limitations of the dataset itself, the small sample size could be impacting the results of the study. However, statistical significance showed that this is likely not the case for the results detailed in this study, as focus has been placed on anomaly signals that showed statistical significance when compared to 1000 random samples from the dataset used. While the sample size does necessitate further investigation into GP pluvial periods, the results from this study are useful for the diagnosis and prediction of GP pluvial events. Utilizing the signals seen during *Pattern* pluvial years can help diagnose climate model simulations to determine the probability of pluvial occurrences across the central United States. While the atmospheric anomalies that define *Pattern* pluvial years were identified on an annual scale, analysis of the 2015 SGP pluvial has shown that these signals can be seen on seasonal time scales, thus analysis of smaller time scales, utilizing the results from this work, could provide more information into seasonal to sub-seasonal pluvial periods across the GP.

References

Alderfasi, A. A., D. C. Nielsen, 2001: Use of crop water stress index for monitoring water status and scheduling irrigation in wheat. *Agric. Water Manage.*, **47**, 69–75, doi: https://doi.org/10.1016/S0378-3774(00)00096-2.

Alexander, M. A., I. Bladé, M. Newman, J. R. Lanzante, N.-C. Lau, and J. D. Scott, 2002: The atmospheric bridge: The influence of ENSO teleconnections on air–sea interaction over the global oceans. *J. Climate*, **15**, 2205–2231, https://doi.org/10.1175/1520-0442(2002)015<2205:TABTIO>2.0.CO;2.

Alfieri, L., P. Claps, P. D'Odorico, F. Laio, and T. M. Over, 2008: An analysis of the soil moisture feedback on convective and stratiform precipitation. *J. Hydrometeor.*, **9**, 280–291, doi:10.1175/2007JHM863.1.

AMS, 2012: Streamfunction. Glossary of Meteorology. [Available online at http://glossary.ametsoc.org/wiki/Streamfunction]

André JC, Bougeault P, Goutorbe JP. 1990. Regional estimates of heat and evaporation fluxes over nonhomogeneous terrain: Examples from the HAPEXMOBILHY Programme. *Bound.-Layer Meteor.*, **50**, 77–108, doi: 10.1007/BF00120519

Ashok, K., S. K. Behera, S. A. Rao, H. Weng, and T. Yamagata, 2007: El Niño Modoki and its possible teleconnection. *J. Geophys. Res.*, **112**, C11007. doi:10.1029/2006JC003798.

Badeck FW, Bondeau A, Böttcher K, Doktor D, Lucht W, Schaber J, Sitch S. 2004. Responses of spring phenology to climate change. *New Phytologist*, **162**, 295–309, doi: 10.1111/j.1469-8137.2004.01059.x

Barsugli, J. J., and P. D. Sardeshmukh, 2002: Global atmospheric sensitivity to tropical SST anomalies throughout the Indo-Pacific basin. *J. Climate*, **15**, 3427–3442.

`

Bartz JA and Brecht JK. 2002. Postharvest physiology and pathology of vegetables. 2nd ed. CRC Press. 744 p.

Basara, J. B., J. N. Maybourn, C. M. Peirano, J. E. Tate, P. J. Brown, J. D. Hoey, and B. R. Smith, 2013: Drought and associated impacts in the Great Plains of the United States - A review. *Intl. J. Geosciences*, **4,** 72-81.

Bates, G. T., M. P. Hoerling, and A. Kumar, 2001: Central U.S. springtime precipitation extremes: Teleconnections and relationships with sea surface temperature. *J. Climate*, **14**, 3751–3766, doi:https://doi.org/10.1175/1520-0442(2001)014<3751:CUSSPE>2.0.CO;2.

Berg, A., and Coauthors, 2015: Interannual coupling between summertime sur`face temperature and precipitation over land: Processes and implications for climate change. *J. Climate*, **28**, 1308–1328, https://doi.org/10.1175/JCLI-D-14-00324.1.

Bertin RI. 2008. Plant phenology and distribution in relation to recent climate change. *J. Torrey Bot. Soc.,* **135**,126–146, doi: http://dx.doi.org/10.3159/07-RP-035R.1

Bluestein HB. 1993.Synoptic–Dynamic Meteorology in Midlatitudes. Oxford University Press: New York, NY.

Blum A. 2010. Plant Breeding for Water-Limited Environments. 11th edn. Springer Science+Business Media, New York.

Branstator, G., H. Teng, 2017: Tropospheric waveguide teleconnections and their seasonality. *J. Atmos. Sci.,* **74**, 1513–1532, doi: https://doi.org/10.1175/JAS-D-16-0305.1.

Bukovsky MS, Karoly DJ. 2011. A regional modeling study of climate change impacts on warm-season precipitation in the central United States. *J. Climate*, **24**, 1985–2002, doi:10.1175/2010JCLI3447.1

Bukovsky, M. S., R. R. McCrary, A. Seth, L. O. Mearns, 2017: A mechanistically credible, Poleward shift in warm season precipitation projected for the U.S. Southern Great Plains?, *J. Climate,* **30**, 8275–8298, doi: https://doi.org/10.1175/JCLI-D-16-0316.1.

Burke, I. C., T. G. F. Kittel, W. K. Lauenroth, P. Snook, C.M. Yonker, and W. J. Parton, 1991: Regional analysis ofthe Central Great Plains. *BioScience,* **41**, 685–692, doi: 10.2307/1311763.

Caesar J, Alexander L, Vose RS. 2006. Large-scale changes in observed daily maximum and minimum temperatures: Creation and analysis of a new gridded data set. *J. Geophys. Res.*, **111**, D05101, doi: 10.1029/2005JD006280

Chen, T-C., 2002: A North Pacific short-wave train during the extreme phases of ENSO. *J. Climate*, **15**, 2359–2376.

Chen, Z., Z. Wen, R. Wu, P. Zhao, and J. Cao, 2014: Influence of two types of El Niños on the East Asian climate during boreal summer: A numerical study. *Climate Dyn.*, **43**, 469–481, doi:10.1007/s00382-013-1943-1.

Chiodi, A. M., and D. E. Harrison, 2013: Impacts on seasonal U.S. atmospheric circulation, temperature, and precipitation anomalies: The OLR-event perspective. *J. Climate*, **26**, 822–837, doi:10.1175/JCLI-D-12-00097.1.

Christian J, K. Christian, J. B. Basara, 2015: Drought and pluvial dipole events within the great plains of the United States. *J. Appl. Meteorol. Climatol.,* **54**, 1886–1898, doi: http://dx.doi.org/10.1175/JAMC-D-15-0002.1.

Ciancarelli, B., C. L. Castro, C. Woodhouse. F. Dominguez, H.-I. Chang, C. Carrillo, and D. Griffin, 2014: Dominant patterns of US warm season precipitation variability in a fine

resolution observational record, with focus on the Southwest. *Int. J. Climatol.,* **34**, 687–707, doi:https://doi.org/10.1002/joc.3716.

Cleland EE, Chuine I, Menzel A, Mooney HA, Schwartz MD. 2007. Shifting plant phenology in response to global change. *Trends in Ecology & Evolution*, **22**, 357–365, doi: http://dx.doi.org/10.1016/j.tree.2007.04.003

Compo, G. P. and Coauthors, 2011: The Twentieth Century Reanalysis Project. *Quart. J. Roy. Meteor. Soc.*, **137**, 1–28, doi:10.1002/qj.776.

Cook, B. I., R. L. Miller, and R. Seager, 2008: Dust and sea surface temperature forcing of the 1930s "Dust Bowl" drought. *Geophys. Res. Lett*., **35**, L08710, doi:10.1029/2008GL033486.

Cook, B. I., R. Seager, and R. L. Miller, 2011: On the causes and dynamics of the early twentieth-century North American pluvial. *J. Climate*, **24**, 5043–5060, doi:10.1175/2011JCLI4201.1

Cook, B. I., T. R. Ault, and J. E. Smerdon, 2015: Unprecedented 21st century drought risk in the American Southwest and Central Plains. *Sci. Adv.*, **1**, e1400082, doi:https://doi.org/10.1126/sciadv.1400082.

Dai, A., and T. M. L. Wigley, 2000: Global patterns of ENSO induced precipitation. *Geophys. Res. Lett*., **27**, 1283–1286.

Daly, C., W. P. Gibson, G. H. Taylor, G. L. Johnson, and P. Pasteris, 2000: High quality spatial climate data sets for the United States and beyond. *Trans. Am. Soc. Ag. Eng.*, **43**, 1957-1962.

Dee, D., and Coauthors, 2011: The ERA-Interim reanalysis: Configuration and performance of the data assimilation system. *Quart. J. Roy. Meteor. Soc*., **137**, 553–597.

`

Deser, C., and J. M. Wallace, 1990: Large-scale atmospheric circulation features of warm and cold episodes in the tropical Pacific. *J. Climate*, **3**, 1254–1281.

Di, L., D. C. Rundquist, and L. Han, 1994. Modelling relationships between NDVI and precipitation during vegetative growth cycles. *Int. J. Remote Sens.,* **15,** 2121–2136, doi: http://dx.doi.org/10.1080/01431169408954231

Ding, Q., and B. Wang, 2005: Circumglobal teleconnection in the Northern Hemisphere summer. J. *Climate*, **18**, 3483–3505.

Ding, Q., and B. Wang, J. M. Wallace, and G. Branstator, 2011: Tropical-extratropical teleconnections in boreal summer: Observed interannual variability. *J. Climate*, **24**, 1878–1896.

Dore M. H. I., 2005: Climatic change and changes in global precipitation patterns: what do we know? *Environment International* **31**: 1167–1181.

Duchon, C. E., C. Fiebrich and B. Illston, 2017: Observing the May 2015 record rainfall at Norman, Oklahoma, using various methods. *J. Hydrometeor.,* **18**, 3043–3049, doi: https://doi.org/10.1175/JHM-D-17-0137.1.

Durre I, Wallace JM, Lettenmaier DP. 2000. Dependence of extreme daily maximum temperatures on antecedent soil moisture in the contiguous United States during summer. *J. Climate*, **13,** 2641–2651, doi: http://dx.doi.org/10.1175/1520-0442(2000)013<2641:DOEDMT>2.0.CO;2

Easterling DR, Robinson PJ. 1985. The diurnal variation of thunderstorm activity in the United States. *J. Climate Appl. Meteor.*, **24**, 1048–1058, doi: http://dx.doi.org/10.1175/1520-0450(1985)024<1048:TDVOTA>2.0.CO;2

Easterling, D. R., G. A. Meehl, C. Parmesan, S. Changnon, T. Karl, and L. Mearns, 2000: Climate extremes: Observations, modeling, and impacts. *Science,* **289**, 2068–2074, doi:https://doi.org/10.1126/science.289.5487.2068.

Fang, X.-H. and M. Mu, 2018: A three-region conceptual model for central Pacific El Niño including zonal advective feedback. *J. Climate.,* **31**, 4965–4979, https://doi.org/10.1175/JCLI-D-17-0633.1.

Fay PA. 2009. Precipitation variability and primary productivity in water-limited ecosystems: how plants 'leverage' precipitation to 'finance' growth. *New Phytologist,* **181**, 5–8, doi: 10.1111/j.1469-8137.2008.02695.x

Feng, S., M. Trnka, M. Hayes, and Y. Zhang, 2017: Why do different drought indices show distinct future drought risk outcomes in the U.S. Great Plains? *J. Climate*, **30**, 265–278, doi:https://doi.org/10.1175/JCLI-D-15-0590.1.

Findell, K. L., and T. L. Delworth, 2010: Impact of common sea surface temperature anomalies on global drought and pluvial frequency. *J. Climate*, **23**, 485–503.

Fischer M. L., D. P. Billesbach, J. A. Berry, W. J. Riley, M. S. Torn, 2007: Spatiotemporal variations in growing season exchanges of CO2, H2O, and sensible heat in agricultural fields of the Southern Great Plains. *Earth Interact*., **11**, 1–21.

Flanagan, P. X., J. B. Basara, and X. Xiao, 2017: Long-term analysis of the asynchronicity between temperature and precipitation maxima in the United States Great Plains. *Int. J. Climatol.,* **37**, 3919–3933, doi:10.1002/joc.4966.

Flanagan, P. X., J. B. Basara, J. C. Furtado, X. Xiao, 2018a: Primary atmospheric drivers of pluvial years in the United States Great Plains. *J. Hydrometeor*., **19**, 643–658, doi: https://doi.org/10.1175/JHM-D-17-0148.1.

`

Flanagan, P. X., J. B. Basara, J. C. Furtado, E. R. Martin, X. Xiao, 2018b: Role of Pacific sea surface temperatures in United States Great Plains pluvial years. *J. Climate, In review.*

Frankignoul, C., and N. Sennéchael, 2007: Observed influence of North Pacific SST anomalies on the atmospheric circulation. *J. Climate*, **20**, 592–606.

Fu, J., M. Zhang, Z. Han, et al., 2013: Sensitivity difference in the extratropical atmosphere to two types of El Nino events. *Atmos. Oceanic Sci. Lett*., **6(5)**, 355–359

Garfinkel, C. I., M. M. Hurwitz, D. W. Waugh, and A. H. Butler, 2013: Are the teleconnections of central Pacific and eastern Pacific El Niño distinct in boreal wintertime? *Climate Dyn*., **41**, 1835–1852, doi: https://doi.org/10.1007/s00382-012-1570-2.

Gershunov, A., and T. Barnett, 1998: ENSO influence on intraseasonal extreme rainfall and temperature frequencies in the contiguous United States: Observations and model results. *J. Climate*, **11**, 1575–1586.

Graef, F. and J. Haigis, 2001: Spatial and temporal rainfall variability in the Sahel and effects on farmers' management strategies. *J. Arid Environments,* **48/2**, 221–231, doi: https://doi.org/10.1006/jare.2000.0747.

Graf, H.-F., and D. Zanchettin, 2012: Central Pacific El Niño, the subtropical bridge, and Eurasian climate. *J. Geophys. Res*., **117**, D01102, doi:https://doi.org/10.1029/2011JD016493.

Griffin, K. S., J. E. Martin, 2017: Synoptic features associated with temporally coherent modes of variability of the north pacific jet stream. . *J. Climate,* **30**, 39–54, doi: http://dx.doi.org/10.1175/JCLI-D-15-0833.1.

Groisman PYa, Knight RW, Karl TR. 2012. Changes in intense precipitation over the central United States. *J. Hydrometeor.,* **13**, 47–66, doi:10.1175/JHM-D-11-039.1.

`

Grotjahn, R., and G. Faure, 2008: Composite predictor maps of extraordinary weather events in the Sacramento California region. *Wea. Forecasting*, 23, 313–335, doi:https://doi.org/10.1175/2007WAF2006055.1.

Guo, Y., M. Ting, Z. Wen, D.E. Lee, Y. Guo, M. Ting, Z. Wen, D.E. Lee, 2017: Distinct patterns of tropical Pacific SST anomaly and their impacts on North American climate. *J. Climate*, **30**, 5221–5241, doi:10.1175/JCLI-D-16-0488.1

Harrison, D. E., and N. K. Larkin, 1998: El Niño–Southern Oscillation sea surface temperature and wind anomalies, 1946–1993. *Rev. Geophys*., **36**, 353–400, doi:10.1029/98RG00715.

Haugland MJ, Crawford KC. 2005. The diurnal cycle of land–atmosphere interactions across Oklahoma's winter wheat belt. *Mon. Wea. Rev.*, **133,** 120–130, doi: http://dx.doi.org/10.1175/MWR-2842.1

Hoerling, M. P., A. Kumar, and M. Zhong, 1997: El Niño, La Niña, and the nonlinearity of their teleconnections. *J.Climate*, **10**, 1769–1786, doi:10.1175/1520-0442(1997)010,1769:ENOLNA.2.0.CO;2.

Hoerling, M., J. Eischeid, A. Kumar, R. Leung, A. Mariotti, K. Mo, S. Schubert, and R. Seager, 2014: Causes and predictability of the 2012 Great Plains drought. *Bull. Amer. Meteor. Soc.*, **95**, 269–282, https://doi.org/10.1175/BAMS-D-13-00055.1.

Hu, Q., and S. Feng, 2001: Variations of teleconnections of ENSO and interannual variations in summer rainfall in the central United States. *J. Climate*, **14**, 2469–2480.

Hu, Z., and B. Huang, 2009: Interferential impact of ENSO and PDO on dry and wet conditions in the U.S. Great Plains. *J. Climate*, **22**, 6047–6065, doi:10.1175/2009JCLI2798.1.

`

Hughes L 2000. Biological consequences of global warming: is the signal already apparent? *Trends in Ecology and Evolution*, **15**, 56–61, doi: http://dx.doi.org/10.1016/S0169-5347(99)01764-4

Hunt, B. G., 2011: Global characteristics of pluvial and dry multi-year episodes, with emphasis on megadroughts. *Int. J. Climatol.*, **31**, 1425–1439, doi:https://doi.org/10.1002/joc.2166.

Illston, B. G., J. B. Basara, and K. C. Crawford, 2004: Seasonal to interannual variations of soil moisture measured in Oklahoma. *Int. J. Climatol.*, **24**, 1883–1896.

Irmak, S., D. Z. Haman, and R. Bastug, 2000: Determination of crop water stress index for irrigation timing and yield estimation of corn. *Agron. J.,* **92**, 1221–1227, doi:10.2134/agronj2000.9261221x.

Jamieson MA, Trowbridge AM, Raffa KF, Lindroth RL. 2012. Consequences of climate warming and altered precipitation patterns for plant-insect and multitrophic interactions. *Plant Physiology*, **160**, 1719–1727, doi: http://dx.doi.org/10.1104/pp.112.206524

Jongen M, Pereira JS, Aires LMI, Pio CA. 2011. The effects of drought and timing of precipitation on the inter-annual variation in ecosystem-atmosphere exchange in a Mediterranean grassland, *Agric. For. Meteorol.*, **151**(5), 595–606, doi: http://dx.doi.org/10.1016/j.agrformet.2011.01.008

Kalnay, E., and Coauthors, 1996: The NCEP/NCAR 40-Year Reanalysis Project. *Bull. Amer. Meteor. Soc.*, 77, 437–471, doi:10.1175/1520-0477(1996)077,0437:TNYRP.2.0.CO;2.

Kang, Y., S. Khan, X. Maa, 2009: Climate change impacts on crop yield, crop water productivity and food security: a review. *Prog. Nat. Sci.,* **1**9, 1665–1674, doi: https://doi.org/10.1016/j.pnsc.2009.08.001.

`

Kao, H. -Y., and J.-Y. Yu, 2009: Contrasting eastern-Pacific and central-Pacific types of ENSO. *J. Climate*, **22**, 615–632, https://doi.org/10.1175/2008JCLI2309.1.

Karl TR, Williams Jr. CN. 1987. An approach to adjusting climatological time series for discontinuous inhomogeneities. *J. Climate Appl. Meteor.*, **26**, 1744–1763, doi: http://dx.doi.org/10.1175/1520-0450(1987)026<1744:AATACT>2.0.CO;2

Karl TR, Williams Jr. CN, Young PJ, Wendland WM. 1986. A model to estimate the time of observation bias associated with monthly mean maximum, minimum, and mean temperature for the United States. *J. Climate Appl. Meteor.*, **25**, 145–160, doi: http://dx.doi.org/10.1175/1520-0450(1986)025<0145:AMTETT>2.0.CO;2

Karl TR, Diaz HF, Kukla G. 1988. Urbanization: Its detection and effect in the United States climate record. *J. Climate*, **1**, 1099–1123, doi: http://dx.doi.org/10.1175/1520-0442(1988)001<1099:UIDAEI>2.0.CO;2

Kirigwi, F. M., M. Van Ginkel, R. M. Trethowan, R. G. Sears, G. M. Paulsen, 2004: Evaluation of selection strategies for wheat adaptation across water regimes. *Euphytica,* **135**, 361–371, doi: https://doi.org/10.1023/B:EUPH.0000013375.66104.04.

Klingaman, N. P., B. Hanson, and D. J. Leathers, 2008: A teleconnection between forced Great Plains snow cover and European winter climate. *J. Climate*, 21, 2466–2483, doi:10.1175/2007JCLI1672.1.

Knippertz, P., and H. Wernli, 2010: A Lagrangian climatology of tropical moisture exports to the Northern Hemisphere extratropics. *J. Climate*, **23**, 987–1003, https://doi.org/10.1175/2009JCLI3333.1.

Koster, R. D., and Coauthors, 2004: Regions of strong coupling between soil moisture and precipitation. *Science*, **305**, 1138–1140, doi:10.1126/science.1100217.

Koster, R., M. J. Suarez, and M. Heiser, 2000: Variance and predictability of precipitation at seasonal-to-interannual timescales. *J. Hydrometeor.*, **1**, 26–46, https://doi.org/10.1175/1525-7541(2000)001,0026:VAPOPA.2.0.CO;2.

Kug, J.-S., F.-F. Jin, and S.-I. An, 2009: Two types of El Niño events: Cold tongue El Niño and warm pool El Niño. *J. Climate*, **22**, 1499–1515, https://doi.org/10.1175/2008JCLI2624.1.

Kumar S, Kinter III J, Dirmeyer PA, Pan Z, Adams J. 2013. Multidecadal climate variability and the ‘‘warming hole’’ in North America: Results from CMIP5 twentieth- and twenty-first-century climate simulations. *J. Climate*, **26**, 3511– 3527, doi:10.1175/JCLI-D-12-00535.1

Kunkel KE, Liang XZ, Zhu JH. 2010. Regional climate model projections and uncertainties of U.S. summer heat waves. *J. Climate*, **23**, 4447–4458, doi:10.1175/2010JCLI3349.1.

Kuo, Y. H., M. A. Shapiro, and E. G. Donall, 1991: The interaction between baroclinic and diabatic processes in a numerical simulation of a rapidly intensifying extratropical marine cyclone. *Mon. Wea. Rev.,* **119**, 368–384.

Kushnir, Y., R. Seager, M. Ting, N. Naik, and J. Nakamura, 2010: Mechanisms of tropical Atlantic SST influence on North American precipitation variability. *J. Climate*, **23**, 5610–5628, doi:https://doi.org/10.1175/2010JCLI3172.1.

Kwon, Y-O., M. A. Alexander, N. A. Bond, C. Frankignoul, H. Nakamura, B. Qiu, and L. Thompson, 2010: Role of the Gulf Stream and Kuroshio–Oyashio systems in large-scale atmosphere–ocean interaction: A review. *J. Climate*, **23**, 3249–3281.

L’Heureux, M. L., M. K. Tippett, and A. G. Barnston, 2015: Characterizing ENSO coupled variability and its impact on North American seasonal precipitation and temperature. *J. Climate*, **28**, 4231–4245, doi:10.1175/JCLI-D-14-00508.1.

Larkin, N. K., and D. E. Harrison, 2005a: On the definition of El Niño and associated seasonal average U.S. weather anomalies. *Geophys. Res. Lett.*, **32**, L13705, doi:10.1029/2005GL022738.

Larkin, N. K., and D. E. Harrison, 2005b: Global seasonal temperature and precipitation anomalies during El Niño autumn and winter. *Geophys. Res. Lett*., **32**, L16705, doi:10.1029/2005GL022860.

Lau, K-M., and H-Y. Weng, 2002: Recurrent teleconnection patterns linking summertime precipitation variability over east Asia and North America. *J. Meteor. Soc. Japan*, **80**, 1309–1324.

Lau, K-M., J-Y. Lee, K-M. Kim, and I-S. Kang, 2004: The North Pacific as a regulator of summertime climate over Eurasia and North America. *J. Climate*, **17**, 819–833.

Lau, N-C., 1997: Interactions between global SST anomalies and the midlatitude atmospheric circulation. *Bull. Amer. Meteor. Soc*., **78**, 21–33.

Linderholm HW. 2006. Growing season changes in the last century. *Agricultural and Forest Meteorology*, **137**,1–14, doi: http://dx.doi.org/10.1016/j.agrformet.2006.03.006

Livezey, R. E., M. Masutani, A. Leetmaa, H. Rui, M. Ji, and A. Kumar, 1997: Teleconnective response of the Pacific–North American region atmosphere to large central equatorial Pacific SST anomalies. J. Climate, 10, 1787–1820, https://doi.org/10.1175/1520-0442(1997)010<1787:TROTPN>2.0.CO;2.

Livneh, B., and M. P. Hoerling, 2016: The physics of drought in the U.S. central Great Plains. *J. Climate*, **29**, 6783–6804, https://doi.org/10.1175/JCLI-D-15-0697.1.

Lobell DB, Asner GP. 2003. Climate and management contributions to recent trends in agricultural yields. *Science,* **299**, 1032, doi: 10.1126/science.1078475

`

Long D, Scanlon BR, Fernando DN, Meng L, Quiring SM. 2012. Are temperature and precipitation extremes increasing over the U.S. high plains? *Earth Interact*., **16**, 1–20, doi: http://dx.doi.org/10.1175/2012EI000454.1

Ma, X., and Coauthors, 2015: Distant influence of Kuroshio eddies on North Pacific weather patterns? *Sci. Rep*., **5**, 17785, doi:10.1038/srep17785.

Ma, X., P. Chang, R. Saravanan, R. Montuoro, H. Nakamura, D. Wu, X. Lin, L. Wu, 2017: Importance of resolving Kuroshio front and eddy influence in simulating the north pacific storm track. *J. Climate*, **30**, 1861–1880, doi: 10.1175/JCLI-D-16-0154.1

Mantua, N. J., S. R. Hare, Y. Zhang, J. M. Wallace, and R. C. Francis, 1997: A Pacific interdecadal climate oscillation with impacts on salmon production. *Bull. Amer. Meteor. Soc.,* **78**, 1069–1079.

Martin, E. R., and C. Schumacher, 2011: The Caribbean low-level jet and its relationship with precipitation in IPCC AR4 models. *J. Climate*, **24**, 5935–5950.

Martyniak L. 2008. Response of spring cereals to a deficit of atmospheric precipitation in the particular stages of plant growth. *Agric. Water Manage.,* **95**, 171–178, doi: http://dx.doi.org/10.1016/j.agwat.2007.10.014

Méndez-Barroso LA, Vivoni ER, Watts CJ, Rodríguez JC. 2009. Seasonal and interannual relations between precipitation, surface soil moisture and vegetation dynamics in the North American monsoon region. *J. Hydrology*, **377**, 59–70, doi: http://dx.doi.org/10.1016/j.jhydrol.2009.08.009

Menne MJ, Durre I, Gleason BG, Houston TG, Vose RS. 2012. An overview of the Global Historical Climatology Network-Daily database. *J. Atmos. Oceanic Technol.*, **29**, 897–910, doi: http://dx.doi.org/10.1175/JTECH-D-11-00103.1

`

Menzel A. 2003. Plant phenological anomalies in Germany and their relation to air temperature and NAO. *Climatic Change*, **57**, 243–263, doi: 10.1023/A:1022880418362

Menzel A, and coauthors. 2006. European phenological response to climate change matches the warming pattern. *Global Change Biology,* **12**, 1969–1976, doi: 10.1111/j.1365-2486.2006.01193.x

McCrary, R. R., and D. A. Randall, 2010: Great Plains drought in simulations of the twentieth century. *J. Climate*, **23**, 2178–2196, doi:https://doi.org/10.1175/2009JCLI3061.1.

Mills, C., and J. E. Walsh, 2013: Seasonal variation and spatial patterns of the atmospheric component of the Pacific decadal oscillation. *J. Climate*, **26**, 1575–1594, doi:https://doi.org/10.1175/JCLI-D-12-00264.1.

Mo, K. C., J. Nogues-Paegle, and R. W. Higgins, 1997: Atmospheric processes associated with summer floods and droughts in the central United States. *J. Climate*, **10**, 3028–3046, doi: https://doi.org/10.1175/1520-0442(1997)010<3028:APAWSF>2.0.CO;2.

Moore, R. W., O. Martius, and T. Spengler, 2010: The modulation of the subtropical and extratropical atmosphere in the Pacific basin in response to the Madden–Julian oscillation. Mon. Wea. Rev., 138, 2761–2778, doi:10.1175/2010MWR3194.1.

Neelin, J. D., 2011: *Climate Change and Climate Modeling*. Cambridge University Press, 304 pp.

Newman, M., and Coauthors, 2016: The Pacific decadal oscillation, revisited. *J. Climate*, **29**, 4399–4427, doi:https://doi.org/10.1175/JCLI-D-15-0508.1.

Newman, M., G. Compo, and M. Alexander, 2003: ENSO-forced variability of the Pacific decadal oscillation. *J. Climate*, **16**, 3853–3857.

Nieto, R., and Coauthors, 2005: Climatological features of cutoff low systems in the Northern Hemisphere. *J. Climate*, **18**, 3085–3103, doi:10.1175/JCLI3386.1.

`

O'Lenic, E. A., D. A. Unger, M. S. Halpert, and K. S. Pelman, 2008: Developments in operational long-range climate prediction at CPC. *Wea. Forecasting*, 23, 496–515, doi:10.1175/2007WAF2007042.1.

Oglesby, R. J., K. A. Maasch, and B. Saltzman, 1989: Glacial meltwater cooling of the Gulf of Mexico: GCM implications for Holocene and present-day climate. *Climate Dyn.,* **3,** 115–133.

Olesen JE, Bindi M. 2002. Consequences of climate change for European agricultural productivity, land use and policy. *Eur J Agron*. **16**, 239–62, doi: http://dx.doi.org/10.1016/S1161-0301(02)00004-7

Onogi, K., J. Tsutsui, H. Koide, M. Sakamoto, S. Kobayashi, H. Hatsushika, T. Matsumoto, N. Yamazaki, H. Kamahori, K. Takahashi, S. Kadokura, K. Wada, K. Kato, R. Oyama, T. Ose, N. Mannoji and R. Taira, 2007: The JRA-25 Reanalysis. *J. Meteor. Soc. Japan*, 85, 369-432, doi:10.2151/jmsj.85.369.

Pal, J. S., and E. A. B. Eltahir, 2003: A feedback mechanism between soil-moisture distribution and storm tracks. *Quart. J. Roy. Meteor. Soc*., **129**, 2279–2297, doi:https://doi.org/10.1256/qj.01.201.

Pederson, N., A. R. Bell, E. R. Cook, U. Lall, N. Devineni, R. Seager, K. Eggleston, and K. P. Vranes, 2013: Is an epic pluvial masking the water insecurity of the greater New York City region? J. Climate, 26, 1339–1354, doi:10.1175/JCLI-D-11-00723.1.

Pielke RA, Dalu GA, Snook JS, Lee TJ, Kittel TGF. 1991. Nonlinear influence of mesoscale land use on weather and climate. *J. Climate*, **4**, 1053–1069, doi: http://dx.doi.org/10.1175/1520-0442(1991)004<1053:NIOMLU>2.0.CO;2

`

Poli, P., and Coauthors, 2016: ERA-20C: An atmospheric reanalysis of the twentieth century. *J. Climate*, **29**, 4083–4097, doi:10.1175/JCLI-D-15-0556.1.

Quayle RG, Easterling DR, Karl TR, Hughes PY. 1991. Effects of recent thermometer changes in the cooperative station network. *Bull. Amer. Meteor. Soc.*, **72**, 1718–1723, doi: http://dx.doi.org/10.1175/1520-0477(1991)072<1718:EORTCI>2.0.CO;2

Randall D. 2014. An Introduction to the General Circulation of the Atmosphere. Department of Atmospheric Science, Colorado State University: Boulder, CO.

Rasmusson EM. 1971. Diurnal variation of thunderstorm activity over the U.S. *Tech. Note* 71-4, U.S. Air Force Environmental Technical Applications Center, Washington, DC, 12 pp. [Available from U.S. Air Force Environmental Technical Applications Ctr., Bldg. 159, Navy Yard Annex, Washington, DC 20333.]

Rasmusson, E. M., and T. H. Carpenter, 1982: Variation in tropical sea surface temperature and surface wind fields associated with the Southern Oscillation/El Niño. *Mon. Wea. Rev.*, **110**, 354–384, doi:10.1175/1520-0493(1982)110,0354:VITSST.2.0.CO;2.

Rayner, N. A., D. E. Parker, E. B. Horton, C. K. Folland, L. V. Alexander, D. P. Rowell, E. C. Kent, and A. Kaplan, 2003: Global analyses of sea surface temperature, sea ice, and night marine air temperature since the late nineteenth century. *J. Geophys. Res.*, **108**, 4407, doi:10.1029/2002JD002670.

Reed, R. J., G. A. Grell, and Y. H. Kuo, 1993: The ERICA IOP 5 Storm. Part II: Sensitivity tests and further diagnosis based on model output. *Mon. Wea. Rev.*, **121**, 1595–1612.

Regonda S, Rajagopalan B, Clark M, Pitlick J. 2005. Seasonal cycle shifts in hydroclimatology over the western United States. *J. Climate*, **18**, 372–384, doi: http://dx.doi.org/10.1175/JCLI-3272.1

`

Rex, D. F., 1950: Blocking action in the middle troposphere and its effect upon regional climate. I. An aerological study of blocking action. *Tellus*, **2**, 196–211.

Ropelewski, C. F., and M. S. Halpert, 1986: North American precipitation and temperature patterns associated with the El Niño/Southern Oscillation (ENSO). *Mon. Wea. Rev.*, **114**, 2352–2362.

Ropelewski, C. F., and M. S. Halpert, 1987: Global and regional scale precipitation patterns associated with the El Niño/Southern Oscillation. *Mon. Wea. Rev*., **115**, 1606–1626,doi: https://doi.org/10.1175/1520-0493(1987)115<1606:GARSPP>2.0.CO;2.

Ropelewski, C. F., and M. S. Halpert, 1989: Precipitation patterns associated with the high index phase of the Southern Oscillation. *J. Climate*, **2**, 268–284, doi: https://doi.org/10.1175/1520-0442(1989)002<0268:PPAWTH>2.0.CO;2.

Rosenzweig C, 1990, Crop response to climate change in the southern Great Plains: A simulation study, *Prof. Geogr.*, **1**, 20–37, doi: http://dx.doi.org/10.1111/j.0033-0124.1990.00020.x

Rosenzweig, C., A. Iglesias, X. Yang, 2001: Climate change and extreme weather events: Implications for food production, plant diseases and pests. *Glob. Change Human Health*, **2**, 90–104. doi:10.1023/A:1015086831467.

Ruiz-Barradas, A., and S. Nigam, 2005: Warm season rainfall variability over the U.S. Great Plains in observations, NCEP and ERA-40 reanalyses, and NCAR and NASA atmospheric model simulations. *J. Climate*, **18**, 1808–1830, https://doi.org/10.1175/JCLI3343.1.

Ruiz-Barradas, A., and S. Nigam, 2010: Great Plains precipitation and its SST links in twentieth-century climate simulations, and twenty-first- and twenty-second-century climate projections. *J. Climate*, **23**, 6409–6429.

Sanders, F., 1986: Explosive cyclogenesis over the west-central North Atlantic Ocean, 1981–84. Part I: Composite structure and mean behavior. *Mon. Wea. Rev.,* **114**, 1781–1794.

Schlenker W, Roberts MJ. 2009. Nonlinear temperature effects indicate severe damages to U.S. crop yields under climate change. *Proc. Natl. Acad. Sc. USA,* **106**, 15594–15598, doi: 10.1073/pnas.0906865106

Schneider, N., and B. D. Cornuelle, 2005: The forcing of the Pacific decadal oscillation. *J. Climate*, **18**, 4355–4373.

Schubert, S. D., and Coauthors, 2016: Global meteorological drought: A synthesis of current understanding with a focus on SST drivers of precipitation deficits. *J. Climate*, **29**, 3989–4019, https://doi.org/10.1175/JCLI-D-15-0452.1.

Schubert, S. D., M. J. Suarez, P. J. Pegion, R. D. Koster, and J. T. Bacmeister, 2008: Potential predictability of long-term drought and pluvial conditions in the U.S. Great Plains. *J. Climate*, **21**, 802–816, doi:10.1175/2007JCLI1741.1

Schubert, S. D., M. J. Suarez, P. Pegion, R. J. Koster, and J. T. Bacmeister, 2004: Causes of long-term drought in the U.S. Great Plains. *J. Climate*, **17**, 485–503.

Schubert, S., and Coauthors, 2009: A U.S. CLIVAR project to assess and compare the responses of global climate models to drought-related SST forcing patterns: Overview and results. *J. Climate*, **22**, 5251–5272.

Schwartz MD, Ahas R, Aasa A. 2006. Onset of spring starting earlier across the Northern Hemisphere. *Global Change Biology,* **12**, 343–351, doi: 10.1111/j.1365-2486.2005.01097.x

Seager, R., and M. P. Hoerling, 2014: Atmosphere and ocean origins of North American drought. *J. Climate*, **27**, 4581–4606, doi:https://doi.org/10.1175/JCLI-D-13-00329.1.

`

Seager, R., L. Goddard, J. Nakamura, N. Henderson, and D. E. Lee, 2014: Dynamical causes of the 2010/11 Texas–northern Mexico drought. *J. Hydrometeor.*, **15**, 39–68, doi:10.1175/JHM-D-13-024.1.

Seager, R., N. Harnik, W. A. Robinson, Y. Kushnir, M. Ting, H. P. Huang, and J. Velez, 2005: Mechanisms of ENSO-forcing of hemisphericallysymmetric precipitation variability, Q. *J. R. Meteorol. Soc.*, **131**, 1501 –1527.

Seneviratne SI, Corti T, Davin EL, Hirschi M, Jaeger EB, Lehner I, Orlowsky B, Teuling AJ. 2010. Investigating soil moisture climate interactions in a changing climate: A review, *Earth Sci. Rev.*, **99**, 125–161, doi: http://dx.doi.org/10.1016/j.earscirev.2010.02.004

Seo, H., Y. Kwon, T. M. Joyce, C. C. Ummenhofer, 2017: On the predominant nonlinear response of the extratropical atmosphere to meridional shifts of the Gulf Stream. *J. Climate*, **30**, 9679–9702, doi: https://doi.org/10.1175/JCLI-D-16-0707.1.

Shi X, Durran D. 2016. Sensitivities of extreme precipitation to global warming are lower over mountains than over oceans and plains. *J. Climate*, **29**, 4779–4791, doi: http://dx.doi.org/10.1175/JCLI-D-15-0576.1

Stewart IT, Cayan DR, Dettinger MD. 2004. Changes in snowmelt runoff timing in western North America under a "business as usual" climate change scenario. *Climatic Change*, **62,** 217–232, doi:10.1023/B:CLIM.0000013702.22656.e8

Symstad, A. J., J. L. Jonas, 2011: Incorporating biodiversity into rangeland health: plant species richness and diversity in Great Plains grasslands. *Rangel. Ecol. Manag.,* **64**, 555–572, doi: https://doi.org/10.2111/REM-D-10-00136.1.

`

Terjung WH, Liverman DM, Hayes JT. 1984. Climatic change and water requirements for grain corn in the North American Great Plains. *Climatic Change*, **6**, 193–220, doi:10.1007/BF00144612

Teuling AJ, Troch PA. 2005. Improved understanding of soil moisture variability dynamics. *Geophys. Res. Lett.*, **32**, L05404, doi:10.1029/2004GL021935.

Thurow, T. L., and C. A. Taylor. 1999: Viewpoint: The role of drought in range management. *J. Range Management*, **52**, 413–419, doi: 10.2307/4003766.

Ting, M., and H. Wang, 1997: Summertime U.S. precipitation variability and its relation to Pacific sea surface temperature. *J. Climate*, **10**, 1853–1873, doi:10.1175/1520-0442(1997)010<1853:SUSPVA>2.0.CO;2.

Trenberth, K. E. , G. W. Branstator, D. Karoly, A. Kumar, N.-C. Lau, and C. Ropelewski, 1998: Progress during TOGA in understanding and modeling global teleconnections associated with tropical sea surface temperatures. J. *Geophys. Res.*, **103**, 14 291–14 324.

Trenberth, K. E., 1997: The definition of El Niño. *Bull. Amer. Meteor. Soc*., **78**, 2771–2777, doi:10.1175/1520-0477(1997)078,2771:TDOENO.2.0.CO;2.

Trenberth, K. E., and C. J. Guillemot, 1996: Physical processes involved in the 1988 drought and 1993 floods in North America. *J. Climate*, **9**, 1288–1298.

Trenberth, K. E., and G. W. Branstator, 1992: Issues in establishing causes of the 1988 drought over North America. *J. Climate*, **5**, 159–172.

Tubiello FN, Rosenzweig C, Goldberg RA, Jagtap S, Jones JW. 2002. Effects of climate change on US crop production: simulation results using two different GCM scenarios. Part I: wheat, potato, maize, and citrus. *Climate Research,* **20**, 259–270, doi:10.3354/cr020259

Tubiello FN, Soussana J-F,Howden SM. 2007. Crop and pasture response to climate change. *Proceedings of the National Academy of Sciences, USA*. **104**, 19686–19690, doi: 10.1073/pnas.0701728104

Turner NC, Begg JE. 1981. Plant–water relations and adaptation to stress. *Plant and Soil*, **58**, 97–131, doi:10.1007/BF02180051

Vivoni ER, Moreno HA, Mascaro G, Rodriguez JC, Watts CJ, Garatuza-Payan J, Scott RL. 2008. Observed relation between evapotranspiration and soil moisture in the North American monsoon region. *Geophysical Research Letters.* **3,** L22403, doi: 10·1029/2008GL036001.

Wallace, J. M., 1975: Diurnal variations in precipitation and thunderstorm frequency over the conterminous United States. *Mon. Wea. Rev*., **103**, 406–419, https://doi.org/10.1175/1520-0493(1975)103<0406:DVIPAT>2.0.CO;2.

Wang, C., 2007: Variability of the Caribbean low-level jet and its relations to climate. *Climate Dyn.*, **29**, 411–422.

Wang, C., and S.-K. Lee, 2007: Atlantic warm pool, Caribbean low-level jet, and their potential impact on Atlantic hurricanes. *Geophys. Res. Lett.*, **34**, L02703, doi:10.1029/2006GL028579.

Wang, F., Z. Liu, and M. Notaro, 2013: Extracting the dominant SST modes impacting North America's observed climate. *J. Climate*, **26**, 5434–5452.

Wang, H., S. Schubert, M. Suarez, and R. Koster, 2010: The physical mechanisms by which the leading patterns of SST variability impact U.S. precipitation. *J. Climate*, **23**, 1815–1836.

Weaver, S., S. Baxter, and K. Harnos, 2016: Regional changes in the interannual variability of warm season precipitation. *J. Climate*, **29**, 5157–5173, https://doi.org/10.1175/JCLI-D-14-00803.1.

Wehner, M., D. R. Easterling, J. H. Lawrimore, R. R. Heim, R. S. Vose, and B. D. Santer, 2011: Projections of future drought in the continental United States and Mexico. *J. Hydrometeor*., **12**, 1359–1377.

Weltzin JF, McPherson GR. 2003. Predicting the response of terrestrial ecosystems to potential changes in precipitation regimes. *In*: Changing Precipitation Regimes and Terrestrial Ecosystems: A North American Perspective, pp. 3–8. University of Arizona Press, Tucson.

Westerling, A. L., A. Gershunov, T. J. Brown, D. R. Cayan, and M. D. Dettinger, 2003: Climate and wildfire in the western United States. *Bull. Amer. Meteor. Soc.*, 84, 595–604, doi:10.1175/BAMS-84-5-595.

Westerling, A. L., H. G. Hidalgo, D. R. Cayan, and T. W. Swetnam, 2006: Warming and earlier spring increase western US forest wildfire activity. *Science,* **313**, 940–943.

Wilhelmi O. V., D. A. Wilhite, 2002: Assessing vulnerability to agricultural drought: A Nebraska case study. *Natural Hazards,* **25**, 37–58.

Wilhite, D. A., 2000: Drought as a natural hazard: Concepts and definitions. *Drought: A Global Assessment,* D. A. Wilhite, Ed., Vol. 1, Routledge, 3–18.

Wirth, V., M. Riemer, E. Chang, and O. Martius, 2018: Rossby Wave Packets on the Midlatitude Waveguide — A Review. Mon. Wea. Rev. doi:10.1175/MWR-D-16-0483.1, in press.

Wuebbles, D., and Coauthors, 2014: CMIP5 climate model analyses: Climate extremes in the United States. *Bull. Amer. Meteor. Soc.*, **95**, 571–583, doi:10.1175/BAMS-D-12-00172.1.

`

Yang, S., X. Ding, D. Zheng, and Q. Li, 2007: Depiction of the variations of Great Plains precipitation and its relationship with tropical central-eastern Pacific SST. *J. Appl. Meteor. Climatol.*, **46**, 136–153.

Yeh, S.-W., J.-S. Kug, B. Dewitte, M.-H. Kwon, B. Kirtman, and F.-F. Jin, 2009: El Niño in a changing climate. *Nature*, **461**, doi:https://doi.org/10.1038/nature08316.

Yin, D., M. L. Roderick, G. Leech, F. Sun, and Y. Huang, 2014: The contribution of reduction in evaporative cooling to higher surface air temperatures during drought. *Geophys. Res. Lett.*, **41**, 7891–7897, doi:10.1002/2014GL062039.

Yu, B., X. Zhang, H. Lin, and J.-Y. Yu, 2015: Comparison of wintertime North American climate impacts associated with multiple ENSO indices. *Atmos.–Ocean*, **53**, 426–445, doi:10.1080/07055900.2015.1079697.

Yu, J.-Y., and H.-Y. Kao, 2007: Decadal changes of ENSO persistence barrier in SST and ocean heat content indices: 1958–2001. *J. Geophys. Res.,* **112**, D13106, https://doi.org/10.1029/2006JD007654.

Yu, J.-Y., H.-Y. Kao, and T. Lee, 2010: Subtropics-related interannual sea surface temperature variability in the equatorial central Pacific. *J. Climate*, **23**, 2869–2884, doi:https://doi.org/10.1175/2010JCLI3171.1.

Zeppel MJB, Wilks JV, Lewis JD. 2014. Impacts of extreme precipitation and seasonal changes in precipitation on plants. *Biogeosciences* **11**, 3083–3093, doi:10.5194/bg-11-3083-2014, 2014.

Zhang Y, Xiao X, Jin C, Dong J, Zhou S, Wagle P, Joiner J, Guanter L, Zhang Y, Zhang G, Qin Y, Wang J, Moore BI. 2016. Consistency between sun-induced chlorophyll fluorescence

and gross primary production of vegetation in North America., Remote Sensing of Environment, 183, 154-169, doi: http://dx.doi.org/10.1016/j.rse.2016.05.015

Zhao, S., Y. Deng, and R. Black, 2017: A Dynamical and Statistical Characterization of United States Extreme Precipitation Events and their Associated Large-Scale Meteorological Patterns. *J. Climate*, **30**, 1307–1326, doi:10.1175/JCLI-D-15-0910.1.

Appendix 1

List of All Pluvial Years from All Datasets Utilized

Table A1. List of all pluvial years for the SGP and NGP found in each of the datasets considered. Bold years are pluvial years that match with observed (PRISM) pluvial years. Length of period for each dataset is located below the datasets name.

Pluvial Years SGP					Pluvial Years NGP				
ERA-20C	20CR	NCEP-NCAR	JRA55	PRISM	ERA-20C	20CR	NCEP-NCAR	JRA55	PRISM
1900-2010	1851-2014	1949-2016	1958-2013	1895-2016	1900-2010	1851-2014	1949-2016	1958-2013	1895-2016
(15)	(10)	(13)	(11)		(15)	(10)	(11)	(4)	
2009	**2009**	2016	**2009**	2015	**2010**	2012	**2013**	**1995**	2015
2008	**2007**	**2015**	**2007**	2009	**2009**	**2011**	**2011**	**1993**	2014
2007	**2004**	2010	**2004**	2007	**2008**	**1993**	**2010**	1991	2013
2004	**2002**	**2007**	1993	2004	**2007**	1991	**2008**	**1986**	2011
2002	2001	**2004**	**1992**	2002	**2005**	**1986**	**2005**	1984	2010
2001	2000	**2002**	**1991**	1997	2004	1985	**1998**	1983	2009
1999	1994	**1997**	**1990**	1992	2000	1984	1997	**1982**	2008
1998	**1990**	1995	**1987**	1991	1999	**1982**	1996	1975	2007
1997	**1974**	**1991**	**1986**	1990	**1998**	**1977**	**1995**		2005
1994	**1968**	**1987**	**1985**	1987	**1995**	1975	**1993**		1998
1993	1967	**1986**	**1981**	1986	1994	1971	1991		1995
1992	**1960**	1984	**1973**	1985	**1993**	1968	**1986**		1993
1991	**1957**	1983		1981	**1986**	1967	**1982**		1986
1990	1955	**1981**		1979	**1982**	**1965**	**1977**		1982
1989	1952	**1973**		1974	**1977**	1964	1975		1977
1987	**1944**	**1968**		1973	1972	**1962**	1973		1965
1984	1933	**1957**		1968	1971	1959	1972		1962
1983	1932	1955		1961	1969	**1957**	1971		1957
1982		**1949**		1960	1968	1956	1970		1951
1979				1959	1967	1954	1969		1946
1978				1958	**1965**	1953	1968		1942
1974				1957	**1962**	**1951**			1941
1971				1949	1954	1945			1927
1969				1946	1953	**1942**			
1968				1944	**1951**				
1967				1942	1941				
1957				1941	1930				
1941				1935					
1926				1926					